LINEAR LIBRARY
C01 0068 0974

18

Void boundaries in the southern sky

Aspects of large scale structure in southern galaxy catalogues

A Maurellis

Department of Applied Mathematics
University of Cape Town
7700 Rondebosch
South Africa

February 17, 1991

University of Cape Town

The University of Cape Town has been given the right to reproduce this thesis in whole or in part. Copyright is held by the author.

The copyright of this thesis vests in the author. No quotation from it or information derived from it is to be published without full acknowledgement of the source. The thesis is to be used for private study or non-commercial research purposes only.

Published by the University of Cape Town (UCT) in terms of the non-exclusive license granted to UCT by the author.

University of Cape Town

IDST 510 MAUR
91/5183

To my grandmother
who is always the first to encourage me to reach for the stars

Summary

The evidence for structure at the largest observable scales has developed considerably in the last two and a half decades since the discovery, in 1967, of significant clustering in galaxy surveys. As will be shown by the review material and galaxy spectrum redshift survey maps presented in chapter 1, it has become generally accepted that the the universe contains a vast, lacunary structure. Naturally, a number of issues arise when the accuracy of the survey maps that display such structure is questioned. For example, visual bias on the part of the observer (chapter 1) and errors induced by the inability of a survey to pick out non-luminous or too distant matter, or errors that exist as a result of observational techniques (see chapter 2) may affect the accuracy with which redshift maps represent real structure in the universe. Attempts at mathematically modelling these effects are also reviewed in chapter 2. Redshift distributions contain more than spatial information however, and potential inaccuracies are further exacerbated by the fact that there is a wide range of *galaxy properties*. This fact is the source of so-called *segregation effects*. However it is argued that the lacunae (more commonly called *voids*) which are evident in redshift surveys that make *use of all available redshifts*, agree with features evident in controlled surveys (ie. surveys for which galaxies are selected subject to some sort of observational criterion). In addition, voids are able to "hide" in the cosmic microwave background. Thus even though the largest structures found in redshift surveys (superclusters) tend to be as large as the extents of the surveys, it is conceivable that one way of fitting a homogeneous and isotropic Friedmann model to the real universe is by assuming that voids are in fact the structural units of the Friedmann model.

The question of examining redshift data for possible interconnections between voids has prompted the discovery of a striking *two-dimensional sheet* of galaxies—the main topic of this thesis. In chapter 2 the southern catalogues from which the data has been drawn are discussed. In fact the use of all available redshifts allows a detailed examination of *large volumes of the 3-d distribution* to be made. Computer software called COELIS has been especially developed for the purpose of providing a number of data manipulation and graphics tools for studying the 3-d distribution and, in particular, flat (ie. 2-d) sub-sets of the real data. A description of COELIS' functions is the subject of chapter 3 (the code is included in an appendix). In chapter 4‡, the discovery of a remarkably planar redshift feature is presented; some 6.5 h^{-1} Mpc thick and approximately 20×20 h^{-2} Mpc^2 wide, at the interface between the southern voids of Sculptor and Eridanus—termed the *Wall*. The planar nature of such a feature allows for 2-d statistical methods to test for significantly under-dense regions (in effect *void interconnections*). There is no evidence for clustering in the Wall (which is highly diffuse) and no evidence for significant under-densities. In fact the distribution of redshifts in the Wall appears to be quite random. A preliminary examination of other void interfaces is inconclusive; it reveals a mixture of apparent interconnections and walls.

When available galaxy-property information is used to derive galaxy-property gradients perpendicular to planar features it is possible to obtain a list of likely formation histories for the feature under study, and hence obtain some idea of the formation events that gave rise to the surrounding voids. This is the subject of chapter 5 . The general implications of finding non-uniform distributions of properties across diffuse redshift features are discussed in terms of the *postulate of uniform thermal histories*. One advantage of studying low density features (such as the Wall) is that if non-uniform property distributions exist (as indicated by segregation effects) then it may be argued that the formation of the features predates galaxy formation, that is, proto-galaxies "know" about their eventual environment. This is the case for the Wall, for which segregation effects are presented in some detail. Thereafter a comparison with generally accepted models of large-structure formation is presented. The existence of the Wall appears to be consistent with two models: cosmic strings in a HDM model, or a class of explosion scenarios with a hybrid HDM/CDM model. Thus not only do segregation effects support the existence of the Wall as a real entity in the data but the list of indicated cosmogonies, for voids in the region of the Wall, is shortened considerably.

‡ The results discussed in chapter 4 have already been published (Maurellis *et al.* 1990),

Acknowledgements

The enjoyment and pleasure obtained from working in a field of such current interest, under people who have been as enthusiastic as I have been new at it, can never be satisfactorily communicated on paper. For many of the seminal ideas, and the enthusiasm that I needed to create COELIS, and to complete this project the credit must go to Professor George Ellis. For directing me to the idea of "casement displays" and for much leading by the statistical hand I thank Professor D.R. Matravers. For keeping me involved in large-scale structure since undergraduate days, for encouraging me in the friendliest of ways, and for teaching me (together with Prof Ellis) the significance of the comma in written English, a deep appreciation must be extended to Professor Anthony Fairall.

For technical assistance in the early stages of computing I thank Peter Martinez, while the criticisms and opinions aired in discussion with Sèan Ardren on the near-final draft of this work proved instructive. I am grateful to the Department for allowing me to print this work on their HPlaserjet II, for letting me use their version of LaTeXand for allowing me to sound off on parts of the research in this thesis at seminars and colloquia. A number of people personally contributed small but essential bits to my understanding throughout the period of this research and I must mention them: Dr Edmund Bertschinger (MIT), Dr Ruth Smart (Applied Maths, UCT), Dr McNeil, Prof Zucchini, and Gerard Farmar (all three from Math Stats, UCT), Robert Ritchie (Theoretical Physics, UCT), Guinevere Kauffmann (Astronomy, UCT).

Finally, I must mention the support and inspiration of my close friends and family over what has been a very trying period for all of us: my friends Max Volpi, Sèan Ardren, and Hillie Fast, my parents Nick and Amalia-Helen Mavrellis, my grandmother Erasmia Plomaritis, and our dear old friend Lehlohonolo Mokoena. With long-suffering patience these fine people have conveyed to me love and encouragement, faith in my choice of career and delicious Greek cakes (special thanks to my family) in ample measure.

Contents

List of Figures

Chapter 1

Structure in the Universe

"For a thinking man, ... pitfalls of misinterpreted phenomena seem to be a much lesser threat than considering the phenomena as non-real"

(Rudnicki 1989, on the morphological approach of Fritz Zwicky)

1.1 Introduction

Man has always occupied himself with finding the extents of his surroundings; witness terrestrial and maritime voyages of discovery and, more recently, space exploration. On the other hand, ancient cosmologies incorporate many mechanisms for explaining the role that the skies play in the life and history of Man, and vice versa. For example, there have always been those who wish to explain the phenomena of day-to-day life according to patterns in the heavens—the astrologers. Perhaps this exemplifies a desire in Man to assign patterns to or categorise phenomena around him. Certainly the constellations are an excellent example of this need to find structure at the largest scales—in ancient times, the dome of the heavens.

More recently, with the nature of stars fairly well understood, the existence of cloud-like nebulae (Hubble 1936) (which we now know to be galaxies) within or just outside our immediate stellar neighbourhood proved a problem not completely solved when Einstein formulated his general relativity. When homogeneous, isotropic world models were proposed it was far from certain that our surroundings were homogeneous and isotropic (the stellar neighbourhood can be seen to be quite lumpy as well as directionally biased from a cursory glance at the night sky). As a result of the many observations (especially those of the microwave background) that have been made since the 1930's the universe appears to be more homogeneous today than it was thought to be in Einstein's time. It is also interesting

to note the use of the word "world" in astronomy papers[1], rather than the currently more popular term "universe", up until about 1930.

Astronomers are presently in the position where they understand not only the nature of stars but also how stars congregate, certainly in our galaxy. They have some idea of how galaxies congregate but almost no standard model of why this is so. And while the existence of features made up of galaxies (galaxy clusters) is readily accepted, there is usually little more than speculation on the existence of structure at the next level up: features called superclusters in which clustering of galaxy *clusters* occurs[2]. At present, the quest for structure at the largest scales is at a point where the largest detectable features are only slightly smaller than the limits of the surveys (eg. the Sculptor Wall of da Costa *et al.* 1988, the Great Wall of Geller & Huchra 1989 and the Cetus Wall of Fairall *et al.* 1990). The implication is that these features may form part of an even larger feature.

1.1.1 Current maps of the Universe

The spatial distribution of galaxies, inferred by positional information (in the sky) and the Hubble redshift relation is what will be termed *large-scale structure*[3] from now on. One interpretation of the observations is that large-scale structure is *lacunary* (Einasto *et al.* 1983, Fairall 1984), ie. this structure is apparently foam-like or cellular, like aqueous foams (Aubert *et al.* 1986). Much of what follows attempts to support this interpretation.

The distance to a galaxy is obtained from a measurement of its recession velocity (under the assumption of universal expansion) as follows. Recession velocity v is determined by an examination of the Doppler shifting of the spectrum of the galaxy, usually into the red. The fractional shift in wavelength of a spectral line from a rest wavelength λ_0 to its observed wavelength λ_1 is usually termed the *redshift* z, ie.

$$z = \frac{(\lambda_1 - \lambda_0)}{\lambda_0}.$$

Recession velocity and luminosity distance d are proportionally related in the linear form[4]

[1] For a survey of the relevant papers see *The expanding universe: A history of cosmology from 1917-1960*, Ellis (1988).

[2] Fairall (1989a), among others, speculates further that superclusters identified in the southern sky may be grouped into supercluster complexes.

[3] As van de Weygaert & Icke (1989) point out, the largest scale of observations should be the scale on which the global structure of the universe becomes evident. Thus what is commonly known as large-scale structure should really be called middle-scale structure. This is not the convention adopted in this thesis, however.

[4] This is the result of considering only the first-order term in the Taylor expansion of the full relativistic luminosity-distance relation (Rowan-Robinson 1977)—sufficient at the scale of observations discussed in this thesis—in which case redshift also satisfies $z \approx v/c$.

of the Hubble relation (Hubble 1929) onto which may be added an additional term $v_{\rm pec}$:

$$v = Hd + v_{\rm pec} \ . \tag{1.1}$$

This additional term may be used to model *peculiar velocities*—velocities which galaxies may possess that are independent of universal expansion and may arise out of dynamical effects (such as hidden masses (Dressler *et al.* 1987) or turn-around velocities of bound clusters (Saslaw 1985)). In the case of low-density regions, such as will be studied in this thesis, $v_{\rm pec}$ may be (arguably) set to zero to yield a fair measure of distance: if v is measured in units of km s^{-1}, and the Hubble parameter (at the present) $H = 100h$ ($h \approx 0.5$–1) is expressed in units of km s^{-1} Mpc^{-1}, then d has units of megaparsecs.

Although the limit of observational astronomy (a quasar) is at $z = 4.73$ (Irwin & McMahon 1990), which is about 10 000 h^{-1} Mpc, and deep redshift surveys of galaxies have gone as far out as 2 000 h^{-1} Mpc (Broadhurst *et al.* 1990), the discussion in this thesis will seldom focus on galaxies further out than 100 h^{-1} Mpc. It may be argued that in so limiting the distance we are constructing samples of the universe which may not be "fair" (Peebles 1973). While this is a valid criticism, it must also be understood that, in practice, one is also constrained by whatever redshift information is available. Then it becomes important to know what principles lie behind the specific choice of galaxy redshifts in the compilation of the survey under study. As Kirshner *et al.* (1987) rightly point out, galaxies in redshift surveys are correlated, ie. have been selected because they share some attribute in common (for example, they could be brighter than a certain minimum intensity or larger than a certain image size, or simply be positioned near each other in the sky). This issue will be discussed in the next chapter along with a discussion of the sources of observational uncertainty. In addition, more fundamental errors may arise in our interpretation of galaxy redshift as an accurate distance indicator. In other words, the assumption $v_{\rm pec} = 0$ may break down (especially in the case of individual galaxies in bound clusters) and any interpretation must be carefully modified to take this into account.

1.1.2 The existence of structure

Assigning constellations to mythical figures is one example of finding structure in the cosmos. It involves finding a pattern (a constellation) in a distribution of points (stars). This pattern is then associated with a process (a mythical figure) for some reason, say, in the study of astrology. Thus a spatial pattern may be used to answer various questions in an astrologer's mind. The study of large-scale structure up until now has been very much the same in principle, albeit more sophisticated[5]. But is the structure really there? In other words, is it there waiting to be found, or is it projected onto the data because of the way in which human neural synapses function?

[5]The first serious analysis of large-scale structure—the Lick Survey as analysed by Peebles, Groth and Soneira (1969) mirrors, in so far as motivation is concerned, the ancient study of the constellations, in that 2-d maps of the sky (sans redshifts, that is) were used.

Figure 1.1: Sufficient examination of this picture should reveal an image of a dalmation sniffing amongst some leaves. Unfortunately, once the image has been "recognised" it becomes very difficult to look for alternative images in the picture. Is this why the paradigm of lacunary (ie. cellular) large-scale structure is still used today?

Bhavsar and Barrow (1983) jokingly speculate on the existence of the 3-d distribution of galaxies as a large-scale Rorschach test[6] for astronomers. The picture in figure 1.1 refers: does one perceive a dalmation sniffing amongst leaves or merely a number of dots and lines scattered on a flat surface. Bhavsar and Barrow would argue that it is a natural tendency of the human mind to perceive an image in any set of discrete visual entities (such as points or lines) given sufficient visual exposure. Furthermore while the dalmation may not be immediately obvious, with enough concentration sufficient mental interpolation will occur for the image to form in the observer's mind. In fact it may require a great deal of mental effort to observe anything different in the picture once the image is "recognised".

This is a caveat for anyone involved in some sort of pattern recognition. In the early part of the century Percival Lowell fell into this trap: he "discovered" waterways or canals on Mars by interpreting variations in the visual intensity of the Martian surface as surface features, and interpolating where necessary (Hoyt 1976). In the case of the three-dimensional distribution of galaxies all we have is a large collection of points which are often studied using 2-d slices or projections. The tendency is always there, when viewing a spatial pattern, to either fill in the area between the dots and "discover" sheets, or alternately "discover" filaments surrounding large, empty holes by joining up the dots in a piecewise, linear fashion.

[6]Commonly known as the ink-blot test, this test is used as a projective method of psychological testing resulting in a description of the testee's personality.

One approach is to assume that the structure that is perceived is an objective reality of some sort. Because galaxies in redshift surveys are selected using criteria of which the limitations are not always fully understood (see chapter 2), the structure in redshift surveys may not fairly represent the universe as a whole. For instance, redshift surveys must contain, at best, only the most visible material in the universe. Even if there may be some substantial dark matter component to the universe, the fact remains that the perceived structure in *surveys*, whether or not it really exists, represents some puzzling aspect of the nature of the *visible* universe. If such structure really exists, and if it cannot be explained away by random or observational effects (such as inadequate sampling of the available data), then it is probable that some *real* property of the universe has been uncovered—perhaps even some property which warrants further investigation.

The next section gives a brief overview of those aspects of large-scale structure, relevant to the present study, that appeared in the literature up to about 1986. Important work in more contemporary papers will be reviewed in the next chapter. The discussion will concentrate, in particular, on what is termed *sub-structure*: visual entities that appear, in the data, as filamentary, void-like, or sheet-like features, or perhaps as part of a supercluster.

1.2 Large-scale structure today

The present epoch of Man's study of large-scale structure began with a monumental work of observational astronomy: the Zwicky *et al. Catalogue of Galaxies and Clusters of Galaxies* published between 1961 and 1968. This was complemented by the Lick observatory galaxy counts of Shane & Wirtanen (1967) who also published all-sky maps of northern galaxy fields. These maps, with positional information on about 10^6 galaxies, revealed filamentary sub-structure if subjected to a cursory visual scan. Barrow & Bhavsar (1987) point out, however, that exponential scales of shade gradation—instead of the usual log-log or log-linear used in the Lick maps—reveal, *to the human eye*, the presence of clumps in the Lick maps rather than filaments! Once again we see the difficulties that arise during visual interpretation of point patterns.

Perhaps with the filamentary sub-structure in mind, Oort (1970), Zel'dovic (1970) and Icke (1973) made the first predictions of highly anisotropic structures in the universe. These have to be classed as little more than speculations, because the 3-d nature of the large-scale distribution of galaxies was far from evident—few redshifts had yet been measured. Peebles and others used the wealth of positional data, however, to develop, over a number of years, the two-point angular correlation functions. This mathematical tool yields the amount of clustering of structure in the Lick maps at different length scales (this early work is well surveyed at the semi-popular level in Groth *et al.* 1977). First attempts to explain the formation of the structure in the Lick maps in terms of correlation function results are Soneira & Peebles (1978), and Peebles (1980)—a milestone work in which the mathematics

of general correlation functions is developed.

By 1978 redshift surveys had improved to the point where Chincarini (1978) could speculate on the existence of voids in the 3-d distribution. The existence of lacunary structure in the universe was initially proposed by Jôeveer & Einasto (1978) at an IAU meeting and later discussed in detail by Einasto *et al.* (1980b). Many of the current themes in the study of large-scale structure can be traced back to this paper which cites the volume around a rich cluster in the constellations of Perseus and Pisces as a candidate for lacunary sub-structure. In discussing the cluster region the authors provide good comments on what can be generally inferred from observations.

Other convincing evidence of superclustering and under-dense regions can be found in the work of Gregory & Thompson (1978) and Davis *et al.* (1981). The existence of large voids was further recognised when Kirshner *et al.* (1981) presented evidence for a large void in Boötes. The evidence was based on a large gap found *between* fields in a non-contiguous survey. More compelling arguments (Kirshner *et al.* 1987—to be discussed in the next chapter) along with newer data confirm their 1981 prediction.

Since 1981, the study of large-scale structure has developed quite vigorously, in that observational discoveries have closely followed on important theoretical developments and vice versa. Ostriker & Cowie (1981), and Ikeuchi (1981) were the first to propose the existence of early-universe explosions as a mechanism for triggering galaxy formation. Until then, the best candidates for formation of large-scale structure had been the *hierarchical clustering model* of Peebles and Dicke (1968) (so called "bottom-up" scenarios because matter clusters on the smallest (sub-galactic) scales, before clustering into galaxies, then galaxy clusters and superclusters, and perhaps even larger structures) and the Zel'dovic *pancake formation* scenarios (summarised in a survey paper by Zel'dovic *et al.* (1982), also known as "top-down" scenarios).

Oort (1983), Matsuda & Shima (1983), Winkler (1983), Fairall (1984b), Fairall *et al.* (1985), de Lapparent *et al.* (1986) and Haynes & Giovanelli (1986) were among the first to identify void and filamentary sub-structure in their surveys. At the same time, the significance of another kind of sub-structure became clear. A filamentary feature on a survey map, if it is sharply defined and chiefly radial in extent, may be modelled in terms of large peculiar velocities, superposed on the Hubble flow. These large peculiar velocities may arise simply from the dynamics of galaxy motion taking place in a dense, bound cluster. The effect is that of a "Finger of God" feature on the survey map—so called because the feature seems to point, perhaps reprovingly, in our direction!

The existence of non-radial filamentary sub-structure was also considered[7]: Chincarini

[7]Filamentary and void sub-structure do not preclude each other as voids may be separated by sheets of filaments.(de Lapparent *et al.* 1986).

(1983), Einasto *et al.* (1983). An off-shoot of the search for filaments was a series of techniques developed to identify significant spatial clustering in the 3-d distribution. Among these are the percolation (or "friend-of-a-friend") methods of Bhavsar & Barrow (1987), and the cluster analysis techniques of Zel'dovic *et al.* (1982), Bhavsar (1984) and Einasto *et al.* (1984).

A comparison of the results of theoretical models with broad features of the real data has been an important feature of the work done on large-scale structures since 1985. The most commonly used tool of comparison has been the two-point *spatial* correlation function of Davis & Peebles (1983). For instance, it has been used to compare the results of numerical simulations of particles under non-linear, gravitational clustering with other simulations and other models of structure formation (Davis *et al.* 1985, Fry *et al.* 1985). Another form of comparison has been one of simply comparing sizes of voids obtained from the data (for eg. the published size of the void in Boötes—see Kirshner *et al.* 1981) with the sizes of voids obtained in numerical simulations (eg. Bertschinger 1985) and n-body simulations (eg. Saarinen *et al.* 1987).

Various studies have attempted to find sufficiently quantitative measures (based on topological measures) of large-scale structure. In particular, Gott *et al.* (1986) and collaborators in successive papers, and Einasto *et al.* (1984) and later collaborators determine the connectedness of regions of different density in the observed data. The technique is to compare the results obtained from the observed data either with analytic functions predicted by theory or with similar measures of connectedness for sets of simulated data, evolved from different sets of initial pertubations. This approach will be discussed in the next section.

1.3 Redshift surveys

The term *survey* will be used, in this thesis, to represent the redshifts and positional information used to plot a map of part of the large-scale distribution. The map is nearly always presented in 2-d projection, apart from the case of stereo plots. A number of surveys of the large-scale distribution of galaxies, both in the northern and southern hemispheres, have been conducted since 1979 (Okamura 1989). The following recent papers have, in particular, high-lighted void, wall and filamentary sub-structure: de Lapparent *et al.* (1986), Kirshner *et al.* (1987), Haynes & Giovanelli (1986), da Costa *et al.* (1988, 1989), Geller & Huchra (1989), Fairall *et al.* (1990). Plots from most of these surveys will now be presented, in order to show the sub-structure that is high-lighted in each paper.

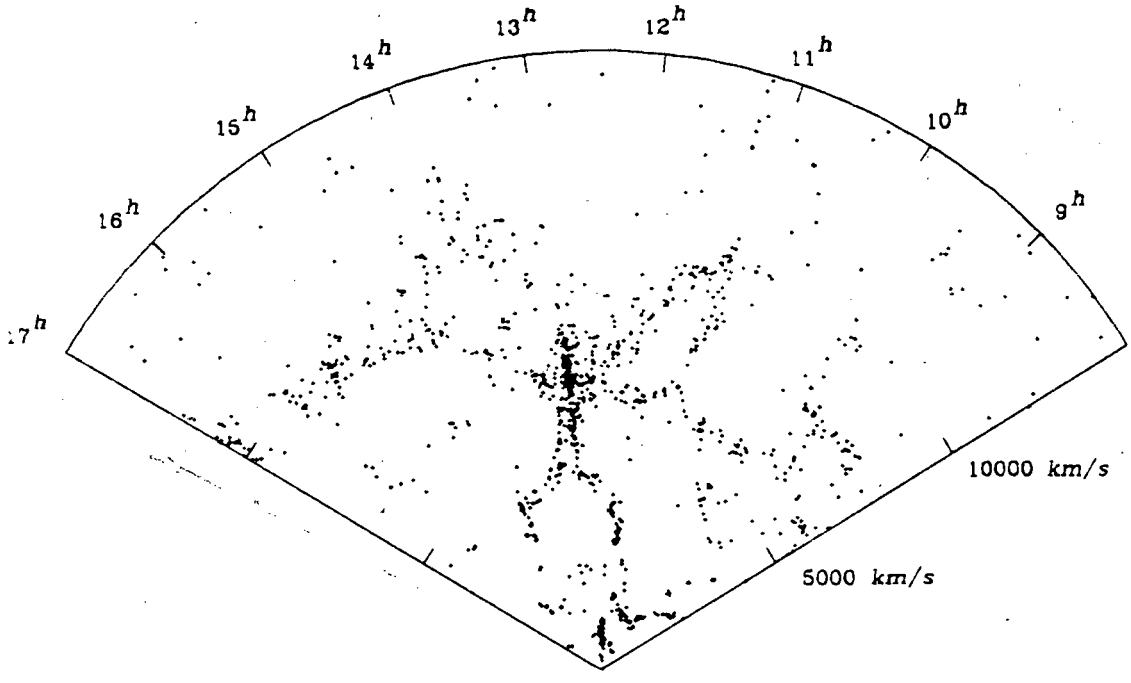

Figure 1.2: Redshifts from a thin strip across the northern sky in the declination wedge $26°.5 \leq \delta \leq 32°.5$. The survey contains 1061 objects satisfying $m_B \leq 15.5$. (Taken directly from de Lapparent *et al.* 1986)

1.3.1 The CfA survey extensions

As the result of an extension to the Centre for Astrophysics survey of Huchra *et al.* (1982), de Lapparent *et al.* (1986) compiled the redshifts of 1100 galaxies in a region which covers a 6° × 117° strip on the sky. This yielded the highly publicised wedge diagram of figure 1.2. In the centre of the diagram, a clear example of a Finger-of-God feature may be found—the so-called Coma cluster. More importantly, voids are identified (on either side of the cluster) as regions of density less than 20% the mean density of the survey. Void diameters range from 14–50 h^{-1} Mpc. Where void boundaries are not part of the Coma cluster (ie. the boundary is formed by field, rather than cluster, galaxies—see chapter 2) the thickness of the boundaries appears to be of the order of a few h^{-1} Mpc. The presence of a filament[8] across the diagram of length $\sim$150 h^{-1} Mpc (passing through the Coma cluster) was detected using a filament-finding algorithm. The term "cellular" is used to describe the overall visual impression, although the authors make the point that the largest structure in the survey (the filament) is comparable with the sample depth.

This sample is considered by the authors to be complete, in a magnitude-limited sense[9], up to $15^m.5$, by the authors. (The magnitudes are taken from Zwicky *et al.* catalogue (1961–68) for which there may be a scatter of up to $\pm$0.4 magnitudes, (Fairall, private communication 1990, also Davis & Huchra 1982). Means of effecting statistical analyses of samples like this one (eg. statistical analyses of de Lapparent *et al.* 1986, 1989) will be briefly reviewed in the next chapter, in the sections devoted to a description of the luminosity and two-point spatial correlation functions. Some discussion of a morphological study (Huchra *et al.* 1990) of the region, including a galactic latitude extension, will also be left to the next chapter.

1.3.2 Pisces-Perseus

The Pisces-Perseus region of the sky was initially investigated by Einasto *et al.* (1980) (as discussed in the introduction). It lies, almost, in the opposite direction in the sky to the Coma cluster and has been surveyed using 21cm HI-emission line observations (Haynes & Giovanelli 1986 and references therein). The survey is not magnitude complete but is once more useful in identifying voids around a rich cluster. The survey also serves as a complement to the morphological studies of Giovanelli *et al.* (1986) to be discussed later.

The nearly 3 000 galaxies in this survey lie in a 50° × 90° strip, predominantly at a

[8]Geller & Huchra (1989) present evidence in favour of this filament being a cross-section through the Great Wall mentioned earlier.

[9]The issue of completeness, and data controls, is one that will be discussed later. However it should become clear, by the time the issue has been discussed, that a survey *without* strict adherence to magnitude (or other) controls can still play a very useful role. See chapter 2 for a fuller discussion of the issues involved.

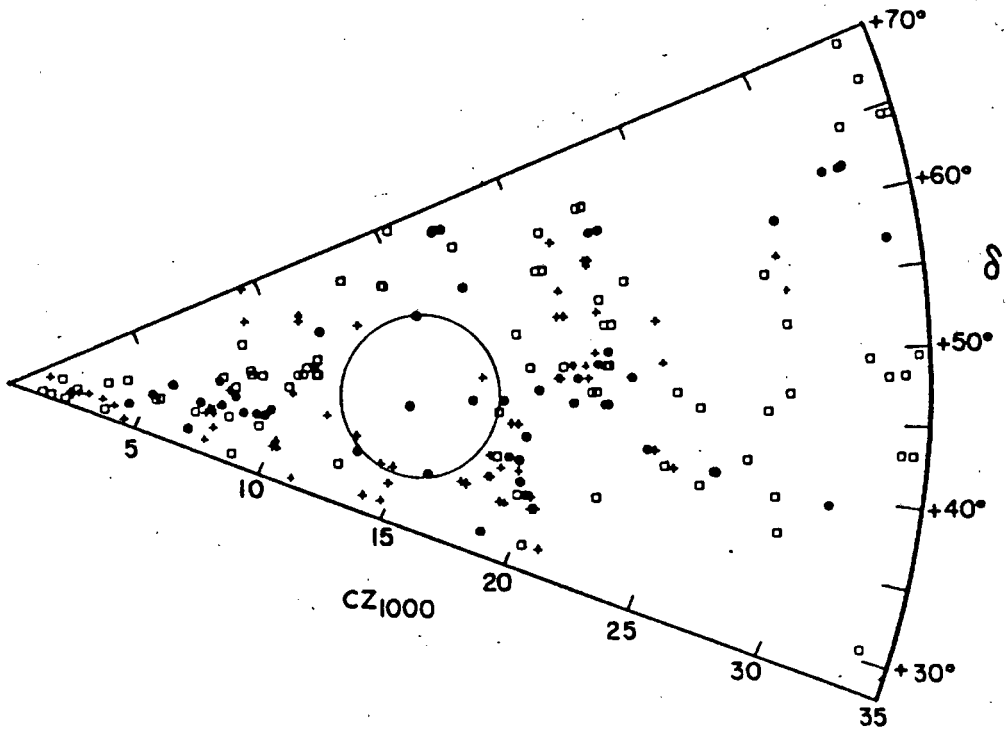

Figure 1.4: The large circle in this redshift map represent a section through the largest empty sphere that fits inside the Boötes void as determined by Kirshner *et al.* (1987). Galaxies with $\alpha > 15^h10'$ are denoted by filled circles; open circles correspond to $14^h20' < \alpha \leq 15^h10'$; pluses to $\alpha \leq 14^h20'$.

into account the selection effects of the survey. The two approaches differ in the kind of smoothing used; Gott *et al.* convolve the discrete distribution with a Gaussian smoothing function (this will be discussed later), whereas Pellegrini *et al.* use a hatbox smoothing function.

Using a similar threshold density criterion for a void ($\rho_{\rm void} < 0.25 < \bar{\rho} >$) as de Lapparent *et al.* (1986) and Kirshner *et al.* (1987), Pellegrini *et al.* find evidence for at least four significant voids in their sample, with volumes ranging from 10^2 to 10^5 h^{-3} Mpc^3 (this corresponds to diameters of 10 to 60 h^{-1} Mpc). Because the smoothing process effectively increases the size of the high-density regions these estimates are probably low, and thus consistent with the Boötes void.

An extension to the da Costa *et al.* (1988) survey, by da Costa *et al.* (1989), allowed an effectively magnitude-complete (to 15.0 in a comparable magnitude system[12] to that of de Lapparent *et al.*, 1986) sample, covering $\approx 135° \times 10°$, to be constructed. The galaxies in this sample are restricted to those of early type and so are not ideal for use in morphology studies.

In particular, da Costa *et al.* (1989) quote the dimensions of a void, with 20% density contrast, as $\sim 60h^{-1}$ by $40h^{-1}$ Mpc (depth by transverse length on wedge diagram—see figure 1.6). This may be construed as further evidence that voids of the dimensions of Boötes are not uncommon (Postman *et al.* 1986 and Kauffmann 1990). The nature of the boundary[13] of this large southern void has been studied in some detail (Maurellis *et al.* 1990) and this will be discussed in chapters four and five. da Costa *et al.* (1989) point out that it does not appear to be a spherical volume, because evidence for sharp corners can be found in the (fairly well-defined) boundary. Finally, sub-structure, in the form of a long filament of length $100h^{-1}$ Mpc, at about 9 000 km s^{-1}, may be discerned.

1.3.5 An all-encompassing view of the universe

Fairall *et al.* (1990) present plots through-out the sky of redshifts obtained from a combination of the updated *Catalogue of Radial Velocities of Galaxies* (Palumbo, Vettolani, Fairall and Baiesi-Pillastrini, to appear) and the *Southern Redshift Catalogue* (Fairall & Jones, 1988); nearly 22 000 redshifts. All available data appear on the survey maps—there are no controls applied to the data. Probably the most interesting result of this approach is that it yields the same qualitative features as, for example, the magnitude-controlled survey, of de Lapparent *et al.* (1986) discussed above. The sub-structure featured in figure 1.2 appears remarkably similar to that in figure 1.7. However the two samples are independent; that is,

[12] These magnitudes were obtained mostly from the Laubert (1982) photometric catalogue—at that stage the only magnitude source that could compare to the Zwicky catalogue in the north.

[13] A term that still needs to be satisfactorily defined—see chapter 2.

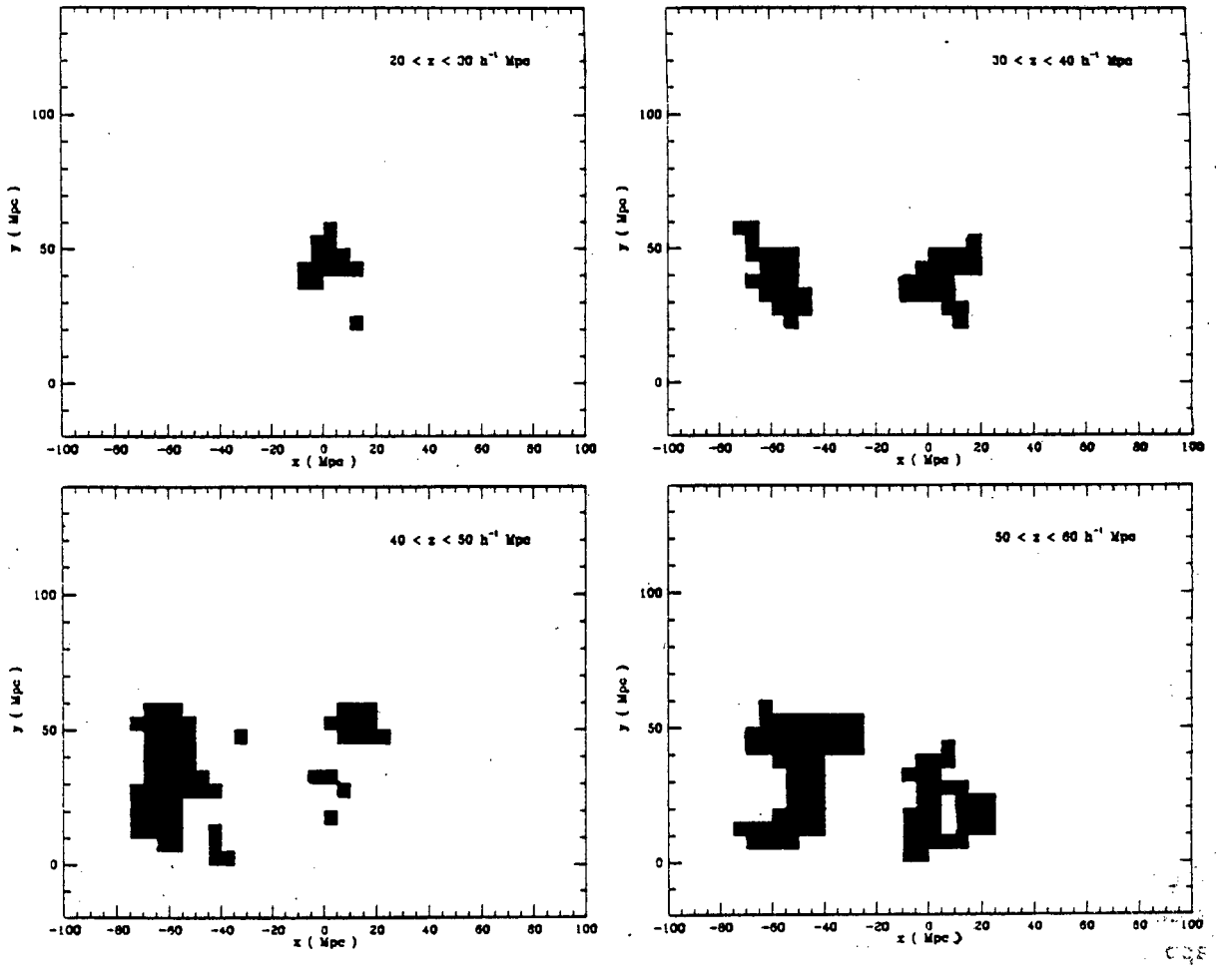

Figure 1.5: The empty cells contained by two large southern voids (diagram from Pellegrini *et al.* 1989) are viewed here in cross-section. Slice thickness and vertical coordinate are displayed in the top right-hand corner of each view. Note that the voids shown form two connected structures (at the zero density level).

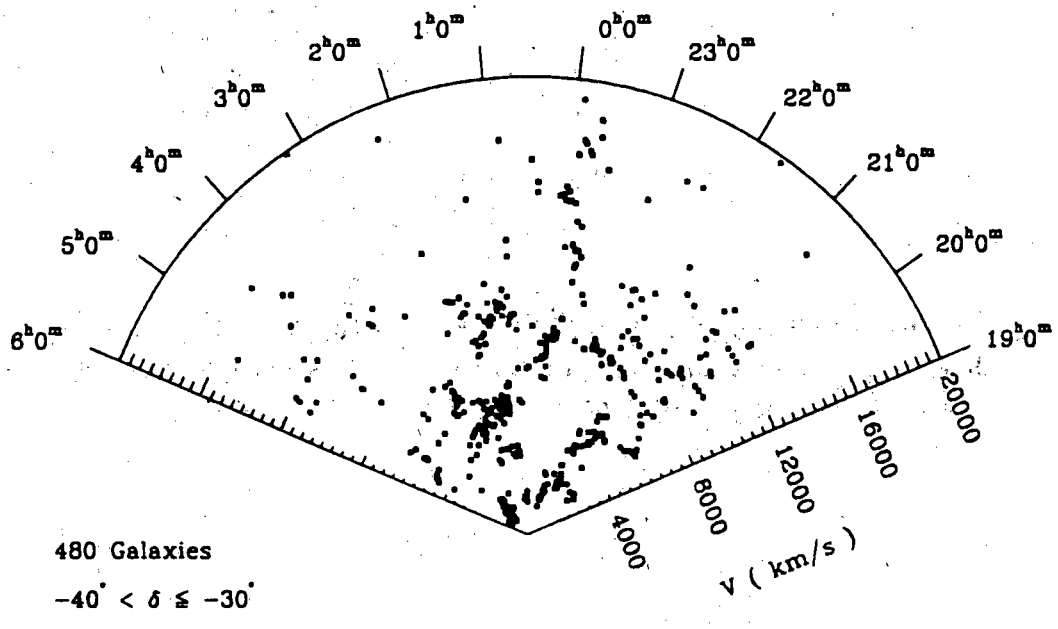

Figure 1.6: This map contains redshifts from the SSRS extension (mostly of early type) in a declination-ascension range as shown. Notice the large, well-defined void with centre at at approximately 6 000 km s^{-1}, $\alpha = 23^h20'$. (Diagram from da Costa *et al.* 1989).

1.4 Aims and modus operandi

Simple, intuitive questions or arguments may successfully form the basis for some discussion of issues in the study of large-scale structure. For example, the well-known explosion model may be easy to compare to the real distribution, as the following illustrates. After explosions occurred in the early universe, it is proposed (Ostriker and Cowie, 1981) that large, empty regions were swept clean by the expanding shock waves, the process yielding voids. One question is then if explosions occurred, can remnants of these explosions be observed today (Ellis *et al.*, 1988)?

The above is an example of the *morphological approach* of Zwicky (see Rudnicki 1988, and references therein to Zwicky)—an investigative style in which perceptions are penetrated to the core, by questions which attack the very basis of the perceptions. Since the appearance of any issue in question is constrained by one's perceptions of the question, the approach is aptly named morphological[14]. In this thesis the morphological approach will be applied to

- the recognition of sheet-like sub-structure in southern redshift maps, in order to establish
- the existence of such sub-structure (ie. how "real" it is) by independent, non-visual methods

Even though cell-like structure has not been established conclusively, it is widely accepted. Perhaps this means that voids constitute the fundamental sub-structure in the universe, rather than the filaments or walls, which appear to have formed on larger scales only because of the way in which adjacent voids are packed. If the existence of voids can be accepted, then it will be shown (chapters 4 and 5) that the investigation of void *boundaries* may be useful in setting the limits on void formation, especially if parts of the boundaries are so flat as to be sheet-like.

[14] Please note that this usage of the term "morphological" is not to be confused with a study of the morphological properties of galaxies—a topic which we will discuss later. In both cases, however, the Greek root refers: "$Μορφή$" can be translated as "shape" or "appearance".

Chapter 2

Structure in redshift surveys

"I remember his insisting very especially ... upon the idea that the principle source of error in all human investigations lay in the liability of the understanding to underrate or overvalue the importance of an object, through mere admeasurement of its propinquity."

(from "The Sphinx" by Edgar Allan Poe)

An important limitation on the usefulness of redshift surveys and catalogues is the extent to which they accurately represent the real matter distribution. The information in the redshift maps presented so far is at least three times removed from the actual matter distribution. In other words, there are four sets of potential data, between which one may construct "mappings", in a pseudo-mathematical sense:

All matter $\longrightarrow$ All luminous matter $\longrightarrow$ All visible matter $\longrightarrow$ Redshift survey

It is the aim of this chapter to present a brief discussion of the issues involved (see sections 2.1–2.4) in these mappings, and hence in the use of redshift catalogues. The mappings are briefly discussed below, as an introduction to the main body of the chapter which contains a more detailed discussion of the issues involved.

A broad aim of this thesis is to suggest that catalogues which consist primarily of a photometric database may be effectively combined with the large amount of positional information that redshift catalogues have to offer, especially for the purposes of studying the segregation effects[1] of diffuse structures. Such a combination of catalogues (Lauberts & Valentijn 1989 and Fairall & Jones 1988) is presented in section 2.5, and has contributed to the results presented in later chapters.

[1] See section 2.4 for a definition of this term.

Luminous and non-luminous matter

The issue in connection with the first mapping is how well the luminous matter distribution traces the total matter distribution. The existence of dark matter, needed to explain spiral galaxy rotation curves (Rubin *et al.*, 1985) or to raise the universal mass-fraction parameter Ω from the observed value of $\Omega_{obs} = 0.2$ to the critical value of $\Omega = 1$, is an issue that has important consequences for large-scale structure formation (Dekel 1987, Rees 1987). Evidence in favour of a one-one mapping *for galaxies* is that voids seem to be empty of both low surface-brightness galaxies as well as the more commonly observed high surface-brightness galaxies[2] (Bothun *et al.* 1986, Oemler 1987 and Rood 1988).

Another way to address the above issue is to deduce upper limits, for the sizes of regions devoid of *all matter*, that are still consistent with the isotropy of the microwave background radiation. If voids in the visible distribution are larger, then there may be a significant dark matter component to the real matter distribution, or alternately, the choice of universe model is inadequate (see section 2.1).

Visible vs. luminous matter

The distinction between luminous and visible matter, in the second mapping, arises out of the problem of source detectability. Even though a source may be luminous, because it lies at great distances from an observer it may not necessarily be visible to the observer. The drop in light intensity, which occurs in observations of distant objects, is a simple yet crucial constraint on the results derived from the observations. Furthermore, galaxies of different morphology may have different luminosities, and thus the selection effects in a redshift survey, if not properly understood, may contribute to errors in studies of the spatial distribution of different morphological types. This issue is discussed in some detail in section 2.2.

Redshift surveys

The final mapping is simply the process of observing redshifts. However this data may be subjected to a further abstraction by a process which indicates the presence of significant sub-structure in the survey. Visual identification of void sub-structure is an example of such a process. In addition, if the effects of the first two mappings can be successfully modelled then the following measures of structure (see section 2.3) can be used on the survey data: the

[2]However, this is not to be confused with the fact that not all luminous matter clusters in the same way. For example, elliptical and lenticular galaxies are more likely to be found in dense clusters than spiral galaxies, which dominate field populations. This issue will be discussed in section 2.4.

two-point correlation function, the void probability function, and the topology of constant density surfaces. Two other methods for determining significant filamentary sub-structure in surveys are: variations (by numerous authors) of the percolation algorithms[3] of Einasto *et al.* (1980); and the minimal spanning tree of Bhavsar & Ling (1988a,b). These methods are not discussed in this thesis as they are of little use in detecting void sub-structure.

An additional problem with the interpretation of structure in redshift surveys is that they contain filamentary or sheet-like features which appear so only because they are "viewed" in redshift, or velocity space rather than in position, or physical space. For instance, dense clusters present as a filamentary Finger-of-God effects in redshift maps while physically separated but co-moving galaxies may present as a sheet-like feature. Attempts to infer the peculiar velocities of galaxies at the surfaces of voids (ie. in the low-density case) in the southern sky, with simple dynamical arguments, have been only partially successful (Matravers & Maurellis 1990). Although these results are consistent with calculations of bound cluster rms velocities of ~ 400 km s^{-1} (Davis & Peebles 1983) it is my intention to use the problem of understanding peculiar velocities of galaxies in low-density regions as the focus for a later study.

2.1 Compatibility with the Friedmann model

As the limits of detection have developed, so too has the common understanding of what constitutes a fundamental observer in the well-understood and well-tried, homogeneous and isotropic universe model of Friedmann, Lemaitre, Robertson and Walker (Friedmann 1922, Robertson 1935, Walker 1936). This is one aspect of the *fitting problem*—the problem of relating the observed "lumpy" universe to the Friedmann model (Ellis 1987). Originally, the "nebulae" (Hubble 1936) (later called galaxies) were perceived as the basic building blocks of the universe. However, if a lacunary structure is regarded as the fundamental structure of the universe, then, if the universe started with a uniform distribution of matter, the radii of today's voids would be the minimum distances required to move points in order to arrive at the the observed inhomogeneous distribution. One of the aims of this thesis is thus to explore the distribution of galaxies, in and around void boundaries, in order to investigate the formation histories of the voids on either side of the boundaries.

One aspect of general observations that is extremely consistent with the Friedmann model is the existence of the 2.7 K cosmic microwave background radiation. Zel'dovic *et al.* (1982) present the following heuristic argument. The microwave background has been measured to be isotropic down to $|\delta T/T| \sim 10^{-5}$ at the 95% confidence level (Vittorio 1988). This

[3]The algorithms are also known as cluster analysis algorithms, or "friends-of-friends" algorithms. Having fixed a parameter called the *neighbourhood radius* to a certain value, chains of galaxies each within a neighbourhood radius of each other may be constructed. A similar procedure is used in chapter 5 to find the clustering of galaxy properties in galaxy property space, rather than clustering in galaxy position space.

indicates very small density fluctuations at the epoch of decoupling of radiation and matter ($z \simeq 1300$) and is consistent with a very homogeneous and isotropic early universe. Now, in an expanding universe, the diameter of voids (expressed in redshift units as Δz) remains approximately constant. It is doubtful that the largest voids, observed at the present epoch, exceed a diameter of 150 h^{-1} Mpc, which corresponds to $\Delta z \simeq 0.05$. If, as expected by any scenario in which galaxies are driven towards the boundaries, cellular structure sets in at $z = 3$–10 (consistent with the cut-off of recently discovered quasar redshifts at $z \simeq 4.4$) then void dimensions, in comparison with the universe as a whole, are still small. Thus if voids are the largest structural units in the universe then there is no need for a revision of two of the fundamental principles of observational cosmology—the homogeneity and isotropy requirements of the Friedmann model—at the scales of void dimensions (even with void volumes as large as the Boötes void $\sim 10^6\, h^{-3}$ Mpc^3).

Shaver *et al.* (1988) find some evidence for smaller void structures at $z \simeq 4$ (as a result of considering line-of-sight statistics through a Voronoi foam of clouds of Lyα absorbers). This result is not inconsistent with the work of Ostriker *et al.* (1988) who find that large voids (of radius 30 h^{-1} Mpc or greater, ie. $\Delta z \geq 0.01$), at $z \simeq 4$, fill less than 15% of the universe. More detailed calculations of the contribution of voids to measurable anisotropies in the microwave background have been attempted than the one presented here—see Nath & Eichler (1989) and references therein—but the details remains essentially outside the scope of this thesis.

Thus it seems as if current limits on the microwave background isotropy cannot be used to test the true emptiness of voids. The issue of deciding whether or not voids are really empty is important, because an expanding Friedmann model, with (empty) voids as the fundamental constituents, would provide a useful model of structure at the largest scales that is consistent with current observations.

2.2 The reliability of redshift surveys

2.2.1 Selection criteria and completeness

As mentioned earlier, the objects in a redshift survey may not constitute an adequate representation of luminous matter in the universe because of the way in which the detectability of a source is affected by attributes of the source, eg. the brightness of the source, or the source size; not to mention the effect that the distance of a source has on its detectability. Thus any conclusions based on a redshift survey may be dependent on the manner in which the galaxies have been selected for the survey. If galaxies have been excluded on the basis of selection criteria decided in advance then any results derived from the survey may suffer from *selection effects*. Commonly-used selection criteria arise either from excluding

galaxies fainter than a certain magnitude or from excluding those smaller than a certain diameter. A survey in which no galaxy that satisfies the selection criteria is missed is said to be *complete*. Therefore surveys in which galaxies are missed because selection effects are not properly understood, may be termed *incomplete*. For instance, galaxies may be missed because of insufficient sky coverage, or by not going deep enough (ie. because of the effects of distance on detectable luminosity).

Conversely, a catalogue which has well-understood selection criteria, that have been systematically applied, may be called *complete*, however severe the selection criteria are. A good example of this is to be found in the procedure adopted by Kirshner *et al.* (1987) to infer the existence of the Boötes void. The redshifts are actually quite strongly correlated because they lie in 283 non-contiguous fields, which are quite distant from each other. Thus it is impossible to draw any conclusions about the existence of the void without taking into account the nature of redshift selection (see chapter one for a brief discussion of their approach).

A good reason for the use of a controlled survey is that a *selection function*—a function which models the way in which galaxies have been included in the survey—may be analytically constructed (although the discussion in section 2.2.2 also refers) or calculated from the data (see section 2.3.3) depending on the degree to which the data is understood. For example, magnitude-controlled surveys may be understood in terms of a *luminosity function* $\phi(L)$ which satisfies

$$\phi(L)\,dL \;=\; \phi^{*}\left(\frac{L}{L^{*}}\right)^{\alpha}\exp\left(-\frac{L}{L^{*}}\right)\,d\left(\frac{L}{L^{*}}\right) \tag{2.1}$$

which was derived (Schechter 1976) from a theoretical analysis of self-similar gravitational condensation in the early universe. The term $\phi(L)\,dL$ is the density of galaxies in the luminosity interval $[L, L+dL]$, and L^{*} and α are constants which depend on the selection effects of the surveys under study. In physical terms, α is the power-law slope for $\phi(L)$ when L is small, while L^{*} can be described as the "break" or "knee" of the luminosity function, where the slope of $\phi(L)$ changes very rapidly (Dickey 1988). In fact, L^{*} is the luminosity below which the survey becomes potentially unreliable, and corresponds to the magnitude limit.

Although the Schechter luminosity function is analytically tractable, it does not give an adequate fit to the observed luminosity distribution (Davis & Huchra 1982). One of the reasons for this is the effect known as *Malmquist bias*: in a magnitude-limited sample, the average (absolute) luminosity of the nearby members of the sample is lower than the average luminosity of the more distant members (Sandage 1987). The result is that any magnitude-limited survey will have an insufficient number of low-luminosity galaxies at higher redshift (see figure 2.1). The consequences of this for studies of the relationship between galaxy morphology and luminosity will be explored in section 2.4.

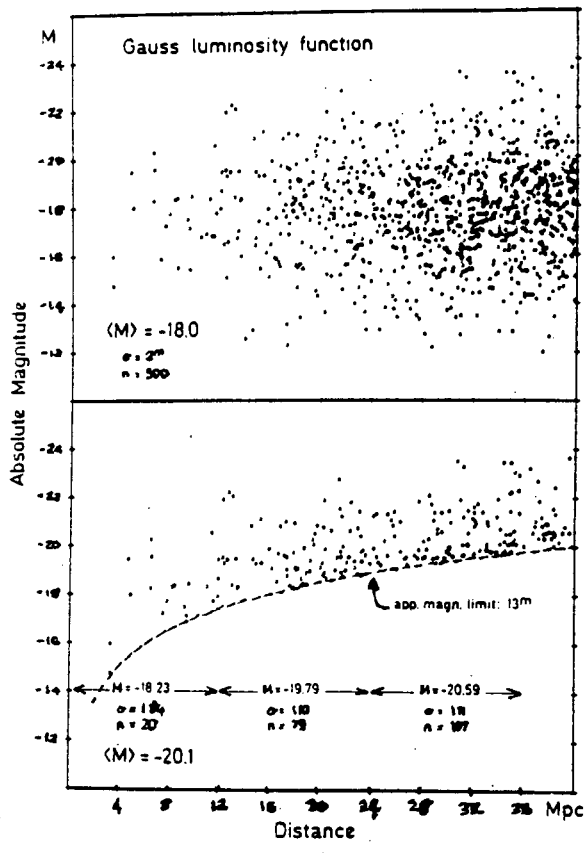

Figure 2.1: A hypothetical catalogue of galaxies of mean absolute magnitude -18, distributed in Gaussian fashion with an intrinsic dispersion of two magnitudes, is displayed in the top panel. A survey drawn from this catalogue, subject to an apparent magnitude limit of 13, will include, at best, only those galaxies above the dashed line in the lower panel. This is the Malmquist bias effect, viz. the average luminosity of an observed sample increases with increasing distance. (Diagram from Sandage 1987).

A selection function, simply in terms of fractional loss of galaxies as a function of distance (Davis & Huchra 1982), may be estimated for surveys without magnitude-control information. This is the case in the work of Pellegrini *et al.* (1989) and Kauffmann (1990). In both cases the procedure is to calculate the Davis & Huchra selection function and then to generate a random catalogue with the same overall density variation and which satisfies the same selection function as the catalogue under study.

2.2.2 Problems with selection criteria

Diameter- or magnitude-controlled surveys need not be the only kind of surveys in current use. This is because surveys that decide on the exclusion of galaxies on the basis of some selection criterion that is easily modelled mathematically may not prove the most efficient. In this connection, Ellis *et al.* (1984), have shown that valid selection criteria depend critically on the intrinsic surface brightness *and* point spread function of each source. Although this topic is not pursued any further in this thesis the implication is that the usefulness of one-parameter selection criteria is highly suspect. Thus the use of *all* available redshifts, as a kind of inclusion criterion, should not be lightly dismissed (see also section 2.5).

2.3 Measures of structure

If all of the above observational constraints are taken into account, can one be sure that the void structure in the above surveys is real? One approach is to determine whether or not the voids have a frequency which cannot be explained simply by random selection effects. Starting at a more simple level, the level of clustering may be determined (see section 2.3.1). This process may be generalised to the probability of finding empty regions of arbitrary shape (see section 2.3.2), and then nearly cubic voids (see section 2.3.3). In addition, the issue of connectedness of voids may be investigated (see section 2.3.4).

2.3.1 Correlation functions

Peebles (1980), in a study of the effects of hierarchical clustering, defines the correlation function $\xi(r)$ for a continuous density function $\rho(\vec{r})$ (with a mean $\bar{\rho} =< \rho(\vec{r}) >$) by

$$1 + \xi(r) = \frac{<\rho(\vec{x})\,\rho(\vec{x}+\vec{r})>}{\bar{\rho}^2} \qquad (2.2)$$

where the average is over $\vec{x}$ in a volume V, and over $\vec{r}$; also $|\vec{r}| = r$. In astronomical terms, the term *hierarchical clustering* describes a scenario in which seeds of galaxy-sized clumps

of matter ($\sim 10^{12} M_\odot$) gravitationally attract more and more matter until clumps of cluster mass, then supercluster mass ($\sim 10^{16} M_\odot$) form.

The power spectrum of initial seeds is often taken to be Gaussian so that kth-order density pertubations of magnitude δ_k satisfy (Baardeen *et al.* 1986)

$$<|\delta_k|^2> \propto k^n. \tag{2.3}$$

In this case Peebles (1974) has shown that the correlation function asymptotically approaches the power law

$$\xi(r) = \left(\frac{r}{r_0}\right)^{-\gamma} \tag{2.4}$$

where r_0 is the so-called correlation length (see below for a description of this constant) so that in the linear regime[4] ($\xi \ll 1$)

$$\gamma = 3 + n \tag{2.5}$$

and in the non-linear regime, assuming a hierarchy of clustering

$$\gamma = \frac{9 + 3n}{5 + n}\ . \tag{2.6}$$

For example, $\gamma = 1.8$ would indicate $n = 0$ ie. random noise and the subsequent absence of clustering on small scales. From real data the correlation function can be calculated using the integral definition

$$1 + \xi(r) = \frac{N_p(r, \Delta r)}{\frac{1}{2} n \bar{V}(r, \Delta r)} \tag{2.7}$$

where $N_p(r, \Delta r)$ is the number of pairs with separations in the interval $(r - \frac{1}{2}\Delta r, r + \frac{1}{2}\Delta r)$ inside a sphere of fixed comoving radius. The denominator corresponds to the number of pairs in a Poisson distribution of N particles inside the same spherical volume, n is the mean number density in the volume and $\bar{V}(r, \Delta r)$ is an edge effect correction term for the Poisson pair count. Dekel & Aarseth (1984) use equation (2.7) to compare to the shape of $\xi(r)$ obtained using equation (2.4) (ie. determined theoretically for hierarchical scenarios) and conclude that hierarchical clustering is not sufficient to explain observed large-scale structure. A note on the broad features of the correlation function is useful at this point. Consider a simple form of the correlation function especially suited to computational purposes—that of Davis & Peebles (1983)

$$1 + \xi(r) = \frac{N_{dd}}{N_{dr}} \tag{2.8}$$

where N_{dd} is twice the number of independent pairs of galaxies with separation r in the real data, and N_{dr} is the number of pairs of galaxies separated by r, the first drawn from the real data and the second drawn from a random distribution of data with the same volume, average density and selection effects.

The relationship to clustering is as follows:

[4] That is, at a pre-clustering epoch, when motion is purely due to linear (Hubble) expansion and gravitational effects have not come into play.

$\xi > 0$ corresponds to the presence of clustering in the data

$\xi < 0$ corresponds to signs of dispersed structure in the data, the very opposite of clustering

$\xi = 0$ gives a value $r = r_0$ called the *correlation length* of the data which corresponds to random, ie. uncorrelated data.

Peebles (1980) finds the correlation length to be approximately 5 h^{-1} Mpc for the Lick data. Davis & Peebles (1983) obtain $r_0 = 5.4 \pm 0.3\ h^{-1}$ Mpc for the early CfA survey of Huchra (1982).

Although its use has pervaded study in large scale structure since its inception (Peebles 1980) its use on galaxy catalogues (in particular the CfA survey 1985) has recently come under attack. Coleman *et al.* (1988) find no evidence for the existence of a correlation length of $r_0 \approx 5\ h^{-1}$ Mpc. Instead they claim the existence of a fractal structure extending up to about 20 h^{-1} Mpc.

2.3.2 Void probability function

Although the correlation function exists as a simple and rigorous means of comparing theory with observations, it is unable to infer the existence of void or other sub-structure. Aarseth & Dekel (1984) find that the correlation function is only mildly sensitive to the existence of structures such as sheets, filaments, or voids. One answer is to move to higher order generalisations of the two-point correlation function (as a void is essentially an n-point correlation where $n \gg 2$) but these methods rapidly become mathematically intractable (although work is progressing in this area; see Szalay 1990, and references therein). An alternate technique is the *void probability function* (VPF) of White (1979), Schaeffer (1984), Fry (1985) and Maurogordato & Lachièze-Rey (1987)

$$P_0(V) = \exp\left[\sum_{i=1}^{\infty} \frac{(-n)^i}{i!} \int_V \cdots \int \xi_i \, dV_1 \ldots dV_i\right] \tag{2.9}$$

which gives the probability that a volume V, placed randomly in a point distribution of galaxies, is empty (expressed in terms of correlation functions of all order ξ_n). A Poisson distribution with number density n (of voids, in this case), for example, has $\xi_1 = n$ and no other correlations. Thus,

$$P_0 = \exp(-nV)\ . \tag{2.10}$$

is the probability (over all space) that a volume V placed in a Poisson distribution of point galaxies will be empty. For a Gaussian distribution, only the one- and two-point correlations are non-zero, so

$$P_0 = \exp(-nV + \frac{1}{2}n^2V^2 <\xi>) \tag{2.11}$$

$$\text{where } <\xi> \equiv \frac{1}{V_1V_2} \int \int \xi_2 \, dV_1' dV_2'\ .$$

Note that ξ_2 is nothing more than the two-point correlation function $\xi(r)$ defined earlier. One of the advantages of this approach is that if the scale variables n and V for a particular survey are related then different samples drawn from the same survey could be compared for similar clustering properties (even if the scales of the samples differ). If the samples exhibit similar clustering properties then the structure in the survey is said to obey a scaling-law. In hierarchically clustered universes, whether or not the probability that a volume placed at random is void of galaxies and obeys a scaling-law in properly chosen variables (Fry 1988 and references therein) is a subject of ongoing investigation.

2.3.3 Void spectra

Of more use than the measure of void sub-structure, which the void probability function offers, is the void-search algorithm of Kauffmann (1990). This generates a spectrum of void sizes by searching for completely empty, approximately cubic, regions in a survey. Although the results are weakly biased by the orientation of the data[5], the selection effects of an observed survey, once understood, can be applied to a randomly generated survey. A comparison of the two surveys can thus give a list of *real* voids (ie. significant under-densities), and hence a distribution of void sizes. The voids thus found are real in the sense that their existence is not consistent, at a confidence level of about 85%, with the null hypothesis that they are the result of random selection effects in the real data.

2.3.4 Smoothed density functions

The work of Gott *et al.* (1989) (and references therein) shows the advantages of working with a smooth, continuous density function for the 3-d distribution of points in a survey. Once the point-distribution is convolved (taking selection effects into account) with a Guassian smoothing function of the form $\exp(-\frac{r^2}{\lambda^2})$, then surfaces of constant density may be constructed. Each surface will have a specific genus, which corresponds to the amount of connectedness it allows (ie. number of holes it contains). Thus the distribution may be viewed at various *contour threshold densities* ν (see figure 2.2).

A further use for this approach is the *genus-threshold density function* $G_s(\nu)$ of Hamilton *et al.* (1986). For the special case of an initial Gaussian power spectrum (see equation (2.3), this has the form

$$G_s \propto (1-\nu^2)\exp\left(-\frac{\nu^2}{2}\right) , \qquad (2.12)$$

[5]This is because a cube is a very poor approximation to some void volumes which are far more successfully fitted by highly eccentric ellipsoidal surfaces, eg. Maurellis & Matravers 1991 (in preparation).

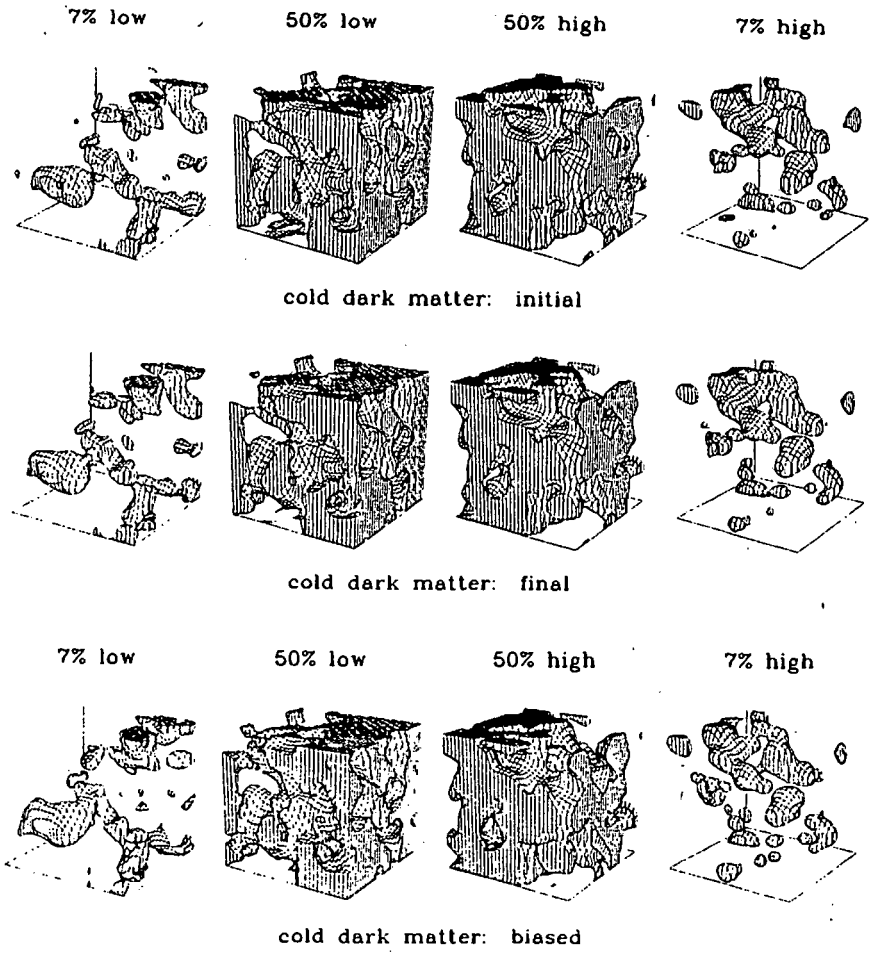

Figure 2.2: Surfaces of constant density are shown here as density contours, for the initial conditions ($z = 25$), the final conditions (the present epoch) and the final biased (see section 5.3.2) conditions of a standard cold dark matter model ($\Omega = 1$). The cubes shown have a co-moving side length of 256 h^{-1} Mpc evaluated at the present epoch. Data sets are smoothed with periodic boundary conditions ($\lambda = 20h^{-1}$ Mpc). The labels 'low' and 'high' refer to the density contained within the shaded region in each cubic representation. Note the sponge-like nature of the 50% threshold surfaces, as well as the apparent similarity of the three simulations, which is indicative of fluctuations that have left the linear regime by the present epoch and whose topology has remained unchanged since structure set in at $z = 25$. (Diagrams from Gott *et al.* 1987).

where ν is the number of standard deviations by which the contour threshold density departs from the mean density. $G_s(\nu)$ has a 'W'- shape (see figure 2.3) which is independent of the coefficients of the power spectrum. Thus this function can be used to indicate how consistent is the topology of large-scale structure in a redshift survey with hierarchical clustering models. Furthermore it gives an idea of the connectedness of the survey studied. For example, Gott *et al.* (1989) find evidence for so-called sponge and meatball topologies in their data. In simple terms, the genus of the contours, at a threshold density level set to the value of the mean density, decides the topology of the large-scale structure. A *sponge* topology would exist when both high and low density regions are multiply connected. In a *meatball* topology the high density regions are isolated by one simply-connected low density region, while the converse situation corresponds to a *swiss cheese* or *bubble* topology.

Of main importance to this thesis is the issue of void connectedness, ie. the topology of large-scale structure at the level of void boundaries. As discussed in chapter 1, da Costa *et al.* (1989) have used a hatbox smoothing procedure (based on a comparison with a random distribution as a model of the selection effects) to investigate the presence of voids (which they define as zero density regions). If the constraint on the density of the void regions is allowed to be increased in value (to 25% of the mean density), *connections* in low-density plots (see figure 1.5) *between* the voids arise. Thus, in a region made up of mostly low-density features, the term *void boundaries* may be used to describe those features in the survey that have a density greater than some fraction of the mean density.

2.4 Segregation effects

Two useful indicators of galaxy properties are intrinsic luminosity (estimated in terms of absolute magnitude) and morphological type. When either of these properties has a range of significantly different clustering profiles (eg. different correlation functions for different morphological types), the sample from which the galaxies are drawn may be said to exhibit *segregation effects.* In more simple terms, the phrase "segregation effects" may be used to describe any correlation between, on the one hand, position of galaxies in a sample, and on the other, either or both of luminosity and morphological type[6].

In a recent review Mo (1989) discusses the considerable evidence for *luminosity segregation* in studies of rich clusters, in which galaxies with greater luminosity tend to cluster more strongly than galaxies with lower luminosity. On the other hand, Einasto (1989), using a sample of the Virgo supercluster drawn from early versions (1983, 1985) of the unpublished Zcat of Huchra, finds evidence that the spatial distributions of bright and faint galaxies are

[6]It should be noted that recent work in progress on segregation effects (Ferguson & Sandage 1990) has generalised the problem to investigating the dependence of the luminosity and the mix of morphological types, in groups and clusters of galaxies, on properties of the groups such as richness, velocity dispersion, central density, etc.

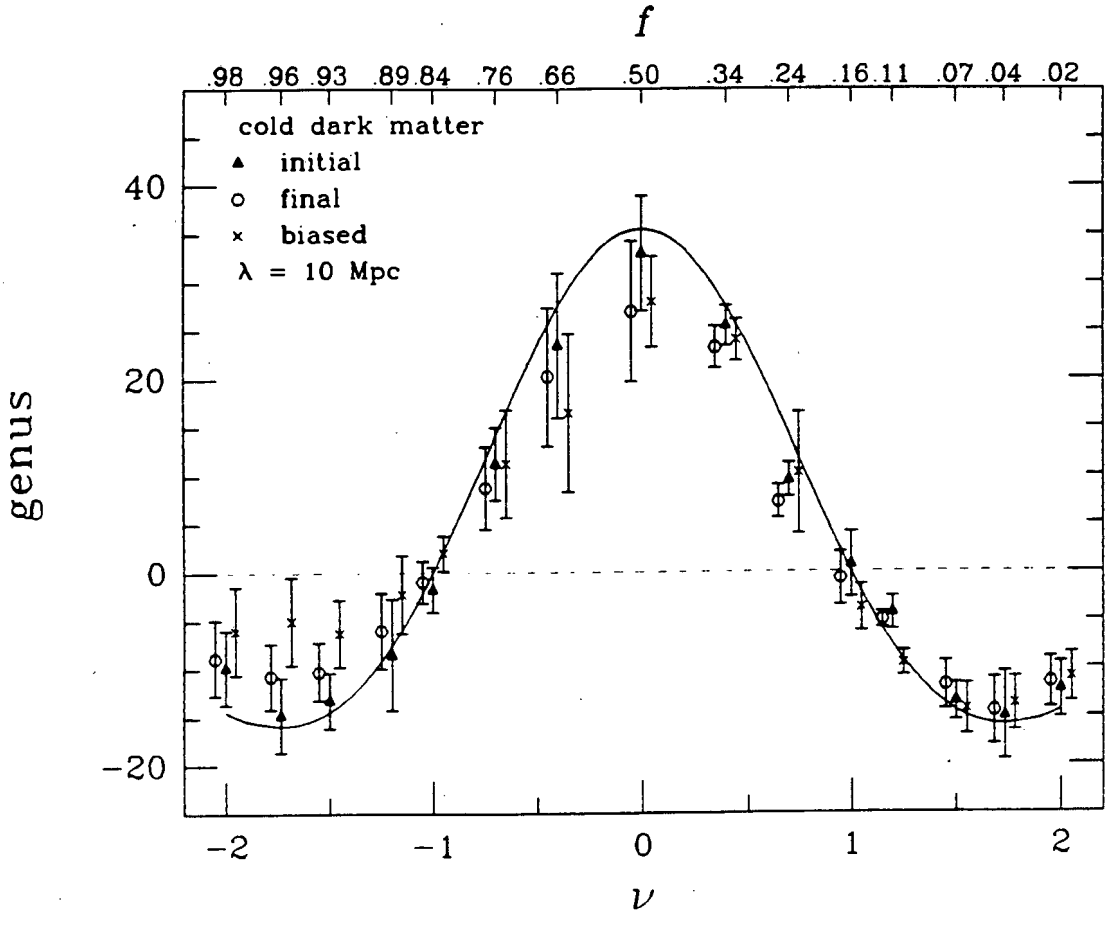

Figure 2.3: The characteristic shape of equation (2.12), in the standard $\Omega = 1$ random-phase model, is drawn as the solid curve in this diagram. Thus the genus, at various threshold densities, of simulations of the type discussed in figure 2.2 (or even of real data), may be compared with the theoretical curve. The 'W'-curve appears quite symmetrical about $\nu = 0$ which indicates both that the simulations have yielded a sponge-like topology and that the simulations are fairly consistent with all models with Gaussian, random-phase fluctuations. (Diagram from Gott *et al.* 1987).

statistically identical down to absolute magnitude -15.0 ($h = 1$), and that only the most giant galaxies are absent in low density regions. However the sample does not include a dominant population of low surface brightness galaxies present in Virgo (Binggeli *et al.* 1985). To this end, the differences between the luminosity functions of dwarf ellipticals (so-called because of their somewhat flat surface brightness profiles) and ordinary ellipticals have been studied, though not completely, by Binggeli (1987).

Morphological segregation may be similarly understood as a correlation of morphological type with position. This has been suggested for some time (Hubble & Humason 1931, Abell 1965, Mo 1989 and references therein). As mentioned earlier, morphological segregation often takes the form of galaxies in low-density regions (so-called *field* galaxies) being predominantly spiral, and galaxies in high-density regions (such as clusters) being predominantly elliptical and lenticular (Davis & Geller 1976 and Dressler 1980, 1984). This situation is often presented in terms of the *morphology-density relations* which are population-fraction functions that vary with density (Postman & Geller 1984—see figure 2.4) from which it is also evident that the number density of galaxies may range in value over six orders of magnitude. It is important to note that at very low densities, where the dynamical time scale is comparable to or greater than the Hubble time, the population fraction will not reflect variations in local density. Thus a catalogue of predominantly field galaxies should exhibit a similar morphological profile to that of low-density features within it. This fact will be used to substantiate a claim of sampling fairness for the low-density feature studied in chapters 4 & 5.

The regions of the Perseus-Pisces cluster and the Coma cluster have been studied by Haynes (1987) and Huchra *et al.* (1990), respectively, for evidence of segregation effects. In both cases ellipticals and lenticulars are more clustered than spirals, and there even appears to be a significant difference in the way in which early- and late-type spirals (see figures 2.5 and 2.6) cluster. However Huchra *et al.* argue that the significant features (such as the Coma cluster) are still visible in maps of only late- or early-type galaxies. Haynes (1987) also finds that higher luminosity objects are more clustered than lower luminosity objects by determining the two-point correlation function for these luminosity classes (see figure 2.7).

If it can be shown that different galaxy types have different luminosity functions, then morphological segregation would imply luminosity segregation (Dickey 1988). This is because varying the population fractions of spiral, elliptical and S0 galaxies varies the contribution of each of their luminosity functions to the overall luminosity function, thus implying that the overall function is a function of position. This is one of a number of issues which revolve around the fact that a description of large-scale structure, solely in terms of positional data, is incomplete without a knowledge of the properties of the galaxies. Therefore the relationship between morphological segregation and luminosity segregation is an important one and fortunately under study (Iovino *et al.* 1990).

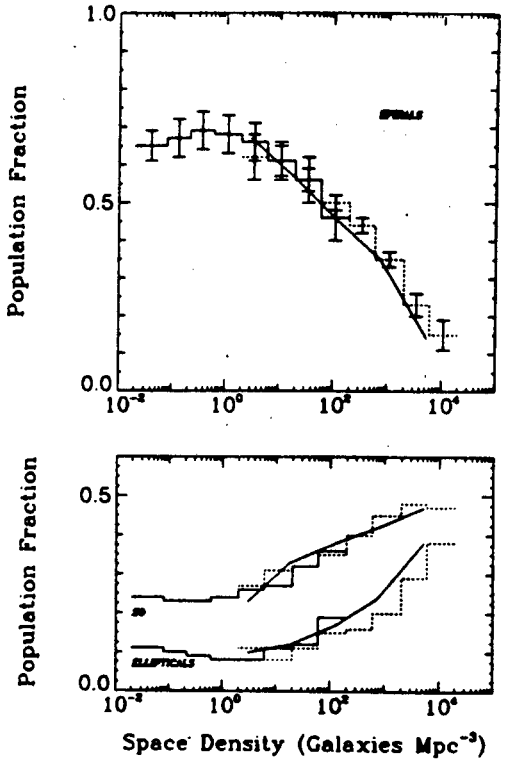

Figure 2.4: The population fraction of morphological types as a function of space density, as determined by Postman & Geller (1984) for groups (solid histogram) and clusters (dashed histogram) of galaxies in the CfA sample. For comparison, the morphology-density relations determined by Dressler (1980) are drawn in as solid curves.

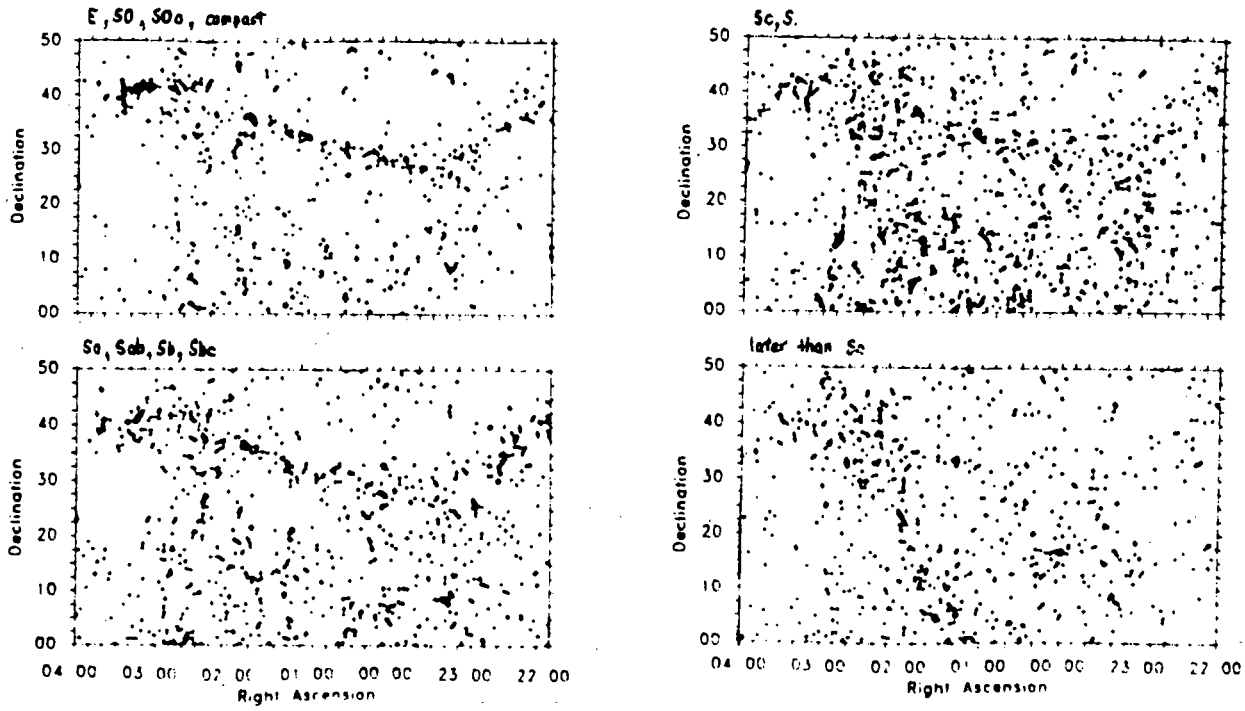

Figure 2.5: Sky distribution of Uppsala Galactic Catalogue galaxies of different morphological classes in the Pisces-Perseus region. (Diagram from Haynes 1987).

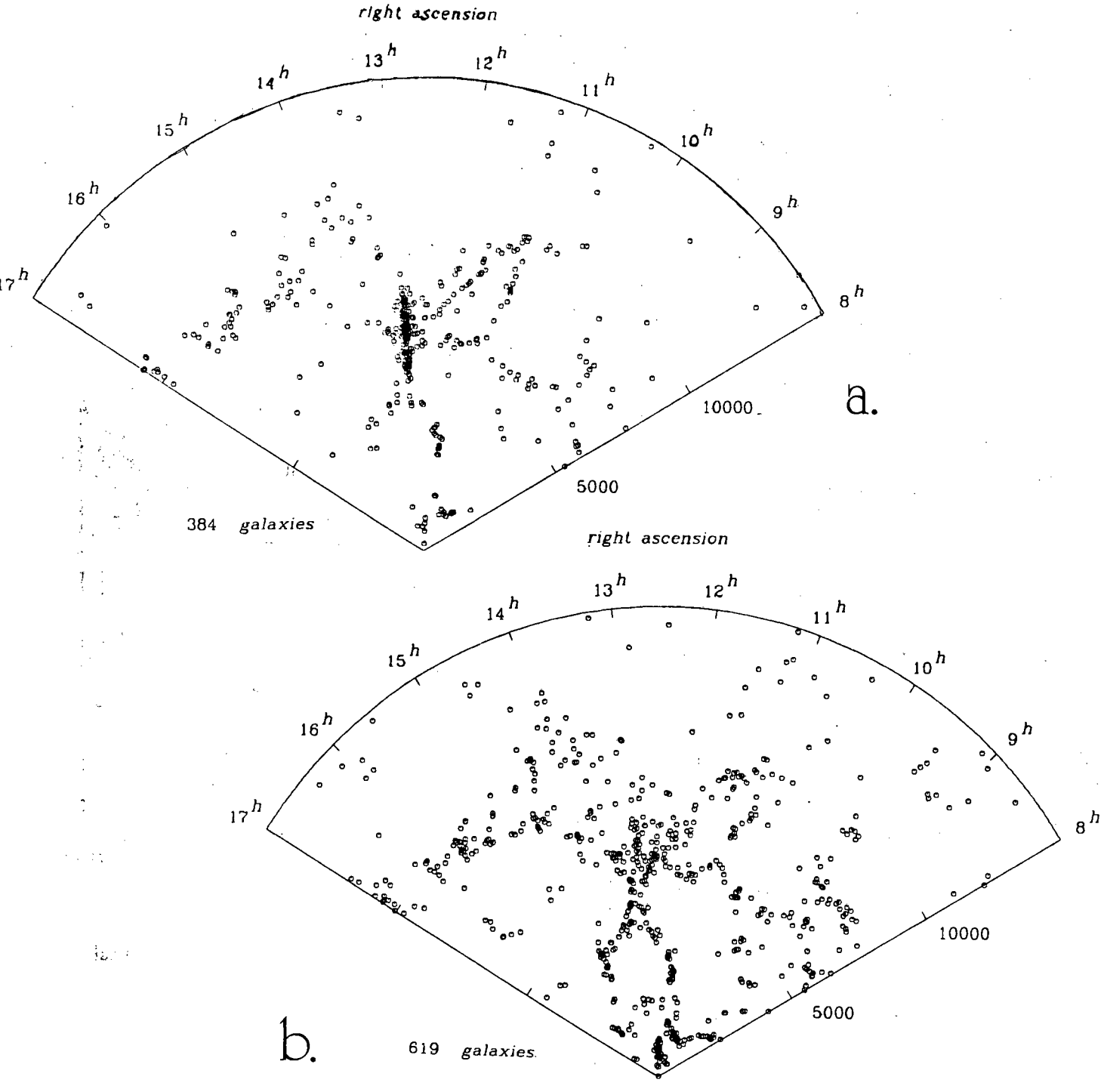

Figure 2.6: Redshift maps of a total of 1058 galaxies in a declination extension ($26.5° \leq \delta \leq 32.5°$) of the CfA survey (Huchra *et al.* 1990). Early-type galaxies are shown in wedge (a), late-type galaxies in wedge (b).

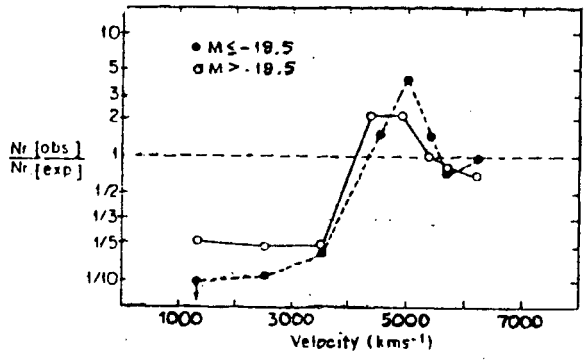

Figure 2.7: Correlation functions for high (solid line) and low (dashed line) luminosity objects in the Perseus-Pisces region. (Diagram from Haynes 1987).

It has been suggested that yet another type of correlation exists; that of position angle with morphology. Djorgowski (1987) reviews the evidence for alignments of galaxy rotation axes with axes of clusters; for example, it appears that ellipticals always tend to align either perpendicular or parallel to the principal axis of the cluster, a phenomenon which cannot easily be explained by selection effects.

2.5 A combination of catalogues

The recent acquisition of data compiled in large and rich catalogues, and the usefulness of uncontrolled surveys in identifying significant structures in the data has prompted the use of data taken from a combination of the following catalogues to obtain the original results discussed in this thesis :

- *The Southern Redshifts Catalogue and Plots* of Fairall & Jones (1988) (hereafter FJ),
- *The Surface Photometry Catalogue of the ESO-Uppsala Galaxies* of Lauberts & Valentijn (1989) (hereafter LV).

The rest of this chapter is devoted to discussing various aspects of these catalogues; survey maps derived from them will be compared and contrasted with some of the results of earlier surveys.

Although LV is a substantial and definitive catalogue, whereas FJ is more of a working database, the two catalogues cover nearly the same survey area: declination[7] south of $-17\frac{1}{2}^{\circ}$.

[7] In 1950 coordinates.

FJ has compiled a catalogue of some 7580 spectroscopic (optical) redshifts, representing some 6214 galaxies up to a range of 75 000 km s^{-1}, from various sources. The aim of this compilation is not only to attempt to produce a collection of *all* available redshifts, but also to provide the most accurate redshift[8] for each galaxy.

In addition to lists of redshift and galaxy positions LV contains a wealth of photometric information. Thus complete diameter-limited, or magnitude-limited sub-samples may be constructed. Furthermore, it contains a number of photometric properties for each galaxy: measures of magnitude (and thus colour), surface brightness, also position angle and morphological type and in a few cases, redshift (often from both HI and optical measurements). In particular the design of this catalogue allows for the study of segregation effects—a feature which we make use of in chapter 5.

2.5.1 Use of catalogues

For a discussion of the sources of error in a photometric catalogue the reader is referred to the excellent introductory chapter of LV. Observational errors in redshift determination may arise in the following manner. Multiple measurements of radial velocities of galaxies suggest that the general error for any single measurement (see FJ) is approximately ±100km s^{-1} although working with higher spectroscopic dispersions may reduce the error to about half of this. This is consistent with da Costa *et al.* (1989) who find that uncertainties in redshift measurements in the CfA and SSRS surveys are less than 40 km s^{-1} (based, as in FJ, on comparisons with various sources). This uncertainty arises simply from the practical difficulties inherent in the process of reducing redshift spectra. Apart from these it is estimated (Fairall 1990, private communication) that at least 1% of spectra are grossly misinterpreted. Thus implicit in any galaxy point on a redshift map is a *radial* error bar, because errors in *position* in the sky are negligible by comparison.

Controls

Although the purely spectroscopic data of FJ does not allow for diameter-limiting or efficient control of magnitudes, the redshift listed for each galaxy is a reflection of a kind of redshift control. Often a number of sources, including additional observations taken by Fairall, are used to determine the redshift of a galaxy because quoted measurement errors are often somewhat optimistic. More precisely, the differences between independent measurements of redshifts are often far larger than the uncertainties quoted by the authors. Thus FJ redshifts are frequently weighted averages and in such cases may offer a more accurate estimate of redshift. In the cases where redshift uncertainties are very large (say $\sim$ 500 km s^{-1}) the

[8]Rather than an opportunity for comparison of redshifts as in Palumbo *et al.* (1989).

catalogue contains relevant warnings in place of redshifts. In other words, use is made of whatever redshifts are available.

In applying her void-search algorithm to a merger of FJ and Zcat[9], Kauffmann (1990) finds evidence for an interesting selection effect. Besides the expected decrease in number of objects surveyed as galactic *latitude* approaches 0° (galactic obscuration) and as *redshifts* get higher, there is a tendency for regions of high ***declination*** (ie. nearer the poles) to be under-sampled. This is related to the whereabouts of observatories (the middle latitudes) and the tendency to point telescopes as close to the overhead direction as possible, to minimise atmospheric obscuration.

LV is a compilation of data from which magnitude- and diameter-limited sub-samples may be drawn. The selection criteria:

1. objects of total magnitude fainter than 14.5 are included ($B_T > 14.5$) in the survey but those brighter than 14.5 appear to constitute a complete sub-sample of the catalogue[10],
2. objects of visual diameter smaller than 1 arcminute are excluded (apart from some interacting systems and compact galaxies below 1 arcminute, of special interest to some observers).

In contrast to FJ, the availability of redshifts has not played an important role in the compilation of the LV catalogue. In fact, there are few redshifts; of the 15 467 galaxies measured, 3 576 of them have redshifts of which roughly 1 600 can be found in FJ as well. LV redshift uncertainties are quoted simply from the literature and do not reflect quite the degree of redshift control to be found in FJ. On the other hand, any redshift survey derived from FJ cannot exhibit the completeness of the LV catalogue which has excellent sky coverage down to galactic latitude −30°, the beginning of galactic obscuration. Out of forty-five plates covering the right ascension-declination range of the data which is used, in this thesis, some six plates are missing (see figure 2.8) from the sky-coverage of the LV catalogue.

A note on control-free surveys

The main advantage of any survey constructed without some formal control is that such a survey can be used to develop a 3-d picture of large-scale structure well in advance of a controlled survey. Because controlled surveys aim at achieving some measure of completeness, only a small area of the sky can be covered at a time. Thus, while it is true that many types of large-scale structure have been posited on the basis of northern surveys

[9]See Fairall *et al.* 1985) for some discussion of this catalogue.

[10]A Malmquist bias trend is evident in a surface brightness-magnitude plot of all galaxies for $B_T > 14.5$.

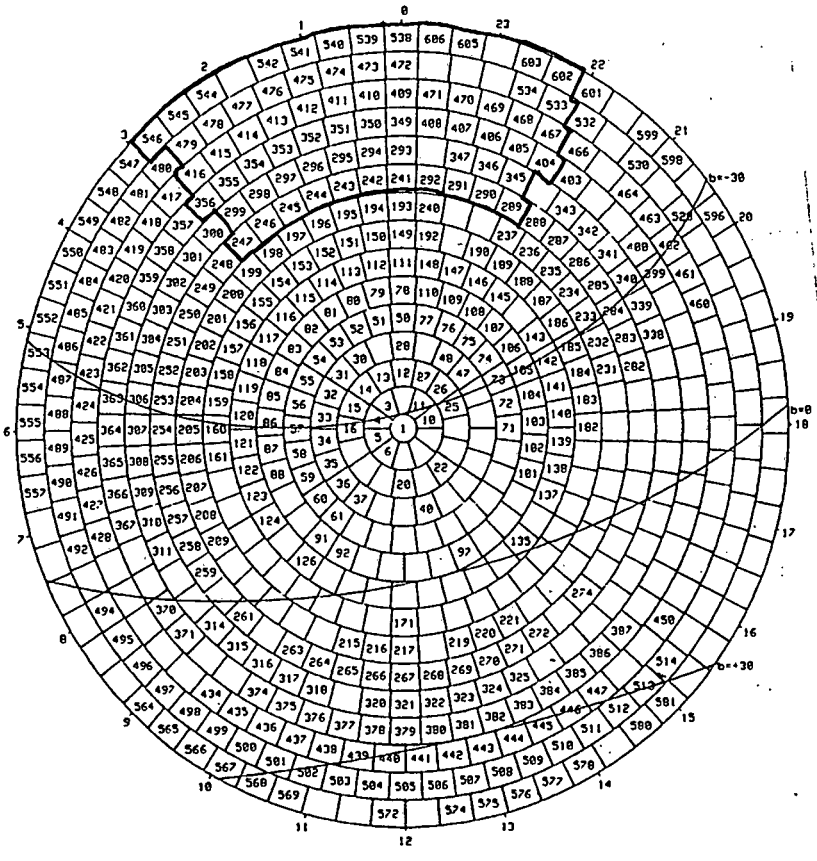

Figure 2.8: The distribution of 407 ESO survey fields in a polar projection (diagram from Lauberts & Valentijn 1989). The south equatorial pole is at the centre while declination $-17.5°$ corresponds to the outermost circle. The plates within the dark solid line contain galaxies found in the Wall region (see chapters 4 and 5) contained in the limits: $2090 \leq cz \leq 5320$, $-57°00' \leq \delta \leq -17°46.8'$, $21^h52'12'' \leq \alpha \leq 02^h52'48''$.

with well-understood controls (for example de Lapparent *et al.* 1986, discussed earlier) the disadvantage with these has been the fact that the data used is taken from a very thin slice through the 3-d distribution, and so very little can initially be said about the nature of the wider distribution. Thus surveys drawn from catalogues which cover a large volume of the sky (such as FJ, or Fairall *et al.* 1990 in which the features that distinguish the "slice of the universe" of de Lapparent *et al.* 1986 are clearly visible), may play a very useful role in understanding the broad features of large-scale structure at an early stage in the study.

Cross-correlation of catalogues

Clearly the paucity of redshifts in a catalogue such as LV makes it difficult to use LV to construct an adequate picture of 3-d structure. However, the fact that it allows a set of galaxies to be drawn from it, complete down to 14.5, means that any study of galaxies in sub-structure found in FJ can be compared in terms of completeness and selection effects to those known for LV galaxies once galaxies common to both catalogues have been cross-correlated. There are bound to be galaxies in LV that are not yet in FJ but a number of galaxies exist in FJ, in the region of interest—see chapter 4 later—that are not found in LV. This indicates that the FJ survey has occasionally gone much fainter. Thus a combination of the two, where appropriate, may yield greater clarity of the structure under study and some measure of completeness. In fact the LV catalogue has the overall distribution of morphological type given in figure 2.9. This is provided for later comparison to a smaller sub-sample of the LV catalogue, originally identified as a feature in FJ, in order to establish some measure of how fairly the data represent the feature. Furthermore, the following conventions will be adopted in future discussion of morphological type of galaxies:

Morph Range	LV Type	Hubble Type
$[-5,-2.5)$	Elliptical	E
$[-2.5,0.5)$	Lenticular	SO
$[0,5,8.5)$	Spiral	Sa–Sc
$[8.5,10)$	Irregular	Irr

where "Morph Range" refers to bounds in the continuous morphological classification scheme used in LV. It should be noted that the concept of a lenticular, or SO galaxy is currently under revision. van den Bergh (1990) suggests that not all SO galaxies are midway between ellipticals and spirals in morphological sequence, but that some are low luminosity, disk-like galaxies of quite unique morphology.

Features of large-scale structure, apparent in the southern sky (or, more accurately, in a survey based on the FJ catalogue) will now be discussed.

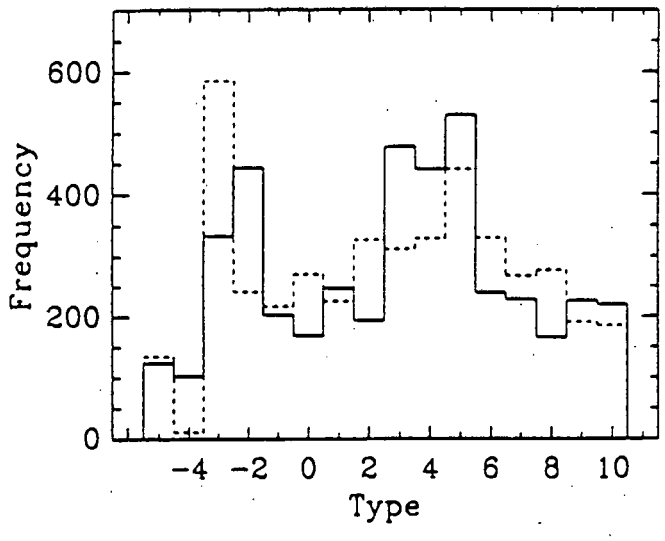

Figure 2.9: Two frequency distributions of morphological types for the same sub-sample of galaxies are shown here: the solid line describes types determined by eye while the dashed line describes automatically determined types. The shapes of both distributions exhibit similar overall trends and are supplied for comparison with that of a sample to be discussed later.

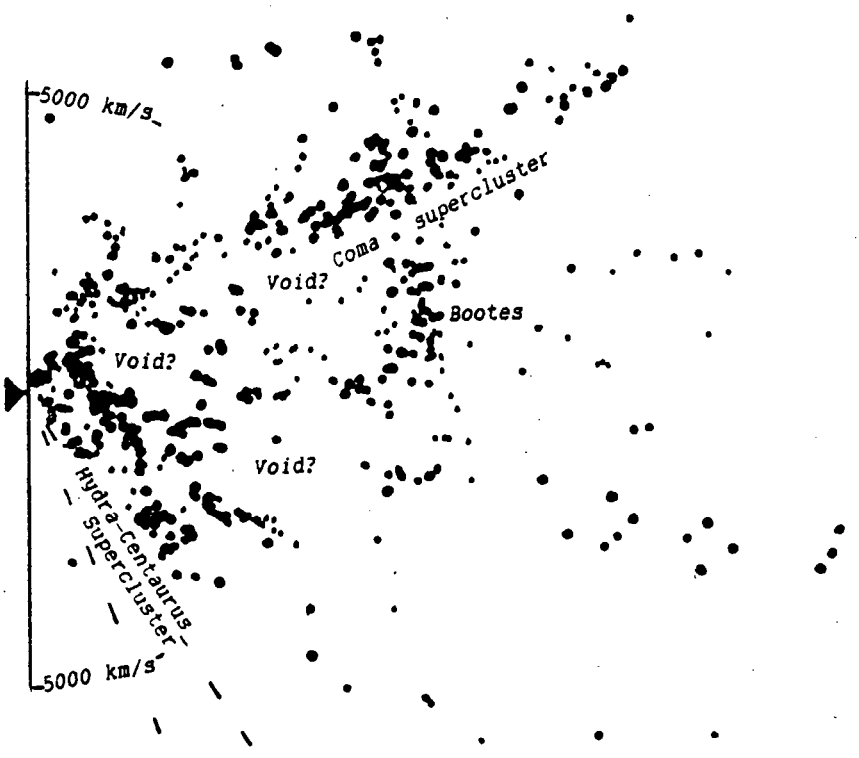

Figure 2.10: A redshift plot of galaxies in the declination wedge $13^h \leq \alpha < 14^h$. The diagram is taken from Fairall *et al.* (1985); redshifts are taken from an early version of Huchra's Zcat.

2.5.2 Sub-structure

It is of interest to note that in contrast to the nearly spherical voids found in northern sky surveys (eg. Fairall *et al.* 1985—see figure 2.10) the southern voids seem to fit into a rectangular structure almost forming a grid—their boundaries have sharp corners (da Costa *al.* 1989). Perhaps this is partly because they are constrained by superclusters which may form a larger structure (see figure 2.11, also Fairall 1988). This may constitute a lacunary structure; ie, there are clearly empty pockets, or gaps (lacunae) in the distribution of galaxies. In other words the reason these lacunae appear so distinct is that they are often (but not always) bounded by very thick, dense concentrations of galaxies.

A number of clusters are evident in plots of FJ (such as the Fornax cluster in the foreground of figure 2.11, and the well-studied Centaurus cluster, not visible in this particular figure) as well as a number of superclusters such as the nearer Sculptor Supercluster (evident as a band across figure 2.11). Fornax, in particular, displays elongations probably due to velocity dispersions of the Finger-of-God type. Other rich clusters have been studied in considerable detail (see Oemler *et al.* 1984, Dekel *et al.* 1986 and references therein) but as West (1989) points out, there is a marked absence of rich clusters in southern data when compared to the abundance of rich clusters identified in the northern skies. As one can hardly assume that all the clusters in the universe lie only in one half of the sky this must be partly symptomatic of the paucity of data in the south.

2.5.3 The case for all available redshifts

The paucity of data in the south may be of some consequence in understanding the nature of the *galaxy* distribution. But it has little effect on the clear definition of *voids*. This has been the experience of Fairall *et al.* (1990a) who compare void predictions of earlier versions of FJ, such as Fairall (1984), with FJ. The result is that new redshifts[11] generally do not remove (by filling in) voids that were evident in earlier catalogues. In other words, while fewer galaxies in a survey may seriously under-define features, the effect on void definition is much more dilute in any wide-angle survey such as FJ. Support for the sub-structure identified in FJ has come from the southern-sky work of da Costa *et al.* (1989), whose controlled samples of many of the same regions covered by the FJ catalogue reveal the same significantly under-dense regions (see chapter 1).

Redshift maps in the region of the southern galactic hemisphere (see figure 2.11), compiled by Fairall & Jones (1988), allow at least four voids, possibly five, to be visually identified:

[11] In particular, measurements of bright galaxies rather than the LSB or dwarf objects discussed earlier (Bothun *et al.* 1986).

Chapter 3

COELIS

"Pleni sunt coeli et terra gloria tua."

(from the Latin Mass)

The idea of searching the sky for remnants from early universe explosions (Ostriker & Cowie (1981) was the original motivation for developing a computer software package called COELIS[1]. If a void formed as the result of an explosion which spread out more or less isotropically, then the centroid might be the site of an unusual vestigial object (Ellis *et al.* 1988) which might still be detectable. (An example of a void with an unusual set of objects at its centre is a void in Pegasus discovered by Fairall *et al.* 1990.).

COELIS has since been developed to investigate the three-dimensional nature of any point pattern in a number of different ways. The software is user-friendly and flexible in that it allows a number of different representations of the point pattern to be viewed, in any order, in a variety of different circumstances. The use of COELIS is described in some detail in section 3.1. A condensed listing of the code is provided in an appendix.

The most useful feature of COELIS is that slices through the distribution may be viewed on a display of the type shown in figure 3.1. Each of the three parts of the display is a slice (of variable horizontal and vertical extent as well as variable thickness) through the point pattern. The three slices are perpendicular to each other. To understand the display technique one must look at any two of the graphics windows and cross-correlate the points viewed, with reference to the coordinate axes. The usefulness of this technique is that slices adjacent to one another may be "cranked" into view (after the *casement display* technique of Chambers *et al.* 1983). In this way, sufficient three-dimensional information can be obtained to build up a mental picture of the structure under study. In the case of a void (discussed in the next section) this is used to obtain a mental picture of the limits

[1] "Coelis", pronounced "chay-liss" or "co-e-liss", is Latin for "the heavens", or "the void above".

of the void and yields an estimate of the void centroid. In the case of a void interface, the casement-display technique allows the matter in and around the interface to be studied in detail. This application will be discussed in chapter 4.

3.1 Visual fitting to voids

COELIS allows a menu-driven approach to void analysis. In particular, it is able to provide a number of useful aids for finding the centroids of voids. The following list of headings represents the menu choices available; words in boldface in the text under each heading indicate the term used by the program:

Choosing the data set

Data in the neighbourhood of a region of visual under-density, (ie. a potential void), is **extracted** from a new catalogue in order to speed up access time in later applications. The extracted data is converted to (x, y, z) coordinates and simultaneously saved into a text file (called a *bubble* file) containing the radial and angular limits of the extracted data, as well as the x, y, z coordinates for each galaxy, and a thirty character alphanumeric string uniquely identifying the galaxy. The data converts as follows

$$\begin{aligned} x &= v \sin\theta \cos\phi \\ y &= v \sin\theta \sin\phi \\ z &= v \cos\theta \end{aligned} \tag{3.1}$$

where the angles (in degrees) relate to right ascension (α) and declination (δ) by

$$\begin{aligned} \theta &= 90^\circ - \delta \\ \phi &= 15\alpha \, . \end{aligned} \tag{3.2}$$

This sets a unique orientation for a right-handed cartesian coordinate system defined by the x-axis parallel to 0^h and the y-axis parallel to 6^h in the plane of declination 0°. The radial coordinate is simply taken to be the heliocentric velocity

$$v = cz \tag{3.3}$$

(not the "galactocentric corrected" velocity[2] $v_0 = v + 300 \sin\alpha \cos\delta$).

Once data has been extracted it can be **loaded** at any time and examined at will.

[2]For some time this formula was considered to be a more absolute way of measuring expansion velocities, but its use is not currently favoured.

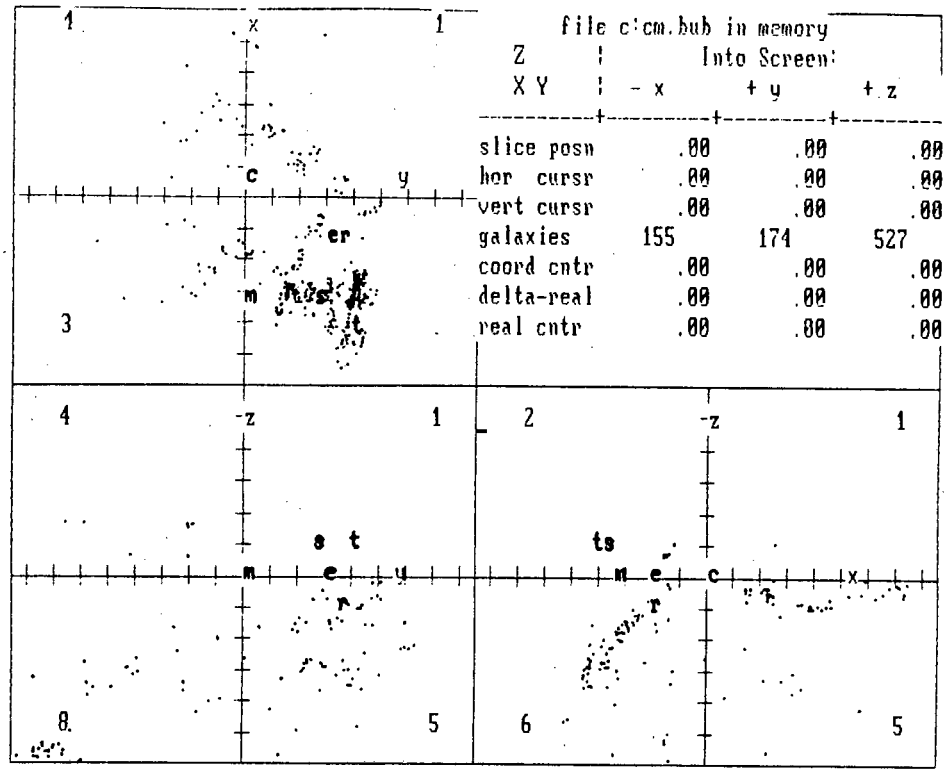

Figure 3.1: This example of the perpendicular slice representations (casement displays) generated by COELIS shows slices through the Sculptor void (the coordinate system is centred at the position of the centroid listed in table 3.1). The views are as labelled in the top right-hand corner. Gradations are in multiples of 1000 km/sec.

By-hand fitting to voids

The nature of the distribution of galaxies in and around the potential void can be conveyed to the user of COELIS in a number of ways. The easiest to work with is the casement display mentioned earlier.

Three perpendicular slices, or **casement displays** through the data set (of thickness set by the user), can be displayed at any one time (see figure 3.1). For a chosen coordinate centre (chosen by the user to be anywhere in the void) the display panel in the top right-hand corner gives the position of the slice in each display relative to the chosen coordinate centre, the number of galaxies in each slice (visible as points), and the coordinates, relative to earth, of the chosen coordinate centre. The slices "fold in" on each other—their relative orientations may be gauged by mentally aligning each display with a right-handed coordinate system according to the axis labels in each display.

In addition, crosshairs may be positioned on each perpendicular slice to mark the centre of some feature, eg. circular sections through a roughly spherical void. This procedure is called **by-hand centreing**. The 'real cntr' row, in the top right-hand corner, displays the coordinates of the centre obtained after centreing on all three displays. The centreing procedure can be repeated at each slice view, as often as needed, until the entry 'delta-real' has values as close to zero as possible. Because each axis is represented twice overall, positioning a centre in one view might give a different x coordinate, say, from another view. Thus 'delta-real' gives a simple means of reconciling all three views.

'Facing' refers to the direction *from* which one is looking in each of the three views (the coordinate system being used is right-handed), and a number is associated with every octant of the three-dimensional system of axes set up by the extraction process. These numbers are for reference when using the histogram procedure (see later) and appear in the four corners of each view. The octants correspond to the following cases:

1	$x \geq 0$	$y \geq 0$	$z \geq 0$
2	$x < 0$	$y \geq 0$	$z \geq 0$
3	$x < 0$	$y < 0$	$z \geq 0$
4	$x \geq 0$	$y < 0$	$z \geq 0$
5	$x \geq 0$	$y \geq 0$	$z < 0$
6	$x < 0$	$y \geq 0$	$z < 0$
7	$x < 0$	$y < 0$	$z < 0$
8	$x \geq 0$	$y < 0$	$z < 0$

Earth's position is indicated in casement displays by the letter **t** (for Terra), and visually chosen centroids[3] are indicated by **c**, **e**, **m**, **r**, **s** for the voids Sculptor, Eridanus, Microscopium, Southern Eridanus and Sagittarius, respectively.

The casement display technique may also be used to analyse redshift features. Any of the views can be enlarged (for better print-outs) or saved to disk for later analysis. In both cases numbers are attached to the galaxies in the view; the numbers index to a list of the names of the galaxies which is simultaneously printed out. This proves to be very valuable for studying galaxy-property gradients (the subject of chapter 5) across redshift features.

Determining the emptiness inside voids

The **histogram** option gives some idea of the distribution of galaxies around the void in relation to the "by-hand" procedure. The input of some centroid coordinates is required. The numbers of galaxies in spherical shells at stepped distances away from the centroid are

[3]Chosen by this method and methods such as scanning declination slice plots of the kind found in Fairall & Jones 1988.

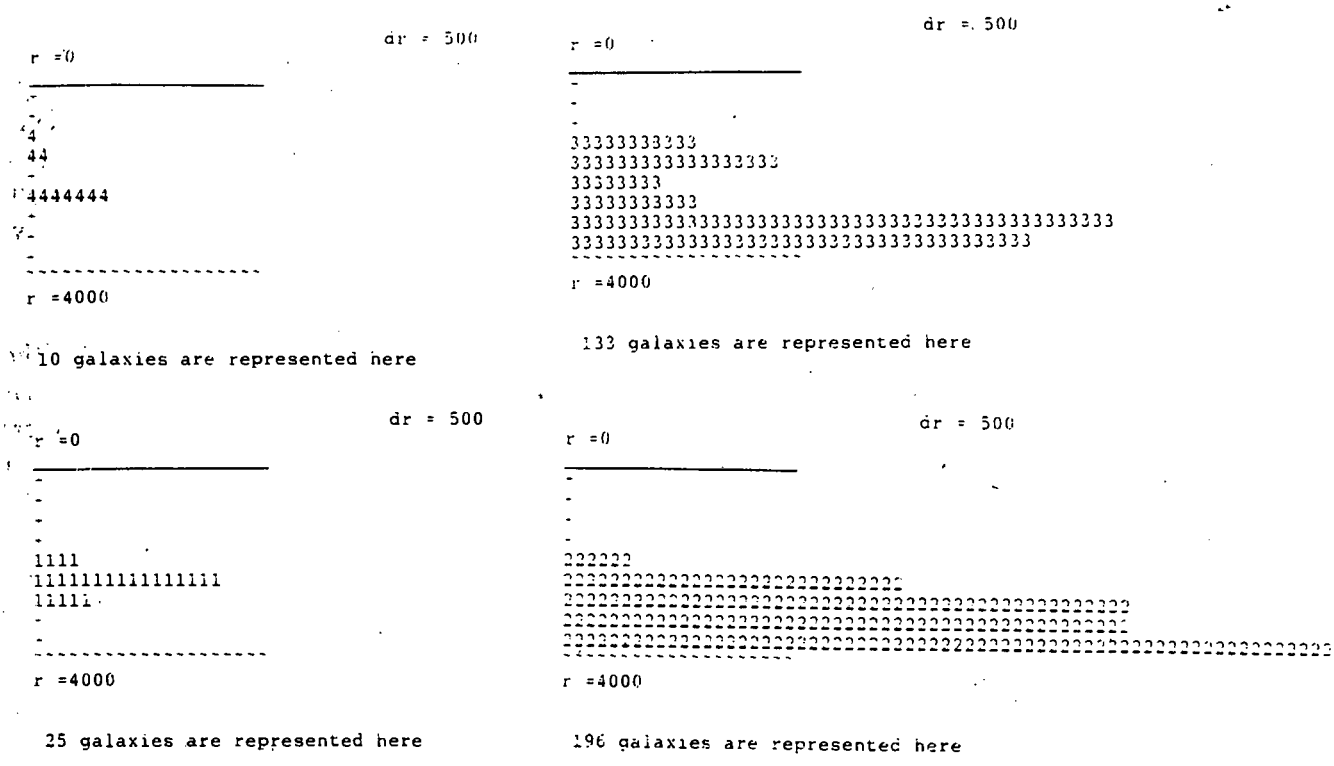

Figure 3.2: The histograms shown represent data for the first four octants of the distribution of galaxies used to define the Sculptor void, in radial steps away from the centroid (see table 3.1) of size 500 km s^{-1}.

counted and presented as eight histograms. The columns of each histogram (see figure 3.2) contain a number of digit entries: each entry is a galaxy, the number reflecting the octant in which it was found (relative to the centroid).

If voids were true spheres, and the chosen centroid was indeed the true centroid, then the histograms would be free of galaxies for all radii up to one or maybe two particular radii. But this is not sufficient. What is also required is that the galaxies are distributed evenly in all octants around the chosen centroid and not excessively distributed in only one or two octants (which would indicate either a centroid that is quite inaccurate, or a data set that suffers from strong selection effects, see below). As observed voids are not ideal spheres what is usually obtained is a level distribution of bin heights that rises sharply at some radius, before levelling off again. Familiarity with the catalogue in use is thus necessary if one is to interpret the octant spread properly, since selection effects may arise from poor sky coverage, and thus one side of a void may not be well-defined, giving rise to what appears to be an offset centre. Similarly, an excess of galaxies on one side (due perhaps to a rich cluster like Fornax) will also contribute a lopsidedness to any more sophisticated fitting technique (eg. that of Matravers & Maurellis 1990) if one is unaware of the extent of the cluster, and the selection effects in the area.

Sky coverage

The galaxy distribution surrounding the test centre may be examined for irregularities of sky coverage with the aid of the **sky-map** feature in the histogram option (see figure 4.3). This technique maps positions of galaxies around the centroid conformally to a plane under the Hammer-Aitoff equal-area projection

$$p_x = \frac{2\sqrt{2}\cos\delta\sin\frac{\alpha}{2}}{\sqrt{1+\cos\delta\cos\frac{\alpha}{2}}} \tag{3.4}$$

$$p_y = \frac{\sqrt{2}\sin\delta}{\sqrt{1+\cos\delta\cos\frac{\alpha}{2}}} \tag{3.5}$$

where coordinates p_x and p_y describe the point in the new plane. It can be shown that this mapping effectively takes all points on the surface of a two-sphere and maps them to a filled ellipse, in the R^2 plane, with submajor axes $\sqrt{2}$ and $2\sqrt{2}$.

The operation of the sky-map is similar to that of the casement displays. Spherical shells measured out from the centroid can be viewed independently on the screen using the equal-area projection and "cranked" into view. Shell thickness can be adjusted by the user and a list of names of galaxies in a view can be saved to disk.

Radial density plots

A more sophisticated way of checking the choice of any centre is to look at **density plots** of the data in each octant (see figure 3.3). This feature requires running the histogram option *followed* by the density plot option which generates two sets of four density plots; for the octants with non-negative z in one set and those with negative z in the other. These plots are very necessary for the process of ellipsoidal fitting to voids because they serve to delineate, often with considerable clarity, the void boundaries.

Rotating the database

One of the representations of an ellipsoid fit (see Matravers & Maurellis 1990) to a potential void is to present the data rotated so that the coordinate axes lie parallel to the submajor axes of the fit. The **transform** option allows for this when the eigenvectors of the two largest eigenvalues, in descending order, are input. The data is then doubly rotated so that the shortest axis (corresponding to the largest eigenvalue) lies parallel to the x-axis and the middle axis lies parallel to the y-axis. Finally, the data set is translated to the centre of the

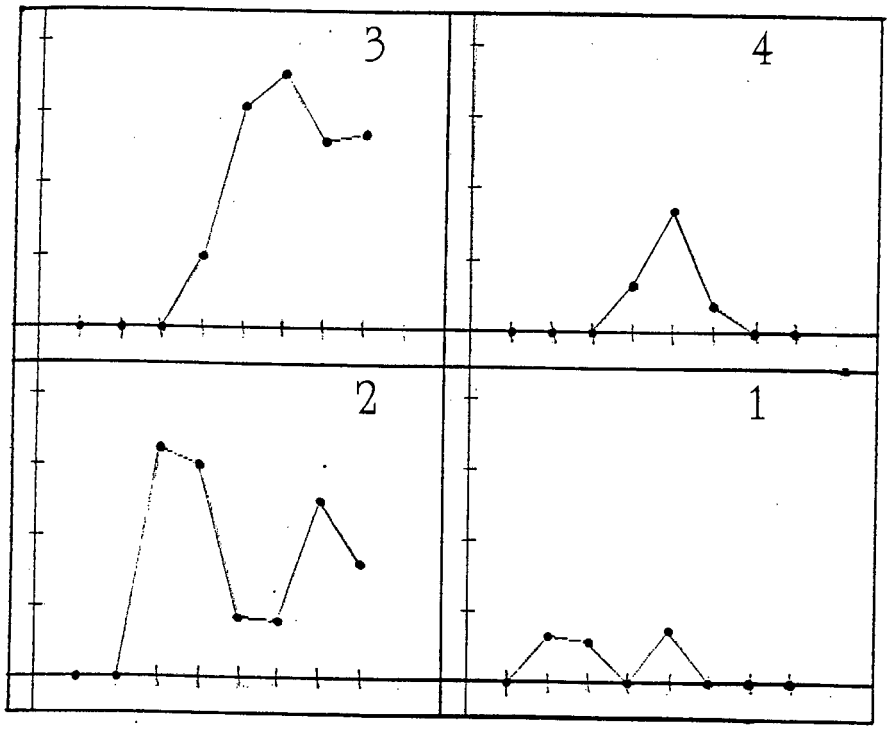

Figure 3.3: Radial density plots for the first four octants of the Sculptor void. Each view represents a density profile, according to the octant number displayed in the view. Vertical axes are in arbitrary units of density. Horizontal axes represent radial distance, increasing from left to right, away from the void centroid (gradations represent units of 500 km s^{-1}).

void and projected in casement display mode following the inputs described in the section on casement displays above. Alternately, the data set can be rotated only once towards a specific direction. This direction becomes the x-axis which allows easy "cranking" in the X view. A feature called the Wall (see chapter 4, also Maurellis *et al.* 1990) was discovered using the latter rotation.

Other options

- A **calculator** for conversion between galactic and cartesian coordinates is provided. This can be used before inputting trial centres, say, if these were obtained from declination slice plots (as in Fairall & Jones 1988).
- COELIS is configured for use with a hard drive but may be used on a PC with at least one floppy drive, 640K resident RAM and TRUE BASIC up and running. The **change device** option has been programmed to allow the input and output configuration to be adapted to the hardware in use.

3.2 A search for remnants

A preliminary search described in Ellis *et al.* (1988) was conducted on the void we now call Southern Eridanus (data was taken from a 1986 version of Fairall 1984b). The void centroid discovered with this data can be found at the following coordinates:

$$\begin{aligned} \alpha &= 2^h 39'.4 \pm 3'.0 \\ \delta &= -67°07' \pm 18' . \end{aligned}$$

The void spans 70° longitudinally and its centre is about 35 h^{-1} Mpc from us. Up to a distance of about 12 h^{-1} Mpc from the centre the void appears quite empty. Although part of it falls slightly out of the data set on one side, it is otherwise well defined, as well as being close to spherical (compare the ellispoidal shape of Sculptor that may be deduced from figures 3.2 and 3.3).

The results of a search for explosion remnants at the Southern Eridanus centre are not conclusive. X-ray and radio source catalogues reveal no strong sources at this location. A recent scan by the NASA Laboratory of High Energy Astrophysics (Boldt, private communication 1988) further confirms the absence of substantial x-ray sources. Infra-red sources abound however; one infra-red source without a corresponding visual image has been located, but no definite conclusions can be drawn since such infra-red objects are not uncommon in this area of the sky.

3.3 Other southern voids

The "by-hand" centreing feature of COELIS has been used on the Fairall & Jones (1988) catalogue to find a set of rough, first estimates of the centroids of voids that have been identified as such by Fairall (see table 3.1). At the same time, some idea of the density in and around voids is obtained, from features of COELIS such as the histogram generator. It is also possible to determine a value for the *maximal emptiness* for each void. If a sphere was constructed with a radius of this value, centred at the void centroid, it would contain no galaxies.

Table 3.1: The coordinates of void centroids chosen "by hand" (ie. using the casement display feature of COELIS) of five prominent voids in Fairall and Jones (1988). Maximal emptiness (ME) and radial distance d are in h^{-1} Mpc. Because of the larger data set the Southern Eridanus centroid given below appears somewhat different to that mentioned earlier.

Void	Centre(d, α, δ)	ME
SCULPTOR	(57.5, 23^h 15′, -32.5°)	12
ERIDANUS	(25.0, 0^h 50′, -32.5°)	6
SOUTHERN ERIDANUS	(33.0, 3^h 16′, -62.0°)	6
MICROSCOPIUM	(40.0, 20^h 26′, -32.0°)	9
SAGITTARIUS	(12.5, 20^h 36′, -34.0°)	5

Chapter 4

The Wall

"For I assure thee, that all these seeming
Extravagancies that I must run through are no jests;
Far from it, they must all be performed seriously and solemnly... "

(Miguel de Cervantes in *Don Quixote*)

4.1 Void boundaries

The question of whether voids are inter-connected or not is relevant to cosmological scenarios such as the hierarchical models discussed earlier. As discussed in chapter 2, Gott and collaborators have determined a measure of the connectedness of the galaxy distribution (or, in reflection, the voids) at various density levels. They find an overall tendency to sponge and meatball topologies. In both cases one would expect *void interconnections*—ie., statistically significant under-dense regions in the void boundaries—to exist.

The term *void boundary* is used to refer to the galaxies in the neighbourhood of the outline of the voids, if the outline is obtained by some sort of visual or computational sphere-fitting interpolation. In this chapter the discovery of a sheet-like (ie. 2-d) void boundary in the FJ catalogue is discussed in the context of the question of whether voids in the southern sky are isolated or inter-connected. In the next chapter we discuss the analysis of properties of galaxies in the region of the sheet-like boundary as a means of reducing the number of models of void formation scenarios from which to choose.

As galaxies are effectively particles, at the scale of interest (galaxy sizes are $\sim 10^{-3}$ void diameter), it will always be possible to find a way through a 2-d structure made up of discrete data. In many ways, the problem of describing void interconnections is much the same as the

problem of describing voids. A void interconnection in a void boundary—hereafter called a *hole*—is merely the two-dimensional case of a void in the distribution of galaxies. However, surveys of thin slices through voids (such as the "slice of the universe" de Lapparent *et al.* 1986) will not reveal whether the voids are totally isolated by sheets of galaxies, or whether interconnections exist between the voids, unless the survey is aligned with the void boundaries in question. For example, a slice perpendicular to a sheet of galaxies between voids will not necessarily reveal void interconnections through the sheet. If significantly large holes occur in a void boundary then the implication is that the boundary is consistent with a sponge topology. Of course, finding under-dense regions in the data is only part of any thorough search for sub-structure in a void boundary; there is also the possibility of finding over-densities. Although some of the tests used to find holes will also indicate the presence of clustering in void boundaries, this is not the focus of this chapter, and tests such as the correlation function have not been applied to the data, for reasons already discussed.

4.1.1 Southern void boundaries

One approach to examining a redshift survey is to do so using the three-dimensional graphics-viewing methods of COELIS. This has yielded the discovery (Maurellis *et al.* 1990) of a very thin sheet of galaxies between two southern FJ voids (in Sculptor and Eridanus). The sheet is thin enough that it may be likened to a 2-d spatial distribution and analysed by statistical methods available for 2-d point patterns. It is anticipated that many sheet-like features will lend themselves particularly well to this 2-d treatment. In this chapter, a spatial analysis of this particular feature—the interface between voids in Sculptor and Eridanus (hereafter denoted by an upper case initial: Wall)—will be discussed in detail. This will include a description of the discovery of the Wall and a detailed discussion of the statistical tests used to arrive at the conclusion that the distribution of galaxies in the Wall is largely Poisson in structure and not gravitationally relaxed.

Although interfaces of one sort or another exist, by definition, between all neighbouring voids, the Sculptor void is one of the most clearly defined in FJ and its boundary with the neighbouring Eridanus void turns out to be an excellent example of a nearly flat interface between two voids. It projects quite clearly as a thin line of galaxies in figure 4.1. This feature is nearly perpendicular to the line of sight, which means it cannot be understood as a Finger-of-God effect. Thus it may be asked whether or not the galaxies at the interface of the Eridanus and Sculptor voids (ie. the Wall) form a *sheet-like* feature—an essentially planar structure with no significantly under-dense regions.

Using COELIS the Wall may be viewed in coordinates optimally suited to studying the planar nature of the interface. The coordinates of the galaxies in the data set were obtained, in the first instance, by searching FJ for all galaxies between approximate right ascension, redshift limits around the feature: (23^h–1^h, 2000 km s^{-1}–5000 km s^{-1}) (bearing in mind

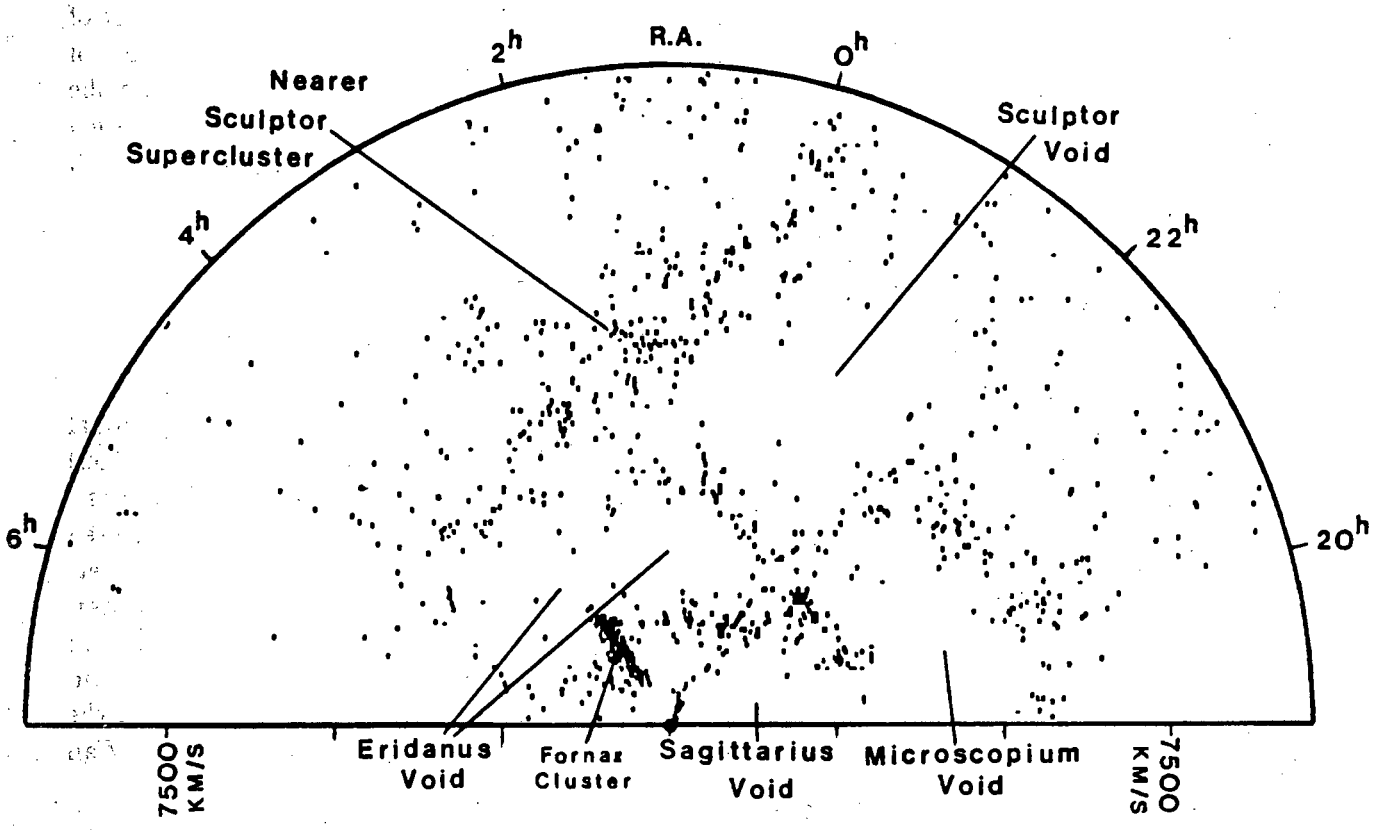

Figure 4.1: A redshift map of southern galaxies, out to about 120 h^{-1} Mpc, for the declination range $-17\frac{1}{2}^\circ$ to $-47\frac{1}{2}^\circ$, taken from FJ. Conveniently, many of the features (such as the interface between the Sculptor and Eridanus voids) may be shown to extend perpendicular to the plane of projection of the data thereby demarcating the under-dense regions fairly clearly.

the declination limits of FJ—see figure 4.1). The subset of the FJ catalogue so obtained was then rotated and translated to achieve the following effect on the data set:

- the centre of the one void formed the origin of the coordinate system, and
- the centre of the other void lay on the x-axis at a negative value[1].

To this end, centres for Sculptor and Eridanus (such as those listed at the end of chapter 3) are needed. With the data suitably rotated the interface can be viewed edge-on and flat-on (in the X window) in which case a series of adjacent views (as in figure 4.2) adjacent to and including what we have called the Wall is obtained. It is clear, after moving through the sequence of figure 4.2, cross-sections a–c, that section b contains a significant over-density of galaxies relative to sections a and c. Measurements off the main view of figure 4.2, that is, off the side view of sections a–c, reveal that the Wall is a thin, nearly planar sheet of galaxies (of approximate dimensions $20 \times 20 \times 6.5\ h^{-3}$ Mpc^3) at the interface of the Sculptor and Eridanus voids, some 25 h^{-1} Mpc and 20 h^{-1} Mpc, respectively, from their centres.

4.1.2 Void interfaces other than the Wall

Void interfaces between other voids can be viewed at a glance using another feature of COELIS—the all-sky view. This uses an Hammer-Aitoff equi-area projection (the details of which are given in chapter 3) to display, in the case of figure 4.3, all the galaxies from the centroid of Sculptor up to a distance of 35 h^{-1} Mpc. Since this distance is greater than the void radius and Sculptor is by no means spherical (da Costa *et al.* 1989, Matravers & Maurellis 1990) the diagram shows all the galaxies at the void boundary as well as some galaxies that lie well into the surrounding voids. Thus an all-round view of the nature of the surrounding void interfaces may be obtained in addition to which the all-sky view can be used to convey some impression of selection effects in FJ. For example the data set around Sculptor suffers from poor definition towards higher declinations (the top of the diagram), a fact which may affect the accuracy of the "by-hand fitting" tool when determining the Sculptor centroid. Notice that the Wall can be readily identified in the centre of this view even though it is reversed to how it appears in figure 4.2b.

4.2 The Wall data

The Wall data set has since been supplemented by searching LV for galaxies in a 22.5^3 h^{-3} Mpc^3 cubical region (hereafter called the Wall region) centered, within the rotated,

[1]The reason for this seemingly odd choice of transformation is discussed in chapter 3.

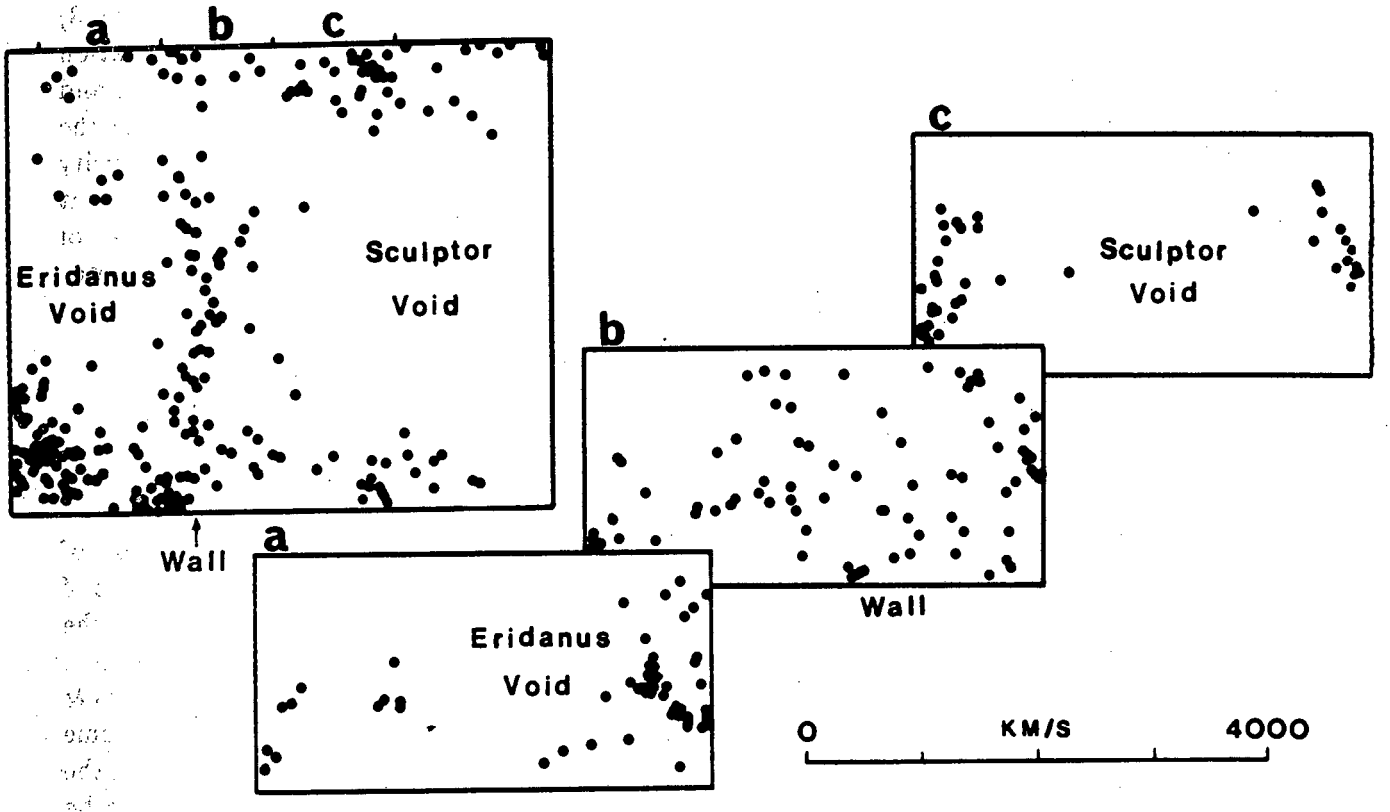

Figure 4.2: This diagram is a montage of three sequential casement displays (or cross-sections) (a–c) viewed from the "left-hand" side of a "top" view (top-left corner diagram) of a block volume, 20 h^{-1} Mpc deep, containing the feature recognisable as a filament in figure 4.1 between the Sculptor and Eridanus void. Each casement view is a slice of thickness 10 h^{-1} Mpc through the volume represented in the "top" view.

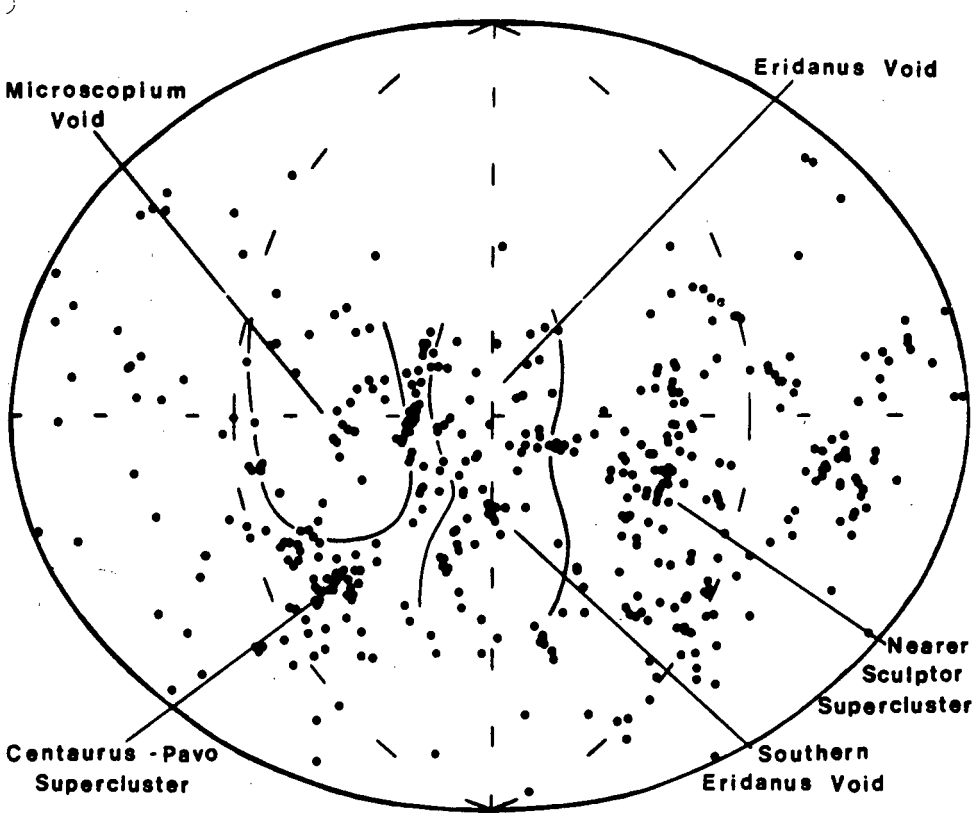

Figure 4.3: An equi-area projection of the distribution of galaxies surrounding the Sculptor void (looking out towards the Eridanus void) as seen from the centre of Sculptor. Neighbouring voids, lying *beyond* the galaxies shown, are indicated. The diagram includes all galaxies within a radius of 35 h^{-1} Mpc— sufficient to include all the interfaces of Sculptor with the surrounding voids. (Although not apparent from the diagram, figure 3.2 shows that no galaxies are found within a radius of 12 h^{-1} Mpc from the centroid of Sculptor.) The data thins towards the top of the diagram because of the declination limit of the data base, and towards the remainder of the periphery because of the generally increasing redshift.

translated coordinate system discussed earlier, on the Wall. As discussed in chapter 3, LV contains a wealth of photometric data although not as many redshifts as FJ. There is a fair degree of overlap between the two catalogues. This has allowed us to construct a catalogue of galaxies in the Wall region. Galaxies in the current version of the Wall to be used for all analysis that follows may thus be divided into three classes:

1. Galaxies only in LV, in which case LV redshifts have been used.
2. Galaxies only in FJ, in which case FJ redshifts have been used.
3. Galaxies in both LV and FJ, in which case FJ redshifts have been used[2].

The corners of the cubical region may be determined from the following radial velocity, declination and right ascension limits on the data: (2090–5320 km s^{-1}, $-57°$– $-17°46.8$, $21^h52'12''$– $2^h52'48''$).

4.2.1 Selection effects

Due to the absence of redshifts for many objects in LV it is possible that some under-sampling in redshifts exists for data in the Wall region. However use is made of all available redshifts in the opinion, ventured earlier (see chapter 2), that this will detract little from structure evident in properly controlled surveys.

Galaxies in the Wall region do appear to form a fair sample of the LV catalogue for the following reason: the frequency profile of morphological type in the Wall region has the same shape as that for the LV catalogue as a whole (see figure 4.4). This is largely because FJ and LV contain so-called *field* galaxies These galaxies are found in regions of galaxy density 10^4–10^5 less than the galaxy densities in Abell clusters (Abell 1958). The region of the Wall has a density of $\sim 10^{-2}$ galaxies h^3 Mpc^{-3}, and is populated by a proportion of morphological types of 70/20/10 (spirals-lenticulars-ellipticals), typical of field galaxies (Postman and Geller 1984).

Thus it may be concluded that the Wall is a real feature[3], rather than an artifact of selective under-sampling, because it appears in a fairly representative sub-sample (namely the Wall region) of the distribution of galaxies in LV.

In section 4.3.1 a number of statistical analyses of the 2-d nature of the Wall will be discussed. Three subsets of the data set (see table 5.5) will be used:

[2]As discussed in chapter 2, this is because most galaxies in FJ are represented by a redshift determined by compilation of a greater number of different sources than is usually the case in LV.

[3]In redshift space, although we do not rule out, at this stage, the possibility that it exists in physical space as an unusually thin structure as well. This possibility is explored in the chapter 5.

1. For the first gridding, all the data will be used.

2. For the second gridding, all points not in LV will be removed, to ensure a sample with more well-understood controls: as mentioned in chapter 2, the FJ objects are often drawn from a much fainter sample than those in LV.

3. For the third gridding, all points closer to the boundary than to another data point will be removed from the data set used in (2). This is one way of taking into account effects of the boundary (that is, the outside edge of the diagram) on the statistics.

Figure 4.4: Frequency profiles of morphological type in the Wall region and the the LV catalogue as a whole appear quite similar (see also figure 2.9). Hence it may be deduced that the Wall region is a fair sub-sample of the catalogue.

4.3 Statistical analysis of the Wall

4.3.1 Chi-squared tests

Elementary techniques of the type outlined in Diggle (1983) and Siegel (1956) have allowed us to compare data in 2-d slices of the real distribution such as the Wall to a Poisson distribution. If T is the total number of data points in the Wall region and N the total number of gridded "squares"[4] then we may compare the Wall to a Poisson distribution in the random variable of *frequency of points per square*. Given that the most likely frequency satisfies $\lambda = T/N$ then

$$P_i = \frac{\lambda^i}{i!}\exp(-\lambda), \tag{4.1}$$

$$\sum_{i=0}^{\alpha} P_i = 1 \tag{4.2}$$

where P_i is the probability of finding $P_i N$ squares with a frequency of i points per square and $\alpha \leq T$ (although $\alpha \ll T$ is true in practice). If we write $E_i = P_i N$ as the expected frequency and O_i as the observed frequency (ie. taken from the observations) then a *chi-squared statistic*

$$\begin{aligned} \chi^2 &= \sum_{i=0}^{\alpha} \frac{(O_i - E_i)^2}{E_i} \\ &= \left(\sum_{i=0}^{\alpha} \frac{O_i^2}{E_i}\right) - N \end{aligned} \tag{4.3}$$

may be used to test goodness-of-fit. (Note that this test is sensitive to the small numbers in the data set, especially at the tail of the distribution. If there is a frequency i for which $E_i < \alpha + 1$ at the tail end of the distribution, then the end bins must be combined until $E_i \geq \alpha$.)

In terms of the definitions above, the degrees of freedom d must satisfy $d = \alpha$, from the one constraint on the data $\sum_{i=0}^{\alpha} O_i = \sum_{i=0}^{\alpha} E_i = N$. In this formulation the null hypothesis is the Poisson nature of the distribution; if the observed $\chi^2 \leq \chi^2(95\%)$ then we are left with the weak result that we cannot reject the null hypothesis; if the converse we may definitely say that the data is inconsistent with a Poisson distribution at the 95% level. The latter case would be strong evidence in favour of sub-structure in the point pattern. Thus if the observed $\chi^2 \approx \chi^2(p\%)$ then there is a $p\%$ probability that the distribution is not random.

[4] See the gridded detail of the X casement display of the Wall viewed head-on (figure 4.5).

Results

If the Wall is gridded into an 8 x 8 square grid (grid spacing = 2400/8 km/s under the first gridding on page 75) (see also figure 4.5), and a frequency distribution table is constructed using the variables described above, then the following is obtained.

i	0	1	2	3	4	5	6
O_i	22	22	7	5	3	4	1
E_i	15.9	22.2	15.4	7.1	2.5	0.7	0.2

The Poisson distribution is calculated from $\lambda = T/N$ where $T = 89$ points and $N = 64$ squares (the second gridding on page 75). Thus $\lambda \approx 1.39$. For goodness-of-fit use $d = 3$ (as $i = 3, 4, 5, 6$ have to be grouped into one class). Thus obtain

$$\chi^2 = 7.52 \approx \chi^2(90\%)$$

which means that there is a 90% chance that the Wall, in 2-d, is non-Poisson. Because the grid spacing may be too small (and hence an unfair representation of the distribution), the analysis may be repeated with a 4 x 4 grid (grid spacing = 2400 km/s /4 see figure 4.9) to yield the following table.

i	0	1	2	3	4	5	6	7	8	9
O_i	1	1	2	2	1	2	1	2	3	1
E_i	0.1	0.6	1.5	2.4	2.9	2.8	2.3	1.6	1.0	0.6

Now $\lambda = 78/16$ and $d = 5$ should be used. Thus obtain

$$\chi^2 = 9.9 \approx \chi^2(90\%)$$

which again shows weak (90%) agreement with the Poisson distribution. The above two tables will be used for fitting to a gravitothermodynamics function described later in the chapter.

Boundary effects

All statistical tests (especially nearest-neighbour tests) on finite data sets will suffer from boundary effects in one way or another. Thus one may remove, prior to calculating the statistics, the data points near the boundaries that are nearer to the boundary than to

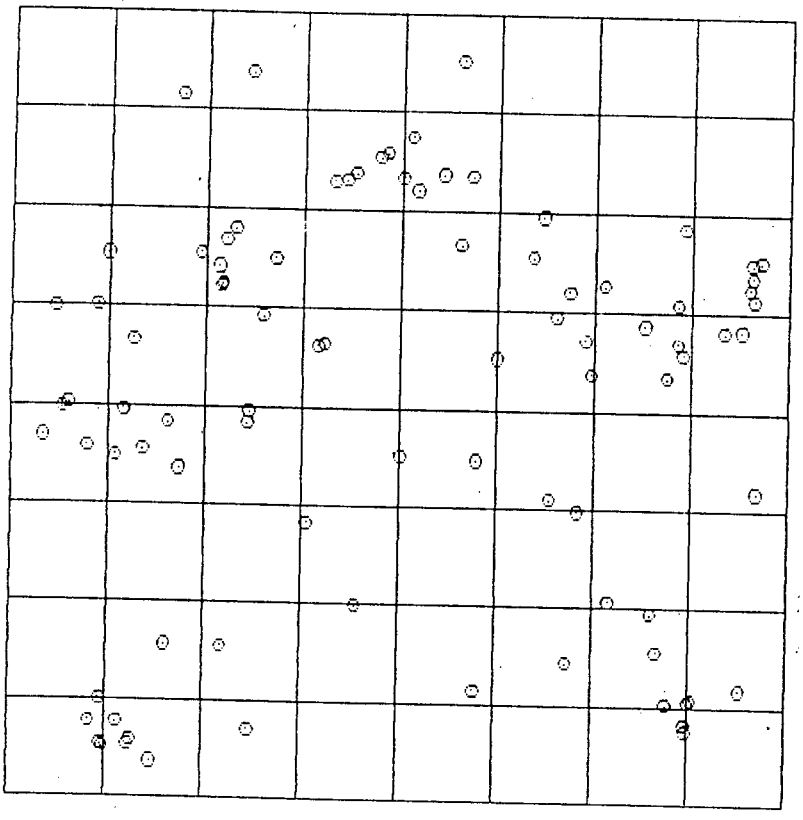

Figure 4.5: Gridded detail of the full data set for the Wall region, viewed face-on, ie. treated as a 2-d point pattern. This (first) gridding is used in the application of a preliminary goodness-of-fit test.

another point (this refers to the third gridding procedure discussed on page 75 and the six removed points on diagram in figure 4.9). In this way a table of frequencies of nearest-neighbour distances is obtained:

i	0	1	2	3	4	5	6	7
O_i	21	11	21	10	0	4	2	3

Here i denotes the distance class (see section 4.3.4). This table will be used in calculations of the Medvedkov entropy function in order to determine random, dispersed and empty components of the distribution in terms of areas.

In section 4.3.6 we discuss a technique to check the degree to which the boundary affects estimates of the nature of the distribution. However, before drawing on more sophisticated statistical tests, a general method for mapping density contours in the Wall will be discussed.

4.3.2 Density maps

Considerable attention has recently focussed on measuring the topology of 2-d representations of large-scale structure. Melott *et al.* (1989) discuss the application of genus threshold density function, discussed in chapter 2, to slices of the universe. Slezak *et al.* (1990) discuss the application of a new mathematical technique—the wavelet transform—to the detection of sub-structure, such as voids or clustering, in 2-d catalogues.

At a simpler level, but one that is equally informative of the gross characteristics of the distribution under study, Cox (1979) has developed a method for mapping the dense and sparse areas in any 2-d point pattern in a simple, visually striking form.

Consider an arbitrary point P in a 2-d slice of data. P is said to be in a *dense* region of size n, or within a *sparse* region of size n according as

$$T_n < d_n \text{ or } T_n > s_n \ . \tag{4.4}$$

T_n is a normally-distributed function of nearest-neighbour distances to P of the form

$$T_n = b_1(n) \sum_{j=1}^{n} \lambda \pi R_j^2 \ + \ b_2(n) \tag{4.5}$$

where R_j is the distance from P to the jth-nearest point, n corresponds to the point most distant from P that will be used to estimate T_n, λ is the density of the spatial pattern as

before, and

$$b_1(n) = \left[\frac{1}{6}n(n+1)(2n+1)\right]^{\frac{1}{2}}$$
$$b_2(n) = -\left[\frac{3}{2}n(n+1)/(2n+1)\right]^{\frac{1}{2}}$$

The d_n and s_n defined earlier are in fact the percentiles of the distribution

$$d_n = d_n(\alpha) \equiv 100\alpha \text{ per cent}$$
$$s_n = s_n(\alpha) \equiv 100(1-\alpha) \text{ per cent}$$

for which a table of values, for $\alpha = 0.05$ and $\alpha = 0.025$, are provided in Cox (1979) (see also a listing of the plot-generating code, included as an appendix) for different values of n.

Cox has tested the method on various data sets. He finds that sparse and dense regions do not arise in a pure Poisson distribution whereas the converse is true in a pattern with strong clustering. A regular pattern displays small amounts of sparse and dense regions (see figure 4.6).

Thus one may determine, for a grid of points laid over a spatial point pattern, whether each point of the grid lies in a region of over- or under-density. It remains to construct contours around the grid points to determine, in a simple way, significant clustering and holes in 2-d pattern.

Cox (1979) uses $n = 10$ a great deal, for reasons which are not discussed in the paper. As with all 2-d methods his method must break down when determining T_n for large n, because of the effect of the sudden drop in density at the boundary. The method has been tested on data in which highly significant sub-structure, ie. clustering or holes, is present. As a rule of thumb it is found that $n = 10$ gives results not too strongly affected by the boundaries when $\alpha = 0.05$ is used on a data set of ~ 100 points, which is consistent with Cox's findings.

By comparing figure 4.7 with figure 4.6 it can be seen that the Wall is not purely random. It appears that the boundary effects induce the only significant under-densities on the density map, ie. there appear to be no significant holes in the Wall. However there are signs of significant clustering (over-dense regions).

4.3.3 Components of a distribution

Further tests of the nature of a 2-d slice require that *components* of the distribution of points in the slice be defined as a subset of points in the distribution relating to some

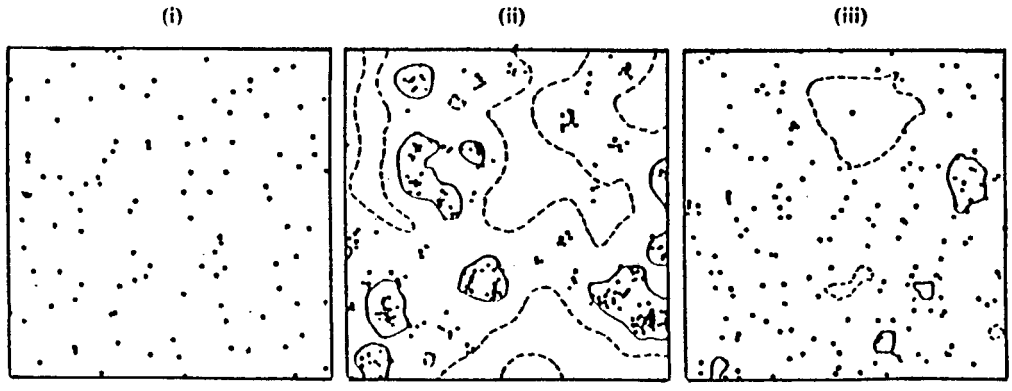

Figure 4.6: Contour diagrams from Cox (1979). The diagrams show clumped and sparse regions within (i) a Poisson distribution, (ii) an aggregated pattern and (iii) a dispersed pattern, for $n = 10$ and $\alpha = 0.05$.

point-generating process. A distribution may have a *random component* in which case some points will evidence clustering, while others may be regularly spaced, or dispersed (Clarke and Evans 1954). A completely dispersed planar distribution displays a hexagonal structure consistent with a gravitationally relaxed system, and a measure of the *dispersed component* in a real distribution may give clues about the manner in which the distribution formed. Depending on the statistical technique used it may or may not be necessary to define an *empty component* which refers to that part of the distribution not generated by a point process, ie. the holes defined earlier.

Simple measures of these components are calculable in terms of nearest-neighbour distances for points in the real distribution. Let p denote surface density λ in units of km s^{-1}. Then the expected *mean nearest-neighbour distances* are

For a random distribution

$$d_R = \frac{1}{2\sqrt{p}}$$

For a dispersed pattern

$$d_D = \frac{1.075}{\sqrt{p}}$$

These may be compared to the observed mean nearest neighbour distance determined directly from the data: d_O.

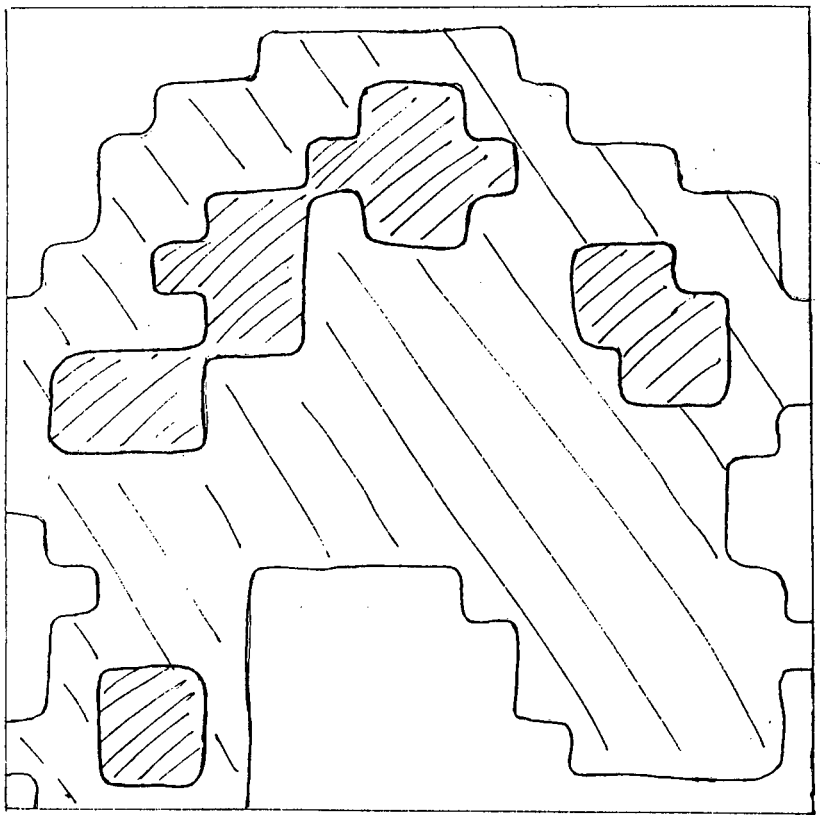

Figure 4.7: A plot of significantly under- and over-dense regions in the Wall, for data in the second gridding, after a method by Cox (1979).

Results

Figure 4.7 shows that the Wall appears of uniform density in that it does not display many significantly under-dense or over-dense regions. It is a simple matter to calculate from the data a mean nearest-neighbour distance. For the Wall this takes the value

$$d_O \approx 96.8 \text{ km s}^{-1}$$

which may be compared with the mean values for pure random or dispersed distributions:

$$\begin{aligned} d_R &\approx 141 \text{ km s}^{-1} \\ d_D &\approx 304 \text{ km s}^{-1} \end{aligned}$$

where p is the number density of the distribution $p = 72/2400^2 \approx 1.25 \times 10^{-5}$ (units of km^{-2} s^2), for data in the third gridding, above. On the basis of this simple comparison it may be conjectured that the Wall has a a slight tendency towards sub-clustering and an insignificant dispersed component.

4.3.4 More on components: Medvedkov's entropy function

A more quantitative idea of the relationship between the components may be obtained via the Medvedkov entropy function (Medvedkov 1966). There are two ways in which this function may be applied; however the net result in both cases is that one may

- determine the dispersed (hexagonal) structure as defined above, in a point pattern, in terms of number density or area,
- determine the random nature, of the point pattern, not related to this regular structure, also in terms of number density or area, and
- determine the amount of "empty area" (the holes, or significantly under-dense regions) in the point pattern.

Application: number densities

The method that yields overall number densities (in units of points per square) for the components will be discussed first. For a gridded point pattern the following quantities will be determined, in the method described below, from the data:

a_R is the mean density of points arranged randomly,

a_D is the mean density of points arranged in a hexagonal pattern,

a_T is the total mean density of points.

The entropy function of Medvedkov (1966), for observed probabilities p_i, is

$$H = -\sum_{i=0}^{d} p_i \log_2 p_i \ . \tag{4.6}$$

The entropy of the data in section 4.3.1 may be estimated using $p_i = O_i/N$ (where O_i is the observed value for the ith frequency as on p.77) to calculate a value $H = H_T$ from equation (4.6). Then, for testing against a random distribution, equation (4.6) is written with

$$p_i = \frac{(a_R)^i}{i!} \exp(-a_R)$$

to obtain a form $H_R = -\sum_{i=0}^{d} p_i \log_2 p_i$ with indeterminate a_R. It may be shown (Medvedkov 1956) that the entropy of a dispersed distribution is zero. Thus a_R may be estimated via

$$H_R = H_T \ .$$

From the definition of a_T it follows that

$$a_D = a_T - a_R$$

can be calculated once a_T is known. To determine a_T requires calculating a quantity similar to λ but without taking empty cells into account. (This is necessary if the entropy of a dispersed distribution vanishes.) Thus

$$a_T = T/N'$$

where $N' = N - E$ and E is the number of empty cells.

Thus are estimates obtained of the densities of different components in the spatial distribution of the Wall.

Results

Equation (4.6) is easily fitted using the observed values O_i in the second gridding of section 4.3.1 (sans $O_0 = 1$) to obtain $H \approx H_T \approx 3.06$. Firstly, $a_T \approx 78/(16-1) \approx 5.2$ Now

$$\begin{aligned} H_R &= H_T \\ \rightsquigarrow a_R &\approx 4.25 \end{aligned}$$

so that the the density of points (per square) in the dispersed component of the Wall arises from

$$a_D \approx 5.2 - 4.25 = 0.95 \ .$$

Thus we find a very strong random component ($4.25 \times (16-1) \approx 64$ points) in the Wall and a small regular component. The degree to which the Wall exhibits significant sub-clustering will arise out of the gravitothermodynamics fit, discussed later.

Application: areas

The second method outlined by Medvedkov (1966) yields the effective areas covered by the various components. For a gridded pattern with points closer to the boundary than to other data points, removed, the following will be determined:

s_D the area covered by the dispersed, or regular, component

s_R the area covered by the random component

s_O the empty area

s_T the total area

α the mean number of points within a unit circle (units of km s^{-1}).

The method requires that a frequency distribution of nearest-neighbour distance must be compiled similar to that in the third gridding of the Wall data set (see section 4.3.1 above). Let bins of constant width r_c, and height N_i, of the number of galaxies with a nearest-neighbour distance in range $[ir_c, (i+1)r_c]$ be defined. (In the range just quoted r_c has units of km s^{-1} and is, as a rule-of-thumb, determined by requiring that there exists at least one point in an area fifty times the size of the r_c^2.) Then Medvedkov (1966) shows that

$$p_i \equiv p(r_{i+1} - r_i) = \exp(-r_i^2\alpha) - \exp(-r_{i+1}^2\alpha) \tag{4.7}$$

is the probability of finding a nearest-neighbour distance $r_i \in [ir_c, (i+1)r_c]$, between two points, in a random distribution (in this case the random variable is nearest-neighbour distance).

Now the probability p_i in equation (4.7) may be substituted into equation (4.6) to yield $H_R = H_R(\alpha)$. As in the number density method above, the aim is to satisfy $H_T = H_R$, and thence to calculate α. (Note that the observed entropy H_T calculated in the number density method is used in the areas method.)

Now, with a given s_T and T for the given 2-d pattern, the mean distance for a purely dispersed distribution is

$$r_D = 1.075\sqrt{\frac{s_T}{T}} \ .$$

Then p_D, the probability of a point in a dispersed pattern occurring randomly, can be calculated from $p_D = p_k$ where k satisfies

$$r_D \in [kr_c, (k+1)r_c] \ .$$

Thus the number of nearest-neighbour distances that would fall randomly into a dispersed pattern is

$$N_D = p_D T \ .$$

From the distribution we obtain N_k, the observed number of nearest neighbours in *distance class* k. Thus the number of points in the dispersed component are

$$n_D = N_k - N_D$$

from which Medvedkov calculates

$$\begin{aligned} s_D &= n_D \frac{s_T}{T} \\ s_R &= \frac{\pi(T - n_D)}{\alpha} \\ s_O &= s_T - s_D - s_R \end{aligned}$$

which are the final forms for the areas of components in a 2-d distribution.

Results

Nearest neighbour distances for the third gridding of the Wall give

$$r_D = 1.075\sqrt{\frac{2400^2 - 2 \times 600^2}{72}} \approx 265 \text{ km s}^{-1}$$

subtracting the area of the two empty squares. Using $r_c = 40\text{km s}^{-1}$ we see $r_D \in [240, 280]$ which corresponds to $k = 6$. Now $H_T \approx 2.41$ for the third gridding, disregarding all empty squares (ie. $O_0 = 2$). Thus $H_R = H_T$ yields $\alpha \approx 7.75 \times 10^{-5}$. This means that $p_D = 0.0092 \rightsquigarrow N_D \approx 0.66$. From the observed nearest-neighbour distribution (the third gridding)

$$\begin{aligned} N_6 = 2 &\rightsquigarrow n_D \approx 1.34 \\ &\rightsquigarrow s_R \approx 1692^2 \\ &\rightsquigarrow s_D \approx 306^2 \\ &\rightsquigarrow s_O \approx 1443^2 . \end{aligned}$$

These results are consistent with the tests so far—the Wall has a significant random component (57%), a considerable empty component (41%) and an almost negligible dispersed component. It is possible that such a structure—a large, very diffuse (planar) group of galaxies, possibly with a few, loosely bound, sparse clusters to be found in it—has an interesting evolutionary history. This topic is explored in some detail in the next chapter.

As the analysis so far, apart from the Cox method, gives no indication of the amount of clustering in the Wall we turn now to the gravitothermodynamics equation of Crane and Saslaw (1986).

4.3.5 A gravitothermodynamics fit

Number counts of galaxies may be fitted by the probability distribution function

$$f(N) = e^{-\bar{N}(1-b)-Nb}\frac{\bar{N}(1-b)}{N!}\left[\bar{N}(1-b) + Nb\right]^{N-1} \tag{4.8}$$

of Saslaw (1986) to determine the degree of *relaxation* in a system, that is, how far a distribution of massive particles is from being in a gravitationally stable state. In equation (4.8), $f(N)$ is the probability of finding N galaxies in a volume V of arbitrary shape and

$$\bar{N} = \bar{n}V$$

is the average number of galaxies in the in the volume V for an average number density $\bar{n}$. The free parameter, b satisfies

$$b = -\frac{W}{2K}$$

which measures the degree of relaxation in terms of the ratio of gravitational correlation energy (W) to kinetic energy (K). (Large values of b correspond to a high degree of relaxation.)

The procedure for fitting equation (4.8) to 2-d data uses the values of O_i obtained from the second gridding of the Wall data (see page 75). The parameter b is obtained as follows: the chi-square statistic, obtained by comparing O_i (from the gridding data) with the expected value $E_i = f(i)$, is minimised with respect to b ($i = N$ in equation (4.8)). A program to achieve this is included in an appendix.

Results

Gridding	b	level
1.	.283	< 75%
2.	.276	< 50%
3.	.385	< 50%

The results of the above procedure are tabulated above. For example, the third gridding yields a value of 0.385 for b and is fitted by the gravitothermodynamic equation (equation (4.8) at the 50% confidence level; that is, there is less than a 50% chance that the gridding is inconsistent with equation 4.8.

Note that equation (4.8) reduces, in the limit when $b = 0$, to the Poisson distribution. Thus fitting the Wall to this equation is actually a refinement on determining the random nature of the data in the Wall. It also allows a measure of comparison with 3-d distributions: Crane & Saslaw (1986) find a value of $b = 0.70 \pm 0.05$ for the Zwicky catalogue which suggests, when compared with $b = 0.65 \pm 0.05$ from N-body simulations of hierarchical clustering, that the observed distribution in the Zwicky catalogue is mostly the result of (relaxed) gravitational clustering. The Wall is evidently even more relaxed (which is consistent with its very diffuse nature) and the values of b obtained for the Wall appear to be too low to indicate any kind of significant clustering, hierarchical or otherwise.

4.3.6 Tests of boundary effects

Because it is difficult to understand the significance of the above results without appreciating their range of validity the idea behind one more test will be outlined. The significance of this method is that it provides a means of graphically estimating the boundary effects in tests of the nature of any 2-d slice through a full 3-d distribution. In principle, this method is similar to the void probability function reviewed earlier.

Consider the probability $f(\omega)$ that a circle of radius ω, placed randomly on a plane of data (such as the Wall), has no galaxy within it. For a Poisson distribution

$$f(\omega) = \exp(-\pi\Sigma\omega^2) \tag{4.9}$$

is expected for a point density Σ (Ostriker & Strassler 1989). Equation (4.9) may be used as follows. Generate a Poisson distribution with the same Σ as the real data set to be studied. For both the Poisson distribution and the real data set determine the shape of $f(\omega)$ by executing the following algorithm.

1. For every ω in a discrete set of values between (ω_1, ω_2)
   (a) generate a set of N random positions in the plane. Then for each random position
      i. measure the distance to all the data points.
      ii. If no data point is found closer than ω then increment a counter N_0 of empty circles. If a data point is found within the ω limit then stop.
   (b) Repeat with the next random position.
2. Calculate $f(\omega) = \frac{N_0}{N}$.
3. Repeat this procedure for the next $\omega \in (\omega_1, \omega_2)$

Thus two discrete sets of values of $f(\omega)$ may be obtained: one for the real data set and one for data generated by a Poisson process. These can be compared on a plot with equation (4.9) to determine both the Poisson nature of the real distribution, as well as the boundary effects that will occur in statistics calculated from a (pseudo)-Poisson point-pattern. Ostriker and Strassler use this approach to compare 2-d slices through their models of a universe with bubble topology (see chapter 6) with 2-d sections through Poisson-distributed data and the CfA "slice of the universe" (see figure 4.8).

Summary

Considerable evidence has been presented for the spatial data in the Wall region to be consistent with the Poisson distribution. Simple statistics, using a grid element size of

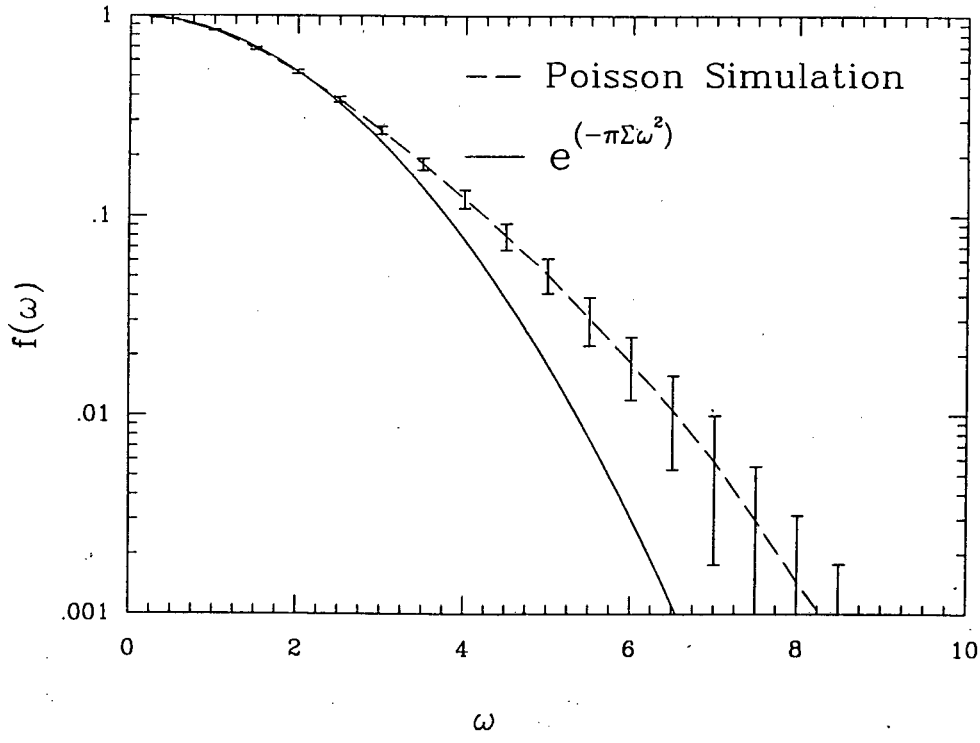

Figure 4.8: The values obtained for the $f(\omega)$ statistic from a sample distribution generated by a Poisson process (dashed line) may be compared with the expected functional form of equation 4.9 (solid line). Notice that the Poisson simulation shows a longer tail than the analytical formula due to boundary effects which cause a greater number of areas of lower surface density to be measured than would be the case for the theoretical average. If, in addition, $f(\omega)$ is determined for a real sample of the universe and the results are then superimposed on the graph, a measure of both the Poisson nature of the real sample and the severity of boundary effects can be obtained.

thickness 1200 km s^{-1} and area (in the plane of the Wall) 600 x 600 km^2 s^{-2} reveal that the Wall is 90% consistent with the Poisson distribution. Also, a method of Cox (1979) designed to find significantly under and over-dense regions in nearly Poissonian 2-d point patterns yields no evidence for significantly under-dense regions, ie. *holes* in the Wall.

Tests which indicate the presence of significant sub-structure reveal little evidence for a dispersed (regular) pattern in the Wall data (no more than 14% of the galaxies in the Wall constitute the regular component). Furthermore the Wall data is shown to be consistent with gravitothermodynamic theory from which the absence of any significant clustering in the Wall region may be inferred.

It has been further stressed that most of the above results are somewhat dependent on choice of grid spacing size and the placement of the grid. The errors incurred by the use of data near the boundary of the data on the Wall, and by the use of small number of points in the available data set still need to be accurately modelled using, for example, equation (4.9).

4.4 Conclusions

A detailed examination of an interface between two southern voids in FJ has been made with the aid of COELIS. The nature of the interface, which takes the form of a flat, sheet-like Wall between voids in Sculptor and Eridanus has been studied. When selection effects are considered in relation to the LV catalogue (from which much of the data has been drawn) it seems reasonable to assume that the Wall is not an artifact of selective under-sampling, but is a real structure. Although it appears to be remarkably diffuse, galaxies are distributed across the Wall in largely random fashion so that it appears to contain no significant holes in relation to its overall density.

For the six other void interfaces there are considerable problems of completeness for the data sets used to define the interfaces. On the basis of a study of only one part of the Sculptor void boundary no definite conclusions may be stated about the topology of this region. Thus alternatives are either that

1. most of the voids are presently so well-defined by their boundaries that they serve merely to support a sponge topology, or
2. that there is a real sparseness of data in void interfaces, from which it may be speculated that, given time, sufficient data will delineate similar complete wall structures at void interfaces other than at the site of the Wall, so supporting a Swiss cheese structure.

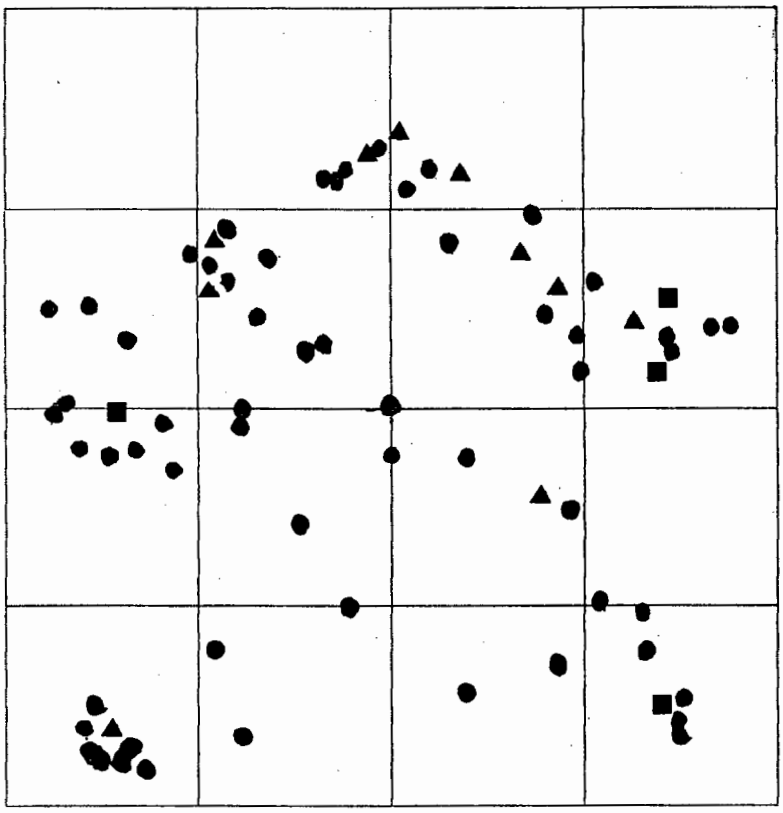

Figure 4.9: This (third) gridding of the Wall is used as the data set for all the methods of statistical analysis discussed in this chapter. It is also used to produce gravitothermodynamics parameters for the Wall. Data points have been removed either because they are nearer to the boundary than to any other point (to minimise boundary effects) or because they are occur in FJ but not in LV. Triangles indicate SO galaxies, boxes ellipticals, the rest are spirals (and one irregular). SO-type galaxies do not appear to be distributed in a strongly correlated fashion.

Methods of graphically viewing and statistically analysing 2-d slices through the 3-d distribution have really been the essence of this chapter. A number of simple yet useful statistical and computational tools for such analysis have been presented. If one considers the availability of 2-d slices of the universe (eg. de Lapparent *et al.* 1986, da Costa *et al.* 1988, Geller & Huchra 1989) with well-understood controls, the methods outlined above may be of considerable use in yielding information on the nature of 2-d subsets of the 3-d distribution. Because of their planar nature, void boundaries and walls lend themselves rather well to this combination of statistics and computer-assisted visual interpretation. The planar nature of these structures is also useful in providing the natural basis for a study of gradients of properties. This is the subject of the next chapter.

Chapter 5

Segregation effects as a cosmogonic indicator

"You must understand the galaxies before you can get the geometry right."
(attributed to Walter Baade (Sandage 1987))

The evidence in favour of a very flat, sheet-like Wall between the Sculptor and Eridanus voids has been presented. Perhaps the processes behind void formation may be understood when void boundaries such as the Wall are examined, the assumption being that the make-up of a void boundary contains some trace of the formation histories of the surrounding voids. Conversely, the existence of a void boundary presents a criterion in the observational data that a successful cosmogonical theory must explain. A further reason for studying the Wall is to ascertain the contribution of galaxy peculiar velocities to the measurements of redshifts in the Wall. These issues beg the main question which is: If the Wall is a real entity then what physical processes contributed to its formation?

5.1 Thermal histories

If it is assumed, on the basis of the evidence presented in chapters one and two, that the lacunary structure is real, (ie. that void sub-structure is statistically significant in the sense that voids have a frequency that cannot be explained simply by random selection effects), then the following issue arises: any distinct feature in the observed distribution must be the product of distinct thermal histories.

More specifically, if a spatially uniform distribution of proto-galaxies evolves uniformly,

then the distribution has the same equation of state and the same density and entropy variations, with respect to the proper times along each of the world lines. Subsequently a uniform distribution of physical properties should result. This is the *postulate of uniform thermal histories* (or PUTH) (Bonnor & Ellis 1986). Conversely, a distribution of galaxies which displays a non-uniform distribution of physical properties is necessarily a region where non-uniform thermal histories have occurred.

One application of PUTH is the possibility that a redshift feature in a survey might exhibit some variation, of physical properties, that correlates with the inhomogeneity in redshift space. If there is a significant correlation then either:

1. the variation of properties with position has been caused by stellar evolution effects or galaxy interaction effects, eg. ram-pressure stripping or galactic cannibalism (Postman & Geller 1984 and Dressler 1984), *subsequent* to galaxy formation, or
2. the inhomogeneity *pre-dates* or is simultaneous with galaxy formation, in which case variations in the physical properties of galaxies might depend on the local over- or under-densities that evolve, during the galaxy formation epoch, into clusters and under-dense regions.

The crucial difference between these two cases involves the different scales at which galaxies and clusters emerge from the homogeneous background (see figure 5.1). If galaxies emerge before features form then the only way a redshift feature could display a non-zero gradient of properties is as a result of environmental effects. If these can be ruled out then it may be concluded, for the first case, that there will be no variation of galaxy properties through-out the feature. Then in order to explain the presence of such a feature, some mechanism must be found to encourage galaxies, after they have formed, to coalesce into redshift features. One such mechanism is a class of explosion scenario (Ostriker & Strassler 1989) in which shells of already-formed galaxies flow away from nearby early-universe explosion sites and intersect. The region of intersection will thus appear as a redshift inhomogeneity only at the present epoch.

In the second case certain features of large-scale structure will emerge before galaxies are formed, say at the scale of cluster-mass pancakes (see also later discussion). This will be followed by galaxy formation with the result that galaxies within a pancake will have undergone quite different thermal histories to those which formed in the low-density region surrounding the pancake (because the initial conditions will differ). Thus if the second case listed above is true then non-zero gradients of galaxy properties, across a pancake, might be expected, and the thermal histories of the galaxies in a void will be different from those of the galaxies in the surrounding boundary.

Of course the above arguments rest on the assumption that all galaxies will start off with uniform properties and features if they form from the same initial conditions. Thus

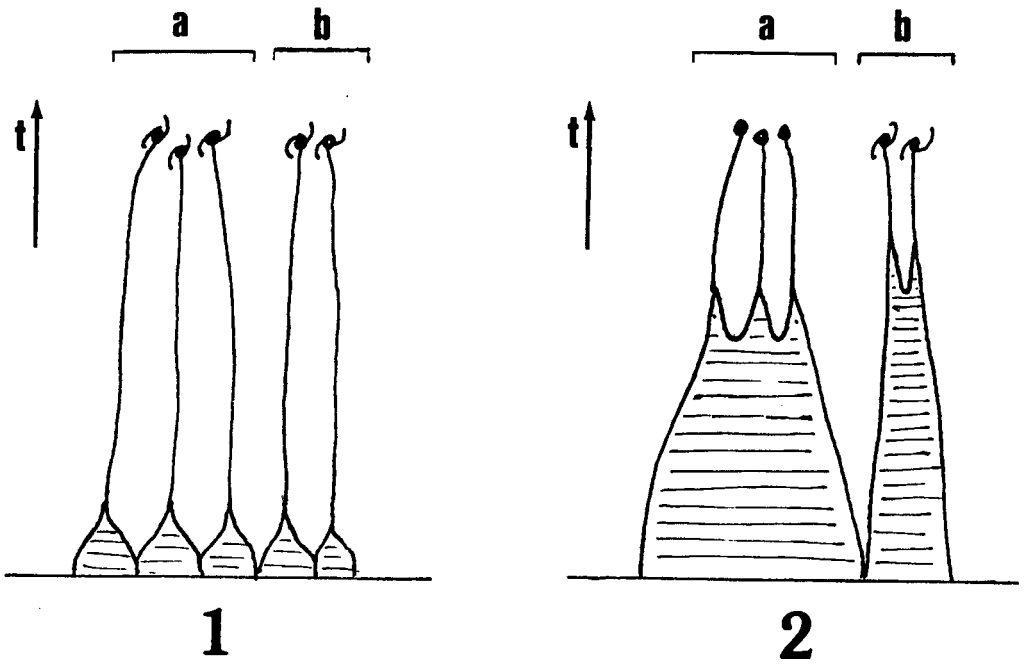

Figure 5.1: If galaxies formed before redshift features (a) and (b) emerged, as in case (1), then the galaxies which constitute both features will have undergone uniform thermal histories, unless interaction between some of the galaxies has occurred. (In the case of the Wall this is unlikely due to its very diffuse nature). Alternatively, if sub-structure at the cluster mass scale emerges before galaxies form, as in case (2), then redshift features have already set in by the time galaxies emerge, in which case the distribution of galaxy properties for the region containing both the features should be non-uniform. This follows from the converse of PUTH; non-uniform thermal histories may be expected for galaxies in the region because the galaxies have evolved from different initial conditions.

whatever the initial conditions are that lead to the production of many galaxies in void boundaries but few in voids, they must also lead to some other variation of properties (such as surface brightness, morphology, etc.) at the transition between high- and low-density regions. In the context of the present study, if a (relatively) high density of galaxies in the Wall and a low density of galaxies in the surrounding voids correlates with some other kind of feature that distinguishes between the two regions, then the Wall must be a product of non-uniform thermal histories.

One of the aims of this chapter is to use segregation effects to classify the thermal histories of galaxies in the Wall region into one of the above two cases. The question of probable formation scenarios of void sub-structure in the Wall region, within the context of PUTH, will then be addressed. Because of the low density nature of the region—the Wall is so diffuse as to have a collapse time of the order of the Hubble time[1]—environmental effects as a result of galaxy interactions may be overlooked. Furthermore if, after galaxy formation, the effects of stellar evolution on the gross physical properties of the galaxies are taken to be negligible[2], then the first case listed above cannot apply. Thus any evidence for non-uniform thermal histories of galaxies in the Wall region will serve to support case (2) above, namely that the Wall pre-dates galaxy formation, and that galaxies reach the non-linear growth phase after the cluster-size pertubations have already done so.

5.2 Segregation effects

As discussed in chapter 4 some 61 galaxies in the region of the Wall are listed in Maurellis *et al.* (1990) along with some of their known characteristics (eg. morphological type, position angle) listed in FJ. This data on the Wall has been supplemented by an additional 30 redshifts most of which have been taken from LV which, as discussed in chapter 2, contains a wealth of information on galaxy properties. Table 5.5 contains a listing of the combined database. It must be noted that all 91 galaxies are used for the least-squares fit procedure to be discussed in section 5.2.1, whereas only galaxies in LV are used in the cluster analysis of galaxy properties to be described (on the basis that this group of galaxies forms a photometrically controlled sub-sample of galaxies in the Wall—see chapter 4).

[1]This is calculated from the collapse time t_c of a region of mass density ρ related by $t_c = 1.43/(G\rho)^{0.5}$ (Gunn & Gott 1972).

[2]Dressler (1984) points out that gas-free disk systems and ellipticals have probably had little star formation within the last several billion years.

5.2.1 The extent of the Wall

A least-squares planar fit to all of the 91 galaxies in the supplemented Wall data set has been carried out: the Wall is best fitted by a plane, with centroid (2577, 136, -1890), that satisfies

$$2.31x - 1.14y - 2.16z = 10^4$$

(using the coordinate system set up in chapter 2). The results of this fit differ little from the fit to the original Wall data set (with 61 galaxies) carried out with graphical methods (discussed in chapter 4). Even though the supplemented Wall contains 50% more data than the original Wall, the planar structure has not disappeared, but instead appears even better defined: $20 \times 20 \times 5.3\ h^{-3}$ Mpc^3.

The parameters of the planar fit yield a means of dividing the cubical Wall region into sub-regions: the Wall *proper* within 1σ of the best-fit plane to the Wall, and the Wall *neighbourhood*, outside the 1σ cutoff points (hereafter labelled by P and N respectively, see also table 5.5). Thus galaxies in the Wall neighbourhood could be interpreted as lying within the voids for which the Wall forms the interface. Figure 5.5 contains casement display views of the Wall in coordinates rotated to position the x-y plane in the bottom left-hand corner. The 1σ region is indicated, in all three views, by means of dashed lines.

5.2.2 Cluster analysis

The block clustering program 3M in the statistical package BMDP (BMDP Statistical Software Inc. 1988) has been used to determine significant clustering of galaxies in galaxy-property space (rather than 3-d space). The term *clustering* is used here to represent galaxies most similar to each other in terms of two or more physical properties (rather than in the sense of close spatial proximity). Galaxies are grouped into *blocks*—the analog of clusters in physical space—which have two or more of the following properties in common:

- morphological type,
- position angle (hereafter pa),
- $(B - R)_T$ integrated colour,
- intrinsic surface brightness μ_B.

All properties scale in terms of measurements set out in LV (see also chapter 2). In the case of data in the region of the Wall the 3M software finds five significant blocks (see table 5.1).

Table 5.1: Results of a BMDP block-cluster analysis of galaxies in the cubic region surrounding the Wall. The *rows* are blocks of galaxies with two or more of the properties indicated in common, in order of decreasing significance. Blank entries indicate properties which are not a common feature of galaxies in the corresponding block.

block	colour	pa	μ_B	morphology	P	N
1	1.0–1.4	30°–60°	21–22	spiral	48	22
2		120°–150°	20–21	lenticular	10	7
3	0.6–1.0	90°–120°			18	6
4		0°–30°	19–20	ellipticals	6	1

Table 5.2: Numbers of galaxies of a given morphological type in the Wall proper compared with the Wall neighbourhood.

Type		P	N
ELLIPTICALS		4	1
LENTICULARS		11	8
SPIRALS		35	20
IRREGULARS	+	3	1
in LV		53	30
in FJ	+	6	2
		59	32

The most significant[3] block in table 5.1 contains galaxies predominantly in the Wall proper: 70 galaxies make up the first block of predominantly spiral character. Of these, 48 are in the Wall proper; the remaining 22 are in the Wall neighbourhood. The second most significant block contains galaxies that happen to lie mostly in the Wall neighbourhood: 17 galaxies constitute this group of predominantly lenticular character (Hubble type S0) of which 10 are in the Wall proper and 7 are in the Wall neighbourhood. Table 5.3 summarises these results and gives the respective properties of the (overlapping) groups of galaxies in each of the blocks. For comparison, table 5.2 contains the populations of the two sub-regions.

[3]Unfortunately the cluster analysis program does not offer the user any adequate measure of significance, so this approach is useful only as a test of very significant clustering.

Clearly, position angle and morphological type are useful indicators of differences in the Wall region. From the percentage probability calculated in table 5.3 there appears to be a greater proportion of lenticulars out of the Wall proper than it. Thus there is evidence for morphological segregation in the Wall region:

- spirals lie predominantly in the Wall proper,
- lenticulars lie predominantly in the Wall neighbourhood.

Table 5.3: Morphological types and relative proportions of populations in the first two blocks of the BMDP cluster analysis (see table 5.1). Group 2 galaxies lie mostly in the Wall neighbourhood whereas group 1 galaxies are found predominantly in the Wall proper. (Note that the groups overlap to some degree, ie. that some of the galaxies are found in both groups.)

Groups:	1		2	
Types	P	N	P	N
ELLIPTICALS	4	1	0	0
LENTICULARS	8	4	7	6
SPIRALS	35	16	3	1
IRREGULARS	1	1	0	0
	48	22	10	7
total # of LV galaxies	53	30	53	30
%	91	73	19	23

From this it may be concluded that galaxies in the Wall region are the products of non-uniform thermal histories. In addition, an investigation of the positions of the lenticulars relative to the plane of the Wall reveals that all of the lenticulars in the Wall neighbourhood lie in the Sculptor void, but otherwise show no signs of spatial clustering in the plane of the Wall (see figure 4.9). This may even point to differences in the formation histories of the voids that are bounded, in part, by the Wall.

5.2.3 Profiles

Histograms of morphological type, surface brightness, magnitude and position angle, *each* with respect to position (ie. in the Wall vs. the Wall neighbourhood) have been investigated to obtain a simple measure of the significance of the segregation effects indicated by the cluster analysis. From amongst the above profiles the following results support segregation effects in the Wall:

- Position angles, of all galaxy types, in the Wall *neighbourhood* (see figure 5.2), appear distributed in a non-Poisson fashion—to the extent that a marked excess at 45° is suggested. The chi-squared test of Hawley & Peebles (1967) may be used to show that there a 90% probability that this profile is not a random alignment. By comparison, position angles in the Wall *proper* are more randomly spread (there exists a 40% probability that the latter distribution is not random). Furthermore, a Kolmogorov-Smirnov 2-sample test can be used to show that there is only a 20% chance that the two profiles are drawn from the same distribution.
- Surface brightnesses, of all galaxy types, in the Wall *neighbourhood* (see figure 5.3) lie in a significantly narrower range than those in the Wall *proper* (the two profiles disagree at the 90% level, using the Kolmogorov-Smirnov 2-sample test).

Thus evidence exists for galaxy orientation effects and luminosity segregation in the Wall region. Once again, there is evidence for differing thermal histories in the Wall region.

Finally, a distribution of morphological type with respect to position angle (after Djorgowski 1987) has also been investigated. This profile shows no significant correlation apart from the following: fourteen of the nineteen lenticular galaxies in the Wall sample have a position angle greater than 90° (see table 5.4). This is probably attributable to the difficulties inherent in observing position angles of lenticulars (Hawley & Peebles 1975).

Table 5.4: Position angles of spirals and lenticulars in the entire cubic region around and including the Wall.

Type	Position angle	
	$> 90°$	$< 90°$
SPIRALS	28	27
LENTICULARS	14	5

5.2.4 Segregation effects as an indicator of thermal histories

Because this analysis is based on small number, *a posteriori* statistics on one sample of the data, the preliminary nature of these findings must be stressed. Nevertheless there is good evidence for significantly different luminosity and position angle profiles between the two regions, and some evidence for an unusual gradient of morphological types through the Wall region. Hence there is evidence for significantly different thermal histories for galaxies in the Wall region. Consequently, there is further support for the existence of the *Wall as a*

real structure in the data.

5.3 Formation scenarios

Probably the most intuitively satisfying processes for forming sheet-like structures between voids may be found in the explosion scenario of Ostriker & Cowie (1981), and the cosmic string scenario of Perivolaropoulos & Brandenberger (1989). In the former, wall-like structures form on the impact of shock wave fronts receding from nearby explosion sites. The blasts may be driven by anything from known sources such as quasars, radio galaxies or supernova ejecta to more exotic sources such as superconducting cosmic strings. Alternatively, sheet sizes with dimensions such as those of the Wall may be obtained directly from certain cosmic string models. It is predicted that long, straight strings, moving at relativistic speeds through a neutrino-dominated universe (see later discussion on hot dark matter models) will accrete matter onto their wakes, thereby triggering galaxy formation. Although both of these models have aspects which are not consistent with some observational results the purpose of this section is to show that they are consistent with the kinds of thermal histories expected for galaxies in the Wall region.

5.3.1 Dark matter models

The question of whether or not the distribution of the luminous matter traces the mass content of the universe has been discussed in chapter 2. For instance, if a significant, non-luminous matter component exists at the present epoch then the history of large-scale structure formation has probably been considerably affected by the gravitational effects of *both* the non-luminous matter as well as the luminous matter. In such circumstances the observed distribution may be the result of *biased galaxy formation.* For example, galaxies may form more readily in the presence of other galaxies—so-called *autonomous biasing* (see Dekel 1987 and Rees 1987). Models of large-scale structure formation usually incorporate biasing in addition to the clustering resulting from hierarchical models in order to adequately explain the observed matter distribution.

Hierarchical clustering may occur in models with either hot or cold dark matter (hereafter HDM or CDM respectively). The term *cold* dark matter usually represents non-baryonic, weakly interacting massive particles (eg. magnetic monopole relics from an early inflationary epoch) although its meaning is sometimes stretched to describe protogalaxies, protostars and Jupiter-type objects[4]. An alternate type of hierarchical clustering is predicted for models with *hot* dark matter—the phrase is frequently used to refer to weakly-interacting,

[4]This kind of dark matter is more accurately described as baryonic dark matter (Peebles & Silk 1990).

high-energy (elementary) particle populations of early-universe origin (such as the neutrino for which a cosmic background at the present epoch is predicted, by big bang nucleosynthesis (Yang *et al.* 1984)).

Some CDM models appear to agree more closely with observations than do the HDM models (White 1987) but there is disagreement on this issue; Peebles & Silk (1990) propose that the general understanding of CDM models only appears to be better than that of HDM models because CDM models have been more extensively studied[5]. Furthermore it seems probable (Peebles & Silk 1990) that HDM models are more efficient at generating Wall-type features with the kind of segregation effects found above (lenticulars predominantly in the Wall neighbourhood). Of particular relevance to this study are the so-called 'top-down' clustering models with HDM, reviewed by Zel'dovic *et al.* (1982). In these models, all but the largest initial density pertubations are damped out, at early times, by the free-streaming of HDM. The result is that initial pertubations of cluster-size arise and then evolve by collapsing along one or more axes into flat (pancake) or thin (cigar) shapes, after which galaxy formation is initiated. Thus a scale of damping may be defined in terms of a *coherence length*—a length scale, $\lambda_{\rm min}$, below which pancake formation is improbable.

It is important to note that the advantages of CDM models are not disadvantages for HDM, nor is the converse true (Kofman 1986). Pancakes also occur in CDM models but at much smaller mass and length scales than in HDM models. Dekel & Aarseth (1984) find evidence that supercluster formation was preceded by galaxy formation. Thus a hybrid scenario is indicated: one in which both galaxy formation and galaxy clustering take place within cluster-mass pancake-fragments while the pancakes simultaneously gravitate together to form superclusters. In other words pancakes form at some intermediate scale in this model. In such a model it is clear that HDM and CDM clustering cannot be mutually exclusive. The role of biased galaxy formation in such a hybrid scenario will now be explored.

5.3.2 Biased galaxy formation

As discussed earlier, it is possible that models which include early-universe density pertubations such as explosions or cosmic strings, *in addition to* dark matter, may yield some of the observed properties of the universe. Because the effects of these pertubations may be superimposed on the purely gravitational effects of hierarchical clustering, they can be thought of as biasing mechanisms. Thus formation of structure in any model may be enhanced if the evolution of the above density pertubations is taken into account.

[5]For example, the following authors attempt to reproduce from their CDM models the 2-pt correlation functions obtained from observations: White *et al.* (1983), White *et al.* (1984), Davis *et al.* (1985), Frenk *et al.* (1985). To the best knowledge of the author there is no list of papers that offers quite the same coverage of HDM simulations, up to 1985, as do these key papers on CDM n-body simulations.

Early explosions

The explosion scenario begins with the formation of a bound stellar system before $z \simeq 100$. Such a stellar system may contain supermassive and hence short-lived stars (short-lived when compared to the Hubble time). The resulting supernova explosions might conceivably seed the intergalactic medium with adiabatic shock waves. Matter surrounding the explosion would be swept up by a "snow-plough" action into a rapidly travelling shell of protogalactic material. If the original energy ($\sim 10^{61}$ergs) was sufficient the matter content of the shock wave would build up to many times the matter contained in the seed explosion—a process called *explosive amplification* (Ostriker & Cowie 1981). Heat transfer in the shell would ultimately occur, leading to fragmentation of the shell into pancakes and, ultimately, galaxy formation. It is expected that this process repeats itself until about $z = 4$. Thus shock waves will sprout anew on the surfaces of many of the shells, especially since shell fragments of high mass ($\geq 10^{12} M_{\odot}$) will not be able to cool sufficiently. This is the process of formation of *detonation waves*—a hydrodynamics phrase used to describe shock waves which give rise to further shock waves (Bertschinger 1985).

After $z = 4$ explosions are expected to subside almost entirely. Later work by Vishniac *et al.* (1985) and Bertschinger (1985) extends this scenario to include heat transfer at all stages. In addition to including a number of other physical effects in a spherically symmetric explosion scenario these papers present numerical solutions of the hydrodynamics equations. They predict the formation of Lyα absorption clouds inside voids[6]—but obtain void radii of the order of $1h^{-1}$ Mpc which are too low to explain the sizes of some voids. The problem with this kind of modelling is to discern when the hydrodynamics picture breaks down and when fragmented shells overlap. The issue is considered, among others, by Fairall (1988) who points out that if galaxies formed before the impinging of adjacent, expanding shells then the galaxies ($\sim 10^{-3}$ void radii) would in most cases move past each other when the shells overlapped. Two possibilities for pancake collapse will now be briefly discussed.

Pancake collapse after shell-shell impact

Icke (1984) proposes an argument applicable to the development of void shapes after the explosion epoch has died away. As pancakes collapse (on the receding shells), they become more aspherical. The result is that the contained void becomes more spherical with time. This is the so-called *bubble theorem* of Icke & van de Weygaert (1987)—a result which is consistent with Bertschinger (1983) who points out that expanding shock fronts are stable to non-spherical pertubations.

[6]This is a result of relevance to an earlier discussion on whether or not luminous matter traces the total matter content.

If it is further assumed that the explosions occurred at roughly the same time and that interacting shells collide rather than pass through each other, then a space-filling tesselation—the so-called *Voronoi tesselation* of Icke & van de Weygaert (1987) and van de Weygaert & Icke (1989)—can be constructed. The tesselation represents the interaction surface of all the receding shells, the essential characteristic being that adjacent explosion centres are equidistant from an intermediate wall of the tesselation (see figure 5.4).

In this model of shell interaction pancakes form at the faces between the polyhedra of the tesselation. Each pancake proceeds to collapse along its shortest axis, a process which is accompanied by a simultaneous process of attraction towards the ends of the pancake. Thus pancakes are predicted to slowly empty towards regions of higher density (the lines of intersection of the void interfaces) which in turn empty in the direction of the highest density concentrations—the points at which the vertices of adjacent Voronoi polyhedra coincide. In fact, van de Weygaert & Icke (1989) give evidence in favour of identifying these high density concentrations with Abell clusters: when correlation functions[7] are determined for the Voronoi vertices a value of $r_0 \simeq 32\ h^{-1}$ Mpc is obtained which is at the upper limit of the range expected (Bahcall 1988) for Abell clusters.

Weinberg *et al.* (1989) use a similar model of what they term *filament* and *knot* development in the aftermath of an explosion scenario, to investigate the consequences for the cluster-cluster correlation function equations. If knots are identified with rich clusters, as above, then the VPF approach (see section 2.3.2) may be used to show that the probability of knots forming as a result of explosions is much greater than that of knots forming purely out of standard dark matter models. A best-fit power-law (equation 2.4) yields a correlation length of $r_0 \simeq 40h^{-1}$ Mpc , which is definitely in excess of the upper limit mentioned above. Thus even though the explosion scenario is probably not the most effective way of obtaining the amount of observed high-density clustering the above results do not rule out the role of explosions in the formation of low-density features such as void interfaces.

Pancake collapse before shell-shell impact

The issue of shell interaction due to overlap of shells of particulate matter, raised in Saarinen *et al.* (1987), is difficult to explore fully, due to the constraints on the accuracy and usefulness of n-body modelling (essentially computational constraints). Saarinen *et al.* use an Aarseth n-body code to evolve the results of explosions on three kinds of gravitating particles: galaxies, gas clouds (such as the Lyα absorbers mentioned above) and dark matter. Void radii $\sim 10\ h^{-1}$ Mpc are a predicted result of the simulations which display a foamy, or lacunary structure which appears quite consistent with observational maps.

[7] As this is used to find a cluster-cluster correlation length it comes as no surprise that it is larger than the galaxy-galaxy correlation length of $\sim 5h^{-1}$ Mpc discussed earlier.

Ostriker & Strassler (1989) model the foamy texture of the universe by an algorithm which generates void structure in the following way: galaxies are placed on the surfaces of expanding voids, or, in the case of overlapping voids, the galaxies are placed *at the ring of intersection* of the two voids. Survey maps for each simulation, much like the redshift slices presented in chapter 1, are generated. These yield a very good match between simulations and the real data for average void radii ($\simeq 13.5 \pm 1.5$) h^{-1} Mpc.

Cosmic strings

Another approach for explaining structure at void interfaces concerns the effects of cosmic strings on the formation of large-scale structure at early epochs. Borden *et al.* (1989) review the role of superconducting cosmic strings as well as explosions as progenitors of features in large-scale structure. In the standard nucleosynthesis scenario (Yang *et al.* 1984), all pertubations on the scale of galaxies are erased by neutrino free-streaming, assuming a HDM model with adiabatic density pertubations. As discussed earlier, galaxies would have to form by fragmentation of larger objects (such as clusters) in such a model. However early epoch, galaxy-sized pertubations survive in a HDM model with cosmic strings because these act as seeds that are not erased by neutrino-free streaming (Perivolaropoulos & Brandenberger 1989, Scherrer *et al.* 1989). Thus galaxies would form simultaneously with the redshift feature with which they are later associated.

In particular, the existence of sheets of galaxies of the dimension of the Wall is fairly consistent with sheet sizes ($5000 \times 5000 \times 500$ km^3 s^{-3}) obtained in cosmic string models with HDM (Perivolaropoulos & Brandenberger 1989). In these models, the wakes of long straight strings (of mass $\sim 10^{21}$ kg m^{-1}) which move at relativistic speeds, are expected to accrete matter onto sheets. Turok (1986) predicts, however, that string wakes are unlikely to have accreted more than about 20% of surrounding galaxies onto them so that sheets of galaxies formed in this way should not stand out very strongly in any redshift survey. Furthermore, a gradient of initial densities of matter is expected in the wake of a cosmic string, so the presence of a low-density feature such as the Wall seems to be quite consistent with a cosmic string in HDM model.

PUTH as a cosmogonic indicator

Hierarchical clustering models have been briefly discussed in an attempt to find large-scale structure formation models consistent with low-density features such as the Wall. A hybrid HDM and CDM model has been suggested to provide the context for discussing the biasing mechanisms of early-universe explosions and cosmic strings. Two kinds of explosion scenario have been examined; the difference lies in the order in which shell interaction and galaxy formation occurs. Although a scenario in which galaxy formation *precedes* shell interaction

agrees well with the observations (Saarinen *et al.* 1987, Ostriker & Strassler 1989) it does not provide features, at shell intersections, with the non-uniform thermal-history distribution that is characteristic of the Wall region.

Explosion scenarios in which galaxy formation *follows* shell interaction, on the other hand, are consistent with the existence of a non-uniform distribution of properties discovered in the Wall region, even though the results of such scenarios contradict current observations of dense clusters[8].

A non-uniform distribution of properties is also expected as a result of galaxy formation in the wakes of relativistic cosmic strings at early epochs. Out of the biasing mechanisms discussed so far it thus seems quite likely that the Wall is a relic of a cosmic string wake, untainted by any other cosmogonical processes, that triggered the seeds of galaxy formation near the end of the inflationary epoch. This would also explain why there has not been sufficient time since the formation of the Wall for any kind of significant collapse to occur.

5.4 Conclusions

In the last chapter the boundary between the voids in Eridanus and Sculptor—the so-called Wall—was presented as being extremely flat and relatively impermeable. As was pointed out such a feature could not be the result of Finger-of-God effects if only because the Wall is almost perpendicular to the line of sight. In this chapter evidence has been presented in favour of non-uniform thermal histories for galaxies in the Wall region. Considering the Wall's orientation the following question then arises: what are the alternatives for the shape of the Wall in real space?

Galaxies that lie in the Wall neighbourhood (ie. inwards towards the voids) in redshift space may be physically separated from galaxies in the Wall proper, but it could be that both sets of galaxies are not physically separated but have different velocities (as is the case with rich clusters of galaxies and the associated Finger-of-God effects). On the other hand, this separation could be reversed: some of the galaxies in the Wall proper, in redshift space, may be physically displaced from its plane. The first case would be remarkable in implying an even tighter distribution of galaxies than we have already supposed (because it would require that the Wall be even narrower than redshift measurements suggest). The second seems unreasonable in the light of the diffuse nature of the Wall. The simplest hypothesis consistent with the concept of differing thermal histories would thus be the alternative possibility that there are quite distinct classes of galaxies, ie. those within the Wall and

[8] *Note added in proof*: It appears, from hydrodynamics simulations by Yoshioka & Ikeuchi (1990), that a wall-like feature between two interacting voids in which galaxy formation follows shell interaction is not stable. Thus the existence of a wall remnant at the present epoch is definitely not indicated in this scenario.

those in the Wall neighbourhood, in real, physical space.

Clearly the real shape of the Wall can be unambiguously determined only by application of independent distance measures to the galaxies in the sample. However, either of the above interpretations still has to account for the *prima facie* evidence in favour of differing thermal histories for galaxies in and out of the Wall in redshift space. This in itself provides evidence for the reality of the Wall as something more than just a random alignment of redshifts.

The use of the postulate of uniform thermal histories (PUTH) as a cosmogonic indicator has been one of the aims of this chapter. Using this approach the existence of the Wall has been shown to be consistent with cosmic strings in HDM models or a class of explosion scenario in a CDM/HDM hybrid. Furthermore, models in which uniform thermal histories should arise are excluded at (approximately) the 80% confidence level.

Putting aside the range of applicability of PUTH, it is rapidly becoming a simple matter to isolate vast regions in maps of large-scale structure that contain various kind of planar densities (such as those mentioned in chapter 2). Thus it may be useful to study gradients of properties through these and other diffuse structures. With detailed and well-understood catalogues such as the Lauberts & Valentijn (1989) catalogue becoming more easily available astronomers are in a position to use the rich, new data sources to understand more about the physics of the formation processes of large-scale structure than, merely, its spatial distribution properties.

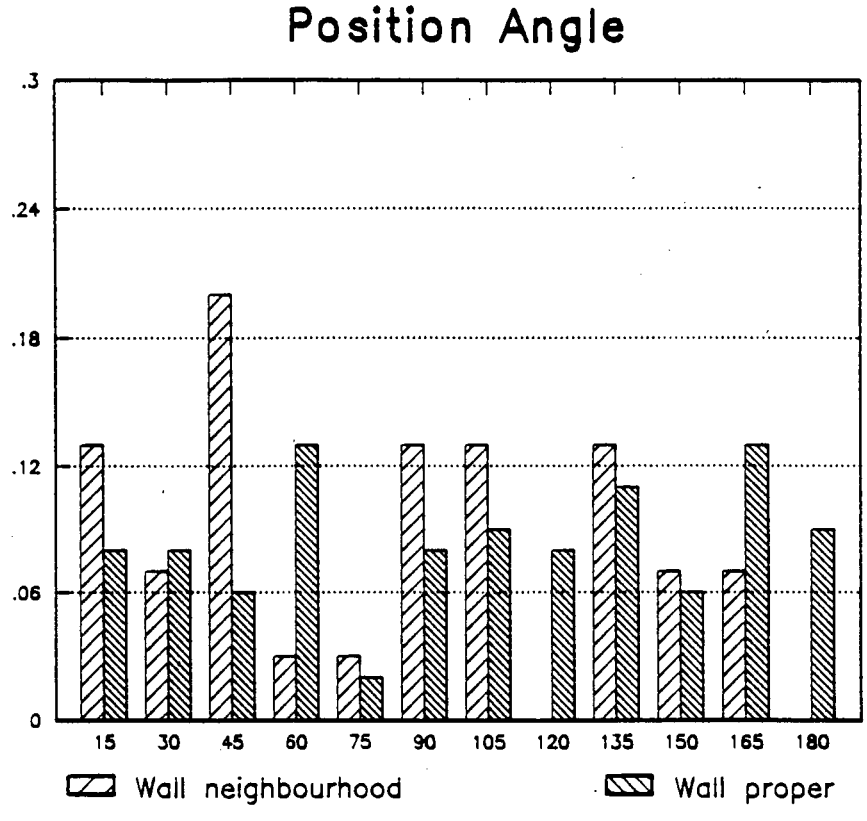

Figure 5.2: Position angles for galaxies in the data subsets of the Wall neighbourhood and the Wall proper, in bins normalised to the total number of galaxies in each of the data sub-sets (see table 5.2). A random spread would yield an average height of 0.07. Clearly the former distribution deviates considerably from a random spread.

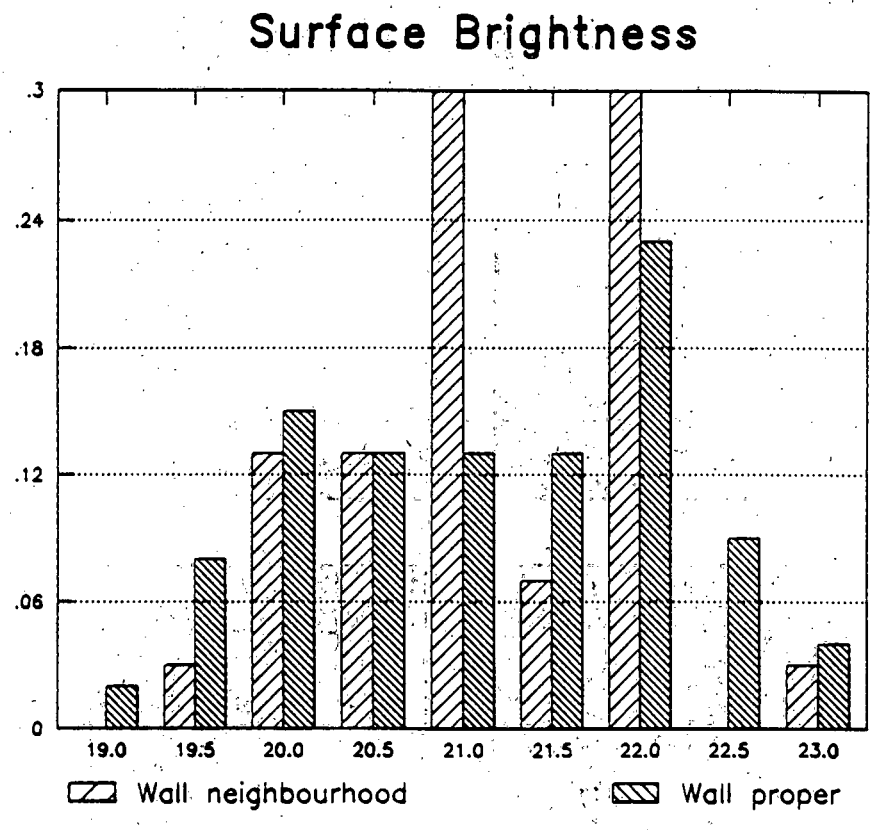

Figure 5.3: Surface brightness μ_B (vertical axis) for galaxies in the Wall neighbourhood and in the Wall proper, in bins normalised to the total number of galaxies in each of the data sub-sets (see table 5.2). Both distributions have a mean of about 20.8 but the standard deviation for the Wall proper is 50% larger than for the Wall neighbourhood. Clearly the two distributions differ significantly from one another.

Table 5.5: Properties of galaxies in the Wall region (see chapter 5) are found in the leftmost section of the tables. Apart from redshift (in km s^{-1}) all other quantities scale in terms of measurements set out in LV. Of interest is morphological type: ellipticals $[-5, -2.5)$, lenticulars $[-2.5, 0.5)$, spirals $[0.5, 8.5)$ and irregulars $[8.5, 10.0)$. Columns headed P/N and dist denote the position of the galaxy in either of the Wall proper or Wall neighbourhood subsets and the distance from the best-fit plane. Designations are as follows: N or I denote NGC or IGC objects, 7-digit numbers denote objects in LV, other labels (eg. CH-2, AQUER78) are taken from FJ. Right ascension (α) and declination (δ) are in 1950 coords.

morph	redshift	app.mag	μ_B	colour	pa	P/N	dist	designation	α	δ
3.6	3204	14.75	20.92	0.91	38.8	N	- 222	3450210	22 29 44	-38 18.4
5.3	2849	14.52	21.87	0.94	141.0	P	111	2890480	22 37 59	-45 55.3
7.6	3070	14.07	21.67	0.93	38.3	P	163	6030060	22 40 05	-21 25.7
-5.0	3050	13.48	19.86	1.34	28.4	P	160	N 7365	22 42 28	-20 12.9
6.5	3113	13.66	21.73	1.08	108.0	P	92	5340240	22 42 32	-22 59.6
3.6	2385	13.16	20.48	1.77	130.0	N	590	N 7368	22 42 40	-39 36.4
8.0	3047	14.74	21.96	1.12	96.0	N	226	6030120	22 43 24	-19 40.7
-1.0	3351	11.39	19.29	0.86	101.0	P	- 60	N 7377	22 45 05	-22 34.6
4.5	2343	14.61	21.73	1.01	65.0	N	632	3460010	22 45 42	-39 54.9
8.0	3171	14.74	21.54	0.80	53.0	P	- 100	6030200	22 48 20	-20 32.0
3.0	3268	12.61	20.08		123.0	P	87	N 7392	22 49 08	-20 52.4
4.0	2919	13.62	20.73	0.98	2.0	P	9	N 7400	22 51 27	-45 36.8
6.0	3452	13.91	21.69	1.01	59.6	P	- 68	I 5261	22 51 44	-20 37.8
9.0	2926	14.63	22.18	0.86	35.0	P	134	4060230	22 53 08	-36 36.0
	3150					P	- 172	F 614	22 54 19	-48 03.0
-1.0	2272	13.48	19.96	1.42	50.4	N	876	I 5269	22 54 57	-36 17.6
2.0	2952	13.57	20.39	1.03	175.0	P	34	N 7476	23 02 22	-43 22.1
-5.0	2743	12.79	19.72	1.53	28.6	N	293	N 7484	23 04 19	-36 32.7
0.3	3779	14.41	19.36	0.95	122.9	N	- 599	4690140	23 04 44	-28 05.2
	2463					N	743	CH-2	23 09 50	-21 47.5
1.0	2812	14.36	20.52	0.77	159.0	P	212	3470030	23 12 08	-38 07.8
3.0	2102	13.84	20.56	0.94	80.0	N	901	N 7545	23 12 48	-38 48.5
	2100					N	902	AQUER78	23 13 00	-38 47.3
5.0	2757	13.48	20.61	1.01	40.0	N	295	4070140	23 14 54	-35 03.9
3.0	2843	13.96	20.54		43.0	N	483	I 5321	23 23 43	-18 13.8
-1.0	4113	14.69	21.56	1.26	161.0	N	- 796	2910280	23 30 33	-45 18.2
-2.5	3136	12.21	19.06	1.38	39.8	P	- 86	I 5328	23 30 35	-45 17.6
7.0	3111	15.04	22.36	0.81	169.0	P	- 75	2910300	23 31 17	-45 29.3
1.0	3093	15.05	20.90	0.67	24.0	P	- 57	2910320	23 32 01	-46 29.0
-2.0	3152	12.97	19.95	1.40	119.0	P	- 74	N 7702	23 32 42	-56 17.2
5.0	2980	13.30	21.38	0.78	76.9	P	96	3470300	23 34 30	-37 59.5
7.0	2918	15.32	22.63	0.90	85.0	P	162	4080120	23 34 55	-37 16.4
-2.0	3195	12.49	19.18	1.34	133.0	P	- 106	2400100	23 35 03	-47 46.9
4.8	2817	13.05	20.31	1.35	129.0	P	218	2400110	23 35 06	-48 00.2
3.0	3178	14.09	20.92	1.10	178.0	P	- 171	2400130	23 36 46	-48 03.0
-2.0	3098	12.50	18.94	1.51	101.6	P	- 30	N 7744	23 42 24	-43 11.3
4.5	2968	12.10	19.76	0.98	20.0	P	218	N 7755	23 45 18	-30 48.0
1.0	3070	14.81	20.67	1.15	85.0	N	232	4720060	23 51 30	-25 44.0
6.0	3240	15.26	22.22	0.86	20.0	P	- 125	2930120	23 52 20	-40 51.5
-5.0	3318	12.36	19.16	1.54	50.0	P	- 187	N 7796	23 56 25	-55 44.1
3.2	3573	15.10	20.61	0.89	85.0	N	- 358	3490160	23 57 07	-34 44.0
4.0	3160	14.40	21.10	1.00	153.0	P	- 4	2930270	23 57 55	-40 45.7

morph	redshift	app.mag	μ_B	colour	pa	P/N	dist	designation	α	δ
5.0	3190	13.53	21.52	1.09	38.0	N	363	5390050	00 14 38	-19 34.7
10.0	3603	14.70	21.30	0.69	14.6	N	- 409	N 87	00 18 48	-48 54.4
-0.3	3533	15.11	20.89	0.91	145.0	N	- 344	N 88	00 18 55	-48 55.1
0.3	3824	14.28	20.42	1.30	148.0	N	- 614	N 89	00 18 57	-48 56.6
1.0	3498	13 71	20.29	1.31	144.2	P	- 134	N 92	00 19 05	-48 54.2
6.0	3400	14.00	21.14	0.97	47.0	P	- 29	1940130	00 20 09	-48 51.5
6.0	3400	13.36	21.04	1.05	83.7	P	- 69	N 101	00 21 24	-32 48.8
	3500					N	- 288	F-653	00 24 51	-47 37.3
1.0	3000	15.45	21.44		15.0	P	176	1940200	00 25 56	-49 21.2
3.0	3351	13.92	20.70	1.10	153.0	N	304	5400030	00 33 10	-20 24.1
0.0	3470	13.82	20.84	1.27	152.0	P	- 11	N 174	00 34 30	-29 45.2
6.0	3553	14.00	21.51	0.85	83.0	N	- 296	2420180	00 34 44	-46 55.1
3.0	3930	12.95	20.42	1.22	108.6	P	- 105	N 175	00 34 52	-20 12.7
	3420					P	- 89	G353719	00 35 00	-37 19.0
1.3	3892	14.14	20 00	1.14	9.0	P	- 185	N 177	00 35 06	-22 49.4
1.0	3604	15.12	20.95	0.99	165.0	P	- 107	4110020	00 35 30	-29 11.9
8.0	3319	14 19	21.90	0.78	141.0	P	- 85	2420200	00 35 40	-46 47.6
3.0	3886	14 92	21.53	0.98	97.0	P	- 226	I 1561	00 36 04	-24 36.9
5.0	3633	13.56	20.54	1.03	49.2	P	- 17	I 1562	00 36 06	-24 33.0
-3.5	3931	13.91	19.61	1.38	9.5	P	- 83	N 209	00 36 34	-18 53.1
7.0	3431	16.81	21.73	0.41	53.8	P	- 154	2420220	00 36 42	-43 21.3
3.0	3927	14.65	21.08	1.28	165.0	P	- 88	5400090	00 36 51	-19 11.6
5.0	3962	13.91	21.21	0.97	128.0	N	- 694	2420230	00 36 52	-43 21.0
6.0	3991	15.60	22.40	0.99	131.0	P	- 184	5400100	00 37 05	-20 39.5
	3992					P	- 142	—	00 37 36	-20 20.3
-1.3	3657	14.58	20.89	1.46	39.0	N	- 371	2420240	00 38 10	-46 15.6
	4500					N	- 942	G403335	00 40 54	-33 35.0
3 0	4113	14.83	21.53	0.87	98.0	N	- 243	5400190	00 43 29	-20 52.9
-2.0	3437	14.06	19.81	1.49	93.8	P	- 66	N 324	00 54 55	-41 13.7
-0.5	3463	13.70	20.06	1.88	170.0	P	29	I 1608	00 57 00	-34 35.9
4.7	3658	14.61	21.46	0.88	80.0	P	- 37	3510280	00 57 08	-36 27.4
1.0	3929	14.62	19.99		45.0	N	- 358	3520060	01 05 01	-37 01.3
7.0	3558	14.38	21.84	1.08	129.0	P	- 77	3520150	01 08 00	-36 00 1
0.0	3496	13.76	20.19	1.38	60.0	P	175	N 424	01 09 10	-38 20.9
2.5	3454	13.63	19.94	1.22	126.4	P	58	N 438	01 11 16	-38 10 0
3.8	3564	13.16	20 18	1.14	170.8	P	66	I 1657	01 11 47	-32 54.9
9.0	3772	14.65	21.75	1.30	130.0	P	57	4750140	01 13 10	-26 42.8
5.5	3059	15.31	21.88	1.07	0.0	N	436	3520360	01 15 34	-36 34.5
8.0	3614	14.32	21.88	0.91	102.0	P	66	3520460	01 17 46	-34 09.8
10.0	3825	15.42	22 35	0.56	73.0	P	- 133	3520470	01 18 16	-34 23.0
3.0	3898	13.28	19.94	1.46	93.0	P	- 184	N 491	01 19 02	-34 19.5
-2.0	3551	14.28	19.92	1.28	157.3	P	113	3520550	01 19 14	-33 25.1
-1.0	3150	14.41	20.25	1.40	3.8	N	271	N 576	01 26 55	-51 51.4
4.0	3651	13.99	22.76	0.91	115.1	P	3	2960380	01 30 15	-38 56.2
-1.0	3841	14.50	21.98	1.25	164.0	P	- 10	3530140	01 31 44	-34 38.6
-2.0	3626	15.13	21.91	1.36	19.0	P	183	3530360	01 41 04	-34 27.4
3.0	3299	13.30	21.69	1.33	3.0	N	644	I 1783	02 07 57	-33 10.5
-2.0	3250	13.45	22.71	1.14	92.2	N	742	N 857	02 10 26	-32 10.7
	3230					N	611	—	02 11 30	-32 04.2

References

Abell, G.O.: 1958, *Astrophys. J. Suppl.*, **3**, 211

Abell, G.O.: 1965, *Ann. Rev. Astron. Astrophys.*, **3**, 1

Aubert, J.H., Kraynik, A.M., Rand, P.B.: 1986, *Scientific American*, **254**, 58

Bahcall, N.A.: 1988, *Ann. Rev. Astron. Astrophys.*, **26**, 631

Bardeen, J.M., Bond, J.R., Kaiser, N., Szalay, A.S.:1986, *Astrophys. J.*, **304**, 15

Barrow, J.D., Bhavsar, S.P.: 1987, *Quart. J. Roy. Astr.*, **28**, 109

Bertschinger, E.: 1983, *Astrophys. J.*, **268**, 17

Bertschinger, E.: 1985, *Astrophys. J.*, **295**, 1

Bhavsar, S.P., Barrow, J.D.: 1984, in *Clusters and Groups of Galaxies*, eds. F. Mardirossian, M. Giuricin, M. Mezzetti, Reidel, Dordrecht, p.415

Bhavsar, S.P., Barrow, J.D.: 1983, *Monthly Notices Roy. Astron. Soc.*, **205**, 61p

Bhavsar, S.P., Ling, E.N.: 1988a, *Astrophys. J. Lett.* **331**, L63

Bhavsar, S.P., Ling, E.N.: 1988b, *Publ. Astron. Soc. Pacific*, **100**, 1314

Binggeli, B.: 1987, in *Proc. 8th Santa Cruz Summer School*, , ed S.M.Faber, Springer (New York) p.195

Binggeli, B., Sandage, A., Tammann, G.A.: 1985, *Astron. J,* **90**, 1681

BMDP Statistical Software Inc. Manual Vol.2: 1988, ed W.J.Dixon, Univ. of California Press, Berkeley, 767

Bonnor, W.B., Ellis, G.F.R.: 1986, *Monthly Notices Roy. Astron. Soc.,* **218**, 605

Borden, D., Ostriker, J.P., Weinberg, D.H.: 1989, *Astrophys. J.,* **345**, 607

Bothun, G.D., Beers, T.C., Mould, J.R., Huchra, J.P.: 1986, *Astrophys. J.,* **308**, 510

Broadhurst, T.J., Ellis, R.S., Koo, D.C., Szalay, A.S.: 1990, *Nature,* **343**, 726

Chambers, J.M., Cleveland, Kleiner, Tukey: 1983, *Graphical Methods for Data Analysis,* Wadsworth International

Chincarini, G.: 1978, *Nature,* **272**, 515

Chincarini, G.: 1983, in *IAU Symp. 104* , eds. G. Chincarini, G.O. Abell, Reidel, Dordrecht, p.159

Clarke, P.J., Evans, F.C.: 1954, *Ecology,* **35**, 445

Coleman, P.H., Pietronero, L., Sanders, R.H.: 1988, *Astron. Astrophys.,* **200**, L32

Cox, T.F.: 1979, *Applied Statistics,* **28**, 14

Crane, P., Saslaw, W.C.: 1986, *Astrophys. J.,* **301**, 1

da Costa, L.N., Pellegrini, P.S., Sargent, W.L.W., Tonry, J., Davis, M., Meiksin, A., Latham, D.W., Menzies, J.W., Coulson, I.A.: 1988, *Astrophys. J.* , **327**, 544

da Costa, L.N., Pellegrini, P.S., Willmer, C.: 1989, *Astrophys. J.,* **344**, 20

Davis, M., Efstathiou, G., Frenk, C., White, S.D.M.: 1985, *Astrophys. J.,* **292**, 371

Davis, M., Geller, M.J.: 1976, *Astrophys. J.,* **208**, 13

Davis, M., Huchra, J.: 1982, *Astrophys. J.*, **254**, 437

Davis, M., Huchra, J., Latham, D.W., Tonry, J.: 1981, *Astrophys. J.*, **253**, 423

Davis, M., Peebles, P.J.E.: 1983, *Astrophys. J.*, **267**, 465

Dekel, A., Aarseth, S.J.: 1984, *Astrophys. J.*, **283**, 1

Dekel, A.: 1987, in *Proc. 8th Santa Cruz Summer School*, , ed S.M. Faber, Springer (New York) p.244

de Lapparent, V., Geller, M.J., Huchra, J.P.: 1986, *Astrophys. J.* **302**, L1

Dickey, J.M.: 1988 in *Minnesota Lectures on Clusters of Galaxies and Large-scale Structure* ed. J.M. Dickey., Astron. Soc. of the Pacific, p.9

Diggle, P.J.: 1983, *Statistical Analysis of Spatial Point Patterns,* Academic Press, New York

Djorgowski, S.: 1987, in *Nearly Normal Galaxies Proc. 8th Santa Cruz Summer School*, ed S.M. Faber, Springer, New York, p.227

Dressler, A.: 1980, *Astrophys. J.*, **236**, 351

Dressler, A.: 1984, *Ann. Rev. Astron. Astrophys.*, **22**, 185

Dressler, A., Faber, S.M., Burstein, D., Davies, R.L., Lynden-Bell, D., Terlevich, R.J., Wegner, G.: 1987, *Astrophys. J.*, **313**, L37

Einasto, J., Jôeveer, M., Saar, E.: 1980, *Monthly Notices Roy. Astron. Soc.*, **193**, 353

Einasto, J., Klypin, A.A., Shandarin, S.F.: 1983, in *IAU Symp. 104* eds. G. Chincarini, G.O. Abell, Reidel, Dordrecht, p.265

Einasto, J., Klypin, A.A., Saar, E., Shandarin, S.F.: 1984, *Monthly Notices Roy. Astron. Soc.*, **206**, 529

Einasto, M.: 1989, in *Morphological Cosmology Proc. XIth Cracow Cosmological School*, eds P .Flin, H.W. Duerbeck, Springer, Berlin, p.134

Ellis, G.F.R.: 1987, UCT pre-print 10/87

Ellis, G.F.R.: 1988, UCT pre-print 88/1

Ellis, G.F.R., Fairall, A.P., Maurellis, A., Matravers, D.R.M.: 1988, in *Large Scale Structures of the Universe, IAU Symp. 130* ed. J. Audouze, M. Pelletan, A. Szalay, Reidel, Dordrecht, p.531

Ellis, G.F.R., Perry, J.J., Sievers, A.W.: 1984, *Astron. J.*, **89**(8), 1124

Fairall, A.P.: 1984, *Monthly Notices Roy. Astron. Soc.*, **210**, 69

Fairall, A.P.: 1984, *A Catalogue of Galaxies South of Declination -30°*, Publ. Dept. Astr. Univ. Cape Town, No.**6** (also 1985 extended version, Publ. No. 7)

Fairall, A.P.: 1987, *Monthly Notices Astron. Soc. South Africa,* **46**, 47

Fairall, A.P.: 1988, *Monthly Notices Roy. Astron. Soc.*, **230**, 69

Fairall, A.P.: 1989a, in *Morphological Cosmology Proc. XIth Cracow Cosmological School*, eds P. Flin, H.W. Duerbeck, Springer, Berlin, p.145

Fairall, A.P.: 1989b, in *Morphological Cosmology Proc. XIth Cracow Cosmological School*, eds P. Flin, H.W. Duerbeck, Springer, Berlin, p.197

Fairall, A.P. Jones, A.: 1988, *Southern Redshifts—Catalogue and Plots* Publ. Dept. Astr. Univ. Cape Town, No.**10**

Fairall, A.P., Maurellis, A., Jones, A., Kauffmann, G.K., Matravers, D.R., Ellis, G.F.R.: 1990, in *Large Scale Structures and Peculiar Motions in the Universe*, eds. D.W. Latham, L.N. da Costa (Astron. Soc. of the Pacific, Provo, in press)

Fairall, A.P., *et al.*: 1985, *Redshift Plots of Huchra's Z Catalogue*, Publ. Dept. Astr. Univ.Cape Town, No.**8**

Ferguson, H.C., Sandage, A.: 1990, *Astron. J.*, **100**(1), 1.

Frenk, C.S., White, S.D.M., Efstathiou, G., Davis, M.: 1985, *Nature*, **317**, 595

Friedmann, A.: 1922, *Zeit. Phys.*, **10**, 377

Fry, J.N.: 1985, *Astrophys. J.*, **289**, 10

Fry, J.N.: 1988, *Publ. Astron. Soc. Pacific*, **100**, 1336

Fry, J.N., Melott, A.L.: 1985, *Astrophys. J.*, **292**, 395

Geller, M.J., Huchra, J.P.: 1989, *Science*, **246**, 897

Giovanelli, R., Haynes, M.P., Myers, S.T., Roth, J.: 1986, *Astron. J.*, **92**, 250

Gott, J.R., Melott, A.L., Dickinson, M.: 1986, *Astrophys. J.*, **306**, 341

Gott, J.R., Miller, J., Thuan, T.X., Schneider, S.E., Weinberg, D.H., Gammie, C., Polk, K., Vogeley, M., Jeffrey, S., Bhavsar, S.P., Melott, A.L., Giovanelli, R., Haynes, M.P., Tully, R.B., Hamilton, A.J.S.: 1989, *Astrophys. J.* , **340**, 625

Gott, J.R., Weinberg, D.H., Melott, A.L.: 1987, *Astrophys. J.*, **319**, 1

Gregory, S.A., Thompson, L.A.: 1978, *Astrophys. J.*, **222**, 784

Groth, E.J., Peebles, P.J.E., Seldner, M., Soneira, R.M.: 1977, *Sci. American*, **237**(5), 76

Gunn, J.E., Gott, J.R.: 1972, *Astrophys. J.*, **176**, 1

Hamilton, A.J.S., Gott, J.R., Weinberg, D.H.: 1986, *Astrophys. J.*, **309**, 1

Hamilton, A.J.S., Saslaw, W.C., and Thuan, T.X.: 1985, *Astrophys. J.*, **297**, 37

Hawley, D.L., Peebles, P.J.E.: 1975, *Astron. J.*, **80**, 477

Haynes, M.: 1987, in *Nearly Normal Galaxies Proc. 8th Santa Cruz Summer School*, , ed S.M. Faber, Springer, New York, p.220

Haynes, M.P., Giovanelli, R.: 1986, *Astrophys. J.*, **306**, L55

Hoyt, W.G.: 1976, *Lowell and Mars*, Univ. of Arizona Press, Tucson

Hubble, E.P.: 1929, *Proc. of the National Academy of Sciences (Washington)*, **15**, 169

Hubble, E.P.: 1934, *Astrophys. J.*, **79**, 8

Hubble, E.P.: 1936, *The Realm of the Nebulae*, Yale

Hubble, E., Humason, M.L.: 1931, *Astrophys. J.*, **74**, 43

Huchra, J.P., Geller, M.J., de Lapparent, V., Corwin, H.G.: 1990, *Astrophys. J.*, **72**, 433

Huchra, J.P., Davis, M., Latham, D., Tonry, J.: 1982, *Astrophys. J. Suppl.*, **52**, 89

Icke, V.: 1973, *Astron. Astrophys*, **27**, 1

Icke, V.: 1984, *Monthly Notices Roy. Astron. Soc.*, **206**, 1p

Icke, V., van de Weygaert, R.: 1987, *Astron. Astrophys.*, **184**, 16

Ikeuchi, S.: 1981, *Pubs. Astr. Soc. Japan*, **33**, 211

Iovino, A., Chincarini, G., Giovanelli, R., Guzzo, L., Haynes, M: 1990 in *Proc. Workshop on Superclusters & Clusters of Galaxies & Environmental Effects*, Sesto-Moso, Italy, eds. Giuricin *et al.*, publ. by the eds. (SISSA, Trieste)

Irwin, M., McMahon, R.: 1990, *Gemini*, No.30, 6

Jôeveer, M., Einasto, U.: 1978, in *IAU Symp. 79*, p.241.

Kauffmann, G.M.: 1990, pre-print, Inst. Theor. Physics and Astrophysics, Univ. Cape Town

Kirshner, R.P., Oemler, A., Schechter, P.L., Schectman, S.A.: 1981: *Astrophys. J.*, **248**, L57

Kirshner, R.P., Oemler, A., Schechter, P.L., Schectman, S.A.: 1987, *Astrophys. J.*, **314**, 493

Kofman, L.: , in *Morphological Cosmology Proc. XIth Cracow Cosmological School*, eds P. Flin, H.W. Duerbeck, Springer, Berlin, p.354

Kraan-Kortweg, R.G.: 1980, *Astron. Astrophys. Suppl.*, **66**, 255

Lauberts, A.: 1982, *The ESO/Uppsala Survey of the ESO(B) Atlas*, European Southern Observatory

Lauberts, A., Valentijn, E.A.: 1989, *The Surface Photometry Catalogue of the ESO-Uppsala Galaxies*, European Southern Observatory

Matravers, D.R., Maurellis, A.: 1990, in *Large Scale Structures and Peculiar Motions in the Universe*, eds. D.W. Latham, L.N. da Costa (Astron. Soc. of the Pacific, Provo, in press)

Matsuda, T., Shima, E.: 1983, Kyoto University pre-print

Maurellis, A., Fairall, A.P., Matravers, D.R., Ellis, G.F.R.: 1990, *Astron. Astrophys.*, **229**, 75

Maurellis, A., Ellis, G.F.R., Fairall, A.P., Matravers, D.R.: 1991, in preparation for *Monthly Notices Roy. Astron. Soc.*

Maurogordato, S., Lachièze-Rey, M.: 1987, **320**, 13

Medvedkov, Y.V.: 1966, *Izvestiya Akademii Nauk SSR, Seriya Geograficheskaya*, **4**, 110

Melott, A.L., Cohen, A.P., Hamilton, A.J.S., Gott, J.R., Weinberg, D.H.: 1989, *Astrophys. J.*, **345**, 618

Mo, H.: 1989 in *Cosmology & Grav. Lensing*, eds. G.Börner, T.Buchert, P.Schneider, publ. Max-Planck-Institut für Phys. & Astrophys., p.24

Nath, B.B, Eichler, D.: 1989, *Astrophys. J.* **337**, 1

Oemler, A.: 1987, in *Nearly Normal Galaxies Proc. 8th Santa Cruz Summer School*, ed S.M. Faber, Springer, New York

Okamura, S.: 1989 in *Proc. Workshop Dark Matter & Structure of the Universe*, Hiroshima University pre-print RRK 89-28

Oort, J.H.: 1970, *Astron. Astrophys.*, **7**, 381

Oort, J.H.: 1983, *Ann. Rev. Astron. Astrophys,* **21**, 273

Ostriker, J.P., Bajtlik, S., Duncan, R.C.: 1988, *Astrophys. J. Lett.,* **327**, L35

Ostriker, J.P., Cowie, L.L.: 1981, *Astrophys. J.,* **243**, L127

Ostriker, J.P., Strassler, M.J.: 1989, *Astrophys. J.,* **338**, 579

Otto, S., Politzer, D., Preskill, J., Wise, M.B.: 1986, *Astrophys. J.,* **304**, 62

Peebles, P.J.E.: 1973, *Astrophys. J.,* **185**, 413

Peebles, P.J.E.: 1974, *Astrophys. J.,* **189**, L51

Peebles, P.J.E.: 1980, *The Large-Scale Structure of the Universe* , Princeton Univ. Press, Princeton

Peebles, P.J.E., Drake, R.H.: 1968, *Astrophys. J.,* **154**, 892

Peebles, P.J.E., Silk, J.: 1990, *Nature*, **346**, 233

Pellegrini, P.S., da Costa, L.N., de Carvalho, R.R.: 1989, **339**, 595

Perivolaropoulos, L., Brandenberger, R.H.: 1989, Brown University pre-print BROWN-HET-711

Postman, M., Geller, M.J.: 1984, *Astrophys. J.,* **285**, 95

Rees, M.J.: 1985, *Monthly Notices Roy. Astron. Soc.,* **213**, 75p

Rees, M.J.: 1987, in *Nearly Normal Galaxies Proc. 8th Santa Cruz Summer School,* , ed S.M. Faber, Springer, New York, p.256

Robertson, H.P.: 1935, *Astrophys. J.,* **82**, 284

Rood, H.J.: 1988, *Ann. Rev. Astron. Astrophys.,* **26**, 245

Rowan-Robinson, M.: 1978, *Cosmology,* , Clarendon, Oxford, p.103

Rubin, V.C., Ford, W.K., Jr., Thonnard, N., Burstein, D.: 1982, *Astrophys. J.*, **261**, 439

Rudnicki, K: 1989, in *Morphological Cosmology Proc. XIth Cracow Cosmological School*, eds P.Flin, H.W. Duerbeck, Springer, Berlin, p.418

Saarinen, S., Dekel, A., Carr, B.J.: 1987, *Nature*, **325**, 598

Sandage, A.:1987, in *Observation Cosmology, IAU Symp. 124*, eds. A. Hewitt, G. Burbidge, L.Z. Fang, Reidel, Dordrecht, p.13

Santiago, B.X., da Costa, L.N.: 1990, *Astrophys. J.*, **362**, 386

Saslaw, W.C.: 1985, *Gravitational Physics of Stellar and Galactic Systems*, Cambridge Univ. Press, p. 245

Schaeffer, R.: 1984, *Astron. Astrophys.*, **134**, L15

Schechter, P.: 1976, *Astrophys. J.*, **203**, 297

Scherrer, R.J., Melott, A.L., Bertschinger, E.: 1989, *Phys. Rev. Lett.*, **62**, 379

Shane, C.D., Wirtanen, C.A.: 1967, *Publ. Lick Observatory*, **22**, Part 1

Shaver, P.A., Iovino, A., Pierre, M.: 1988, in *Large Scale Structure and Motions in the Universe* , SISSA, Trieste, eds. G. Giuricin *et al.*, (in the press)

Siegel, S.: 1956, *Nonparametric Statistics*, McGraw-Hill, New York, p.47ff, p.127ff, p.156ff

Sky and Telescope: 1988, **76**, 601

Slezak, E., Bijaoui, A., Mars, G.: 1990, *Astron. Astrophys.*, **227**, 301

Soneira, R.M., Peebles, P.J.E.: 1978, *Astron. J.*, **83**845

Szalay, A.: 1990, in *Large Scale Structures and Peculiar Motions in the Universe*, eds. D.W. Latham, L.N. da Costa (Astron. Soc. of the Pacific, Provo, in press)

van de Weygaert, R., Icke, V.: 1989, *Astron. Astrophys.*, **213**, 1

van den Bergh, S.: 1990, *Astrophys. J.*, **348**, 57.

Vishniac, E., Ostriker, J.P., Bertschinger, E.: 1985, *Astrophys. J.*, **291**, 399

Vittorio, N.: 1988, in *Large Scale Motions in the Universe–Vatican Study Week*, eds. V.C. Rubin, G.V. Coyne, Princeton

Walker, A.G.: 1936, *Proc. London Math. Soc.(2)*, **42**, 90

Weinberg, D.H., Ostriker, J.P., Dekel, A.,: 1989, *Astrophys. J.*, **336**, 9

West, M.J.: 1989, *Astrophys. J.*, **344**, 535

White, S.D.M.: 1979, *Monthly Notices Roy. Astron. Soc.*, **186**, 145

White, S.D.M., Frenk, C.S., Davis, M.: 1983, *Astrophys. J. Lett.*, **271**, L1

White, S.D.M., Davis, M., Frenk, C.S.: 1984, *Monthly Notices Roy. Astron. Soc.*, **209**, 27p

Winkler, H.: 1983, *Monthly Not. Astron. Soc. of Southern Africa*, **42**, 74

Yang, J., Turner, M., Steigmann G., Schramm, D., Olive, K.:1984, *Astrophys. J.*, **281**, 493

Yoshioka, S., Ikeuchi, S.: 1990, *Astrophys. J. Lett.*, **360**, 352

Zel'dovic, Y.B.: 1970, *Astron. Astrophys.*, **5**, 84

Zel'dovic, Y.B., Einasto, J., Shandarin, S.F.: 1982, *Nature*, **300**, 407

Zwicky, F., Herzog, E., Wild, P., Karpowicz, E., Cowal, C.T.: 1961–8, *Catalogue of Galaxies and of Clusters of Galaxies*, 6 volumes, Pasadena: Calif. Inst. of Technology

Appendix A

Misc programs

Gravitational relaxation

```
rem Testing of relaxation of a gravitating system
rem after a formula of Crane & Saslaw (1986)

dim f(0:15)
declare def fact
let nbar = 72 / 16          ! first gridding
let q = 16                  ! number of squares

for b = 0.2 to .4 step .01
mat f = (0)
let fsum = 0
for r = 0 to 15        ! 15 is enough for convergence
  let f(r) = exp(-nbar*(1-b)-r*b) * nbar*(1-b)/fact(r)
  let f(r) = f(r) * (nbar*(1-b) + r*b)^(r-1)
  let fsum = fsum + f(r)
next r
let a = q / fsum       ! normalisation factor
restore
let chisq = 0
for r = 0 to 15
  read or
  let chisq = chisq + (a*f(r) - or)^2/a/f(r)
next r
print b, chisq
```

```
next b

!data 22, 22, 7, 5, 3, 4, 1, 0,0,0,0,0,0,0,0,0   ! from first gridding
!data 1, 1, 2, 2, 1, 2, 1, 2, 3, 1, 0,0,0,0,0,0  ! from second gridding
data 2, 1, 1, 2, 2, 2, 1, 2, 2, 1, 0,0,0,0,0,0  ! from third gridding

def fact(n)
let p = 1
for i = 1 to n
  let p = p * i
next i
let fact = p
end def
end
```

Cox contour maps

```
rem Density contour mapping based on a method devised by Cox
rem Set up for the Wall

dim event(1:2, 1:81), r(0:15, 0:15, 1:22), d(2:22), s(2:22), temp(1:81)

let irange = 15
let jrange = 15
let lambda = 81/2400^2
let total = 81      ! see dims above
let scrn = 1200
let size = scrn/50
for i = 1 to 10
  read entry
next i
for i = 2 to 22
  read entry
  let d(i) = entry
next i
for i = 2 to 22
  read entry
  let s(i) = entry
next i

input prompt "Input galaxy-file name : ": picname$
  let picname$ = "c:" & picname$ & ".gal"
```

```
  open #9 : name picname$, access input, create old, org text
  let i = 1
    do while more #9
      line input #9 : pic$
      let event(1,i) = val(pic$[18:18]&str$(val(pic$[19:22])))
      let event(2,i) = val(pic$[26:26]&str$(val(pic$[27:30])))
      let i = i + 1
   loop
  close #9

  open #1 : screen 0, 1, 0, 1
  set window -scrn * 1.25, scrn * 1.25, -scrn, scrn
  let i = 1
  do
    let x = event(1, i)
    let y = event(2, i)
    plot x, y
    box circle x - size*.75, x + size*.75, y - size*.75, y + size*.75
    let i = i + 1
  loop until i = total
  let total = i
  close #1
  get key zz
  set mode ("text")

rem Calculate r_j for each grid point
clear
print "Please wait while distances are calculated..."
for i = 0 to irange
  for j = 0 to jrange
    let k = 0
    mat temp = (1e30)        ! must calculate all distances,
    do                       !    n selects later
      let k = k + 1
      let x = i * 2 * scrn / irange - scrn
      let y = j * 2 * scrn / jrange - scrn
      let temp(k) = ((x - event(1,k))^2 + (y - event(2,k))^2)
    loop until k = total
    call quicksort(temp(), k)
    for l = 1 to 22
      let r(i, j, l) = temp(l)
    next l
  next j
next i
```

```
print
print "Ready to plot contour points"
get key zz

rem Calculate and display T_n for each grid point, for each n
open #1: screen 0,1,0,1
set window -scrn * 1.25, scrn * 1.25, -scrn, scrn
restore
do
  clear
  read n
  let b1 = (n * (n + 1) * (2 * n + 1) / 6)^(-.5)
  let b2 = -(n * (n + 1) / (2 * n + 1) * 3 / 2)^(.5)
  for i = 0 to irange
    for j = 0 to jrange
      let x = i * 2 * scrn / irange - scrn
      let y = j * 2 * scrn / jrange - scrn
      box circle x - size, x + size, y - size, y + size
      let t = 0
      for k = 1 to n
        let t = r(i, j, k) + t
      next k
      let t = b1 * lambda * pi * t + b2
      if t <= d(n) then
        flood x, y
      else if t > d(n) and t < s(n) then
        plot x - size, y ; x + size, y
        plot x, y - size ; x, y + size
      end if
    next j
  next i
  get key zz
loop until zz = 113 or n = 10
get key zz

data 2, 3, 4, 5, 6, 8, 10, 12, 17, 22
!rem Data for alpha = .025
!data -1.19, -1.30, -1.37, -1.43, -1.47, 0, -1.53, 0, -1.57, 0, -1.60
!data 0,0,0,0, -1.66, 0,0,0,0, -1.69
!data 2.57, 2.50, 2.46, 2.42, 2.40, 0, 2.35, 0, 2.31, 0, 2.28
!data 0,0,0,0, 2.24, 0,0,0,0, 2.21

rem Data for alpha = .05
data -1.13, -1.20, -1.26, -1.30, -1.32, 0, -1.36, 0, -1.39, 0, -1.42
data 0,0,0,0, -1.45, 0,0,0,0, -1.48
```

```
data 1.95, 1.92, 1.90, 1.89, 1.87, 0, 1.85, 0, 1.84, 0, 1.82
data 0,0,0,0, 1.80, 0,0,0,0, 1.78

end


sub QUICKSORT( list(), upperbound )

rem Quicksort sorts the array 'list' into ascending order.
rem Original algorithm by C A R Hoare.
rem This routine created on 11 August 1987
rem by A Maurellis

dim s( 0:50 ), f( 0:50 )        ! sufficient for ten thousand entries
let d = 0
let s( d ) = 1
let f( d ) = upperbound
let start = s( d )
let fin = f( d )
call sort
sub sort
call partition
let d = d + 1
if pvp - start >= fin - pvp then
  let s( d ) = start
  let f( d ) = pvp - 1
  let start = pvp + 1
else
  let s( d ) = pvp + 1
  let f( d ) = fin
  let fin = pvp - 1
end if
if start < fin then
  call sort
end if
let start = s( d )
let fin = f( d )
if start < fin then
  call sort
end if
let d = d - 1
end sub

sub partition
let pvp = int( ( start + fin ) / 2 )
```

```
let pv = list( pvp )
let left = start
let right = fin
do
  do while left <= fin and list( left ) <= pv
    let left = left + 1
  loop
  do while list( right ) > pv
    let right = right - 1
  loop
  if left < right then
    let temp = list( left )
    let list( left ) = list( right )
    let list( right ) = temp
    if list( left ) = pv then let pvp = left
    if list( right ) = pv then let pvp = right
  end if
loop until left = right + 1
let temp = list( right )
let list( right ) = pv
let list( pvp ) = temp
let pvp = right
end sub

end sub
```

Appendix B

Coelis

Gratias agimus tibi, propter magnan gloriam tuam

```
rem FUNCTIONS
rem To work on galaxy catalogs, to extract suitable data,
rem to save the data for later use, and to perform histogram checks.
rem Also to present graphics representations of galaxy data and to fit
rem using least-squares methods to a plane.

rem created by A Maurellis. Coelis 3.0 completed 15/12/90

dim pt(1:3, 1:5500)          ! 1 to 3 correspond to x, y, z
dim r(1:5500), oct(1:5500)
let maxdatano = 5500         ! Change this when changing the dims. above
dim cocentre(1:3), realcentre(1:3), deltareal(1:3), range(1:3)
dim sliceposn(1:3), galtot(1:3), horcursor(1:3), vertcursor(1:3)
dim corner(1:3), number(1:8), numbertot(1:8)
dim radcursor(1:3), longcursor(1:3), dl(1:2)
dim runresults(1:40, 1:10)
dim fitresults(10)
dim histos(1:8, -10:40)
dim centres(1:3, 1:6)          ! 1 to 3 correspond to x, y, z
dim v1(1:3), v2(1:3)           ! transform to these new vectors
dim ptsub(1:3, 1:700)          ! subset of pt for ellipsoidal fit
dim octlimit(1:8)              ! bounds of ptsub
dim res(1:700)                 ! residuals in ellipsoidal fit
```

```
library "graphlib"
library "fntlib.trc"          ! Trigonometric functions (radians)
declare def cot, sec, csc, asin, acos, acot, asec, acsc
declare def projx, projy      ! Equal-area projection
declare def arctan            ! Returning correct arctan angles

rem Fixed centre info
let no_centres = 6             ! Change centres above too
data t, c, e, m, s, r
data 0, 0, 0
data 4750, -950, -3100
data 2000, 500, -1350
data 2000, -2700, -2100
data 650, -800, -700
data 1000, 1150, -2900
for i = 1 to no_centres
  read qu$
next i
for i = 1 to no_centres
  read centres(1, i), centres(2, i), centres(3, i)
next i

rem Galaxy Catalogue Format
let lname_col = 25
let rname_col = 53
let lra_col = 1
let rra_col = 8
let ldec_col = 10
let rdec_col = 16
let lglong_col = 1          ! glong = galactic longitude
let rglong_col = 7
let lglat_col = 9           ! glat = galactic latitude
let rglat_col = 15
let lv_col = 18              ! v = cz
let rv_col = 23
let end_col = 59

let v_lim0 = 0                !
let v_lim1 = 5000             !       S A M P L E
let phi_lim0 = 20             !   D A T A    L I M I T S
let phi_lim1 = 4              !         F O R
let theta_lim0 = -90          !          F J
let theta_lim1 = 45           !

let devicein$ = "c:"
let deviceout$ = "c:"
let format$ = "-----#.## "

do
```

```
  call menu(choice$)
  when error in
    if choice$ = "e" then call extractbub
    if choice$ = "l" then call loadbub
    if choice$ = "h" then call histo
    if choice$ = "g" then call casementgrid
    if choice$ = "f" then call fitting
    if choice$ = "c" then call calc
    if choice$ = "d" then call changedevice
    if choice$ = "t" then call transformdata
    if choice$ = "p" then call densityplots
  use
    set mode "text"
    clear
    . "ERROR !!!!!!!!!!!!!!!!!!"
    print "Start again........"
    print "(Press any key to continue) "
    get key zz
  end when
loop until choice$ = "q"


!    FIN    !


sub fitting   !!!!! Least-squares menu
do
  clear
  print "Fitting to a plane using least squares"
  print "--------------------------------------"
  print "Fitting data            (f)"
  print "Returning to main menu  (m)"
  print "What is your choice ";
  input choice$
  if choice$ = "m" then exit sub
  if choice$ = "f" then call fit
loop until choice$ = "m"
end sub

sub fit      !!!!! Least-squares procedure
mat runresults = 0
print "NB: Run your trial centre through histograms first."
print "Trial centre so far :-"
print xc, yc, zc
input prompt "Output to screen, printer or disk file (0/1/2) : " : op
  if op = 1 then
    print "Output on printer."
    open #1 : printer
  else if op = 2 then
    print "Output on disk."
```

```
    input prompt "Fit output file name :" : fop$
    let fop$ = deviceout$ & fop$ & ".fop"
    open #2 : name fop$, org text, create newold, access output
    erase #2
    close #2
  end if
  input prompt "Distribution plots ? (y/n) " : qu$
  let ll = 0
  let i = 0
    call leastsq(pt,fitresults,suitable_gals,xc,yc,zc,res,(5000),op,fop$,ffeed)
    let galsinvoid = 0
    let galsinwall = 0
    let se = fitresults(7)^2
    for ll = 1 to suitable_gals
      if res(ll) > - se then
        if res(ll) < se then
          let galsinwall = galsinwall + 1
        end if
      else if res(ll) <= - se then
        let galsinvoid = galsinvoid + 1
      end if
    next ll
    let galsinbubl = galsinvoid + galsinwall
    let galsoutside = gals_ptsub - galsinbubl
      if op = 2 then
        open #2 : name fop$, org text, create newold, access output
        set #2: pointer end
      end if
      print #op: "Galaxies in void = " ; galsinvoid
      print #op: "Galaxies in wall = " ; galsinwall
      print #op: "Galaxies outside = " ; galsoutside
      if op <> 0 then close #op
      if qu$ = "y" then    ! print distribution plots
        call histogram(op,(.04),(-.2),(.2),suitable_gals,
                       histos,res,oct,maxdensity,(1),fop$)
      end if
      if op = 0 then get key zz
end sub


sub densityplots
clear
print "Density plots for generated histograms"
print "--------------------------------------"
print "NB: This choice only applies once histograms have been generated"
print
do
  print "Enter the value for dr used in the last histogram : "
  input dr
  input prompt "Happy ? (y/n)" : qu$
```

```
loop until qu$ = "y"
print
print "Use  ""SPACE BAR"" to toggle between views 2 1  and 6 5 ,"
print "                                          3 4      7 8  "
print "and ""Q""to quit."
print "Press any key to continue..."
get key zz
open #1 : screen .5, 1, .5, 1
open #2 : screen 0, .5, .5, 1
open #3 : screen 0, .5, 0, .5
open #4 : screen .5, 1, 0, .5
rem  1.25 seems to be a good aspect ratio for the Bondwell.
for i = 1 to 4
  window #i
  set window -250 * 1.25, maxradius * 1.25, -5, maxdensity + 5
next i
let dr = dr / 2
let zflag = 0
do
  for ll = 1 to 4
    window #ll
    clear
    call frame
    call ticks(500, 10)
    plot text, at maxradius - 300, 52 : str$(ll + zflag)
    for r0 = 2 * dr to maxradius step 2 * dr
      let hbin = int(r0/2/dr)
      call point(r0,histos(ll+zflag,hbin)
                          /((r0+dr)^3-(r0-dr)^3)*1e10, 50, .5)
    next r0
    plot
  next ll
get key zz
if zz = 32 then
  if zflag = 0 then
    let zflag = 4
  else
    let zflag = 0
  end if
end if
loop until zz = 113
close #4
close #3
close #2
close #1
end sub

sub histo
clear
print "Histogram generator for a trial centre"
```

```
print "---------------------------------------"
if bubblefile$ = "" then
  print "Newly created bubble-data, or no bubble-data in memory."
else
  print "Bubble-file " ; bubblefile$[3:10] ; " in memory."
end if
print "Data chunk limits:"
print "-----------------"
print "v goes from: " ; v_lim0 ; " to " ; v_lim1
print "longitude   : " ; phi_lim0 ; " to " ; phi_lim1
print "latitude    : " ; theta_lim0 ; " to " ; theta_lim1
print "Co-ord centre so far : " ;
mat print cocentre
print "Real centre so far : " ;
mat print realcentre
print "Previous centre : " ; xc, yc, zc
if xc = 0 and yc = 0 and zc = 0 then
  input prompt "Trial centre in rectangular co-ords ? (y/n) " : qu$
  if qu$ <> "y" then call calc
end if
input prompt "Input centre for 'gram/skyview check as
                                        x, y, z : " : xc1, yc1, zc1
print "Trial centre    : " ; xc1, yc1, zc1
print "Extreme radial distances of the bubble data : "
if (xc <> xc1 or yc <> yc1 or zc <> zc1) or
                        (xc1 = 0 and yc1 = 0 and zc1 = 0) then
  let xc = xc1
  let yc = yc1
  let zc = zc1
  print "    Largest  (from the previous  centre) " ; rmax
  print "    Smallest (from the previous  centre) " ; rmin
  print "         Closest galaxy was in oct : " ; octrmin
  let rmax = 0
  let rmin = 1e10
  for i = 1 to suitable_gals
    if pt(3, i) >= zc then let oct(i) = 0 else let oct(i) = 4
    if pt(2, i) >= yc then
      if pt(1, i) < xc then let oct(i) = oct(i) + 1
      let oct(i) = oct(i) + 1
    else
      if pt(1, i) >= xc then let oct(i) = oct(i) + 1
      let oct(i) = oct(i) + 3
    end if
    let r(i)=((pt(1,i) - xc)^2 + (pt(2,i) - yc)^2 + (pt(3,i) - zc)^2)^.5
    if rmax < r(i) then let rmax = r(i)
    if rmin > r(i) then
      let rmin = r(i)
      let octrmin = oct(i)
    end if
  next i
```

```
end if
print "    Largest  (from this trial centre) " ; rmax
print "    Smallest (from this trial centre) " ; rmin
print "         Closest galaxy now in oct : " ; octrmin
print "There are" ; suitable_gals ; "suitable galaxies."
input prompt "To what radius should the 'gram/proj. extend : ": maxradius
input prompt "Suggest an initial value for the radial increment : " : dr
print
print
do
  clear
  print "Choose from:-"
  print "  Histogram to screen ..... (h)"
  print "  Histogram to printer ..... (p)"
  print "  Sky-map ..... (s)"
  print "  Exit ..... (q)"
do
  input prompt "What is your choice ? : " : qu$
loop until qu$ = "h" or qu$ = "p" or qu$ = "s" or qu$ = "q"
if dr = 0 and qu$ <> "q" then
  input prompt "Suggest again a value for dr : " : dr
end if
if qu$ = "h" or qu$ = "p" then
  if qu$ = "p" then
    let op = 1
    print "Output on printer, please wait a moment."
    open #1 : printer
  else
    let op = 0
    print "Please wait a while."
  end if
  do
    call histogram(op,dr,(0),maxradius,suitable_gals,histos,
                                                  r,oct,maxdensity,2,"")
    input prompt "Quit, new centre, or new radial increment ?
                                                    (0/1/new_dr) " : dr
    print
  loop until dr = 0 or dr = 1
  close #1
else if qu$ = "s" then
  open #2: screen 0, 1, 0, 1          ! equal-area projection here
  window #2
  set window 2 * sqr(2), -2 * sqr(2), -sqr(2), sqr(2)
  do
    window #2
    let dr = dr / 2
    let r0 = 0
    do
      window #2
      clear
```

```
for phi = pi to 0 step -pi/2
  for theta = pi/2 to 0 step -pi/10
    let xplot0 = projx(phi, theta)
    let yplot0 = projy(phi, theta)
    let xplot1 = projx(phi, theta - pi/40)
    let yplot1 = projy(phi, theta - pi/40)
    plot  xplot0,  yplot0 ;  xplot1,  yplot1
    plot -xplot0,  yplot0 ; -xplot1,  yplot1
    plot -xplot0, -yplot0 ; -xplot1, -yplot1
    plot  xplot0, -yplot0 ;  xplot1, -yplot1
  next theta
next phi
for phi = 2 * pi to 0 step -pi/5
  plot projx(phi, 0), 0 ; projx(phi - pi/40, 0), 0
next phi
plot text, at 2.7, -1.2 : str$(r0 - dr) & " -> " & str$(r0 + dr)
restore
for i = 1 to no_centres              ! plot centres of other voids
  read name$
  let rt = sqr((xc-centres(1,i))^2+(yc-centres(2,i))^2+
                                        (zc-centres(3,i))^2)
  if rt <> 0 then
    let thetat = pi / 2 - acos((centres(3, i) - zc) / rt)
    let phit = arctan(centres(2, i) - yc, centres(1, i) - xc)
    plot text, at projx(phit, thetat), projy(phit, thetat) : name$
  end if
next i
let galcounter = 0
for i = 1 to suitable_gals
  if abs(r(i) - r0) <= dr then
    let theta = pi / 2 - acos((pt(3, i) - zc) / r(i))
    let phi = arctan(pt(2, i) - yc ,  pt(1, i) - xc)
    let px = projx(phi, theta)
    let py = projy(phi, theta)
    plot px, py
    let galcounter = galcounter + 1
    if zz = 110 then
      print #6 : str$(galcounter); " : " ; str$(i) ; " : " ,
      print #6 : px, py
      plot text, at px, py: str$(galcounter)
    end if
  end if
next i
plot text, at -2.4, -1.2 : str$(galcounter)
get key zz
if zz = 110 then
  let galname$ = deviceout$ & "r="
  let galname$ = galname$ & str$(r0) & ".gal"
  open #6 : name galname$, org text, access output, create newold
  erase #6
```

```
        print #6 : "Galaxies in slice @ " ; str$(r0)
        print #6 : "Thickness =" ; 2*dr
        print #6
      end if
      if zz = 101 or zz = 110 then
        get key zz
        if zz = 115 then
          box keep left, right, bottom, top in picture$
          let picname$ = deviceout$ & "r="
          let picname$ = picname$ & str$(r0) & ".pic"
          open #10 : name picname$,access output,create newold,org text
            erase #10
            print #10 :  picture$
          close #10
        end if
        let zz = 101
      end if
      if zz = 44 and r0 >= 2 * dr then let r0 = r0 - 2 * dr
      if zz = 46 then let r0 = r0 + 2 * dr
      if zz = 100 then
        open #4 : screen .5, 1, .5, 1
        window #4
        clear
        print "Current value of step length is " ; 2 * dr
        input prompt "New value ? " : dr
        let dr = dr / 2
        close #4
      end if
    loop until zz = 113
    set mode "text"
    print "Present centre:-"
    print xc, yc, zc
    input prompt "Quit, new centre, or different
                          radial increment ? (0/1/new_dr) " : dr
  loop until dr = 0 or dr = 1
  close #2
  close #6
end if
loop until dr = 1 or qu$ = "q"
if dr = 1 then call histo

end sub


sub casementgrid
clear
print "Graphics centering : Casement displays"
print "-------------------   ------------------"
print "File " ; bubblefile$ ; " in memory "
print
if cocentre(1) = 0 and cocentre(2) = 0 and cocentre(3) = 0 then
```

```
  mat input prompt "Input the co-ord centre as x, y, z : " : cocentre
else
  print "Previous co-ord centre : " ;
  mat print cocentre
  print "The real centre so far : " ;
  mat print realcentre
  do
    print"Do you wish to use the previous or the real centre, or new " ;
    input prompt "co-ords (p/r/n) : " : qu$
  loop until qu$ = "p" or qu$ = "r" or qu$ = "n"
  if qu$ = "r" then mat cocentre = realcentre
  if qu$ = "n" then
    mat cocentre = 0
    exit sub
  end if
end if
mat range = 0
for i = 1 to suitable_gals
  for ll = 1 to 3
    if range(ll) < abs(pt(ll, i) - cocentre(ll)) then
      let range(ll) = abs(pt(ll, i) - cocentre(ll))
    end if
  next ll
next i
print "The data set covers a region, in the x, y, z directions of : "
mat print range
input prompt "What is the greatest general range of interest ?" : maxrange
input prompt "Increment : " : ds
let ds = ds / 2
print "Graphics options reminder:"
print "--------------------------"
print "No CAPS or NUM or SCROLL locks."
print "X  Y  Z  :  x, y, z -view selection     0    :  start/restart view"
print "  <  >   :  decr/incr slice posn        Q    :  quit graphics"
print "   C     :  activate cursor           Enter  :  deactivate cursor"
print "   D     :  change step length          R    :  change range"
print "   E     :  enlarge a view              S    :  save enlarged view "
print "   N     :  print galaxy nos."
print "(Hit any key when ready ...)"
get key zz
set mode "hires"
rem set up
open #1 : screen 0, .5, 0, .5          ! x view
open #2 : screen .5, 1, 0, .5          ! y view
open #3 : screen 0, .5, .5, 1          ! z view
open #4 : screen .5, 1, .5, 1          ! text
rem  NB:Remember to adjust the window 4 text routines below when adjusting
rem     these OPEN statements---also realcentre & deltareal statements.
rem  Note:See final subroutine ORIENTATION for adjusting axes' orientation.
rem  1.25 seems to be a good aspect ratio for the Bondwell.
```

```
for i = 1 to 3
  window #i
  set window - maxrange * 1.25, maxrange * 1.25, - maxrange, maxrange
next i
mat sliceposn = 0
mat galtot = 0
let view = 0
do
  window #4
  clear
  call frame
  print "Bubble-file " ; bubblefile$ ; " in memory"
  print "   Z      |        Into Screen:"
  print "   X Y    |  - x       + y       + z    "
  print "----------+---------+---------+---------"
  print "slice posn ";
  print using format$ : sliceposn(1), sliceposn(2), sliceposn(3)
  print "hor  cursr ";
  print using format$ : horcursor(1), horcursor(2), horcursor(3)
  print "vert cursr ";
  print using format$ : vertcursor(1), vertcursor(2), vertcursor(3)
  print "galaxies   ";
  print using "######    " : galtot(1), galtot(2), galtot(3)
  print "coord cntr ";
  print using format$ : cocentre(1), cocentre(2), cocentre(3)
  print "delta-real ";
  print using format$ : deltareal(1), deltareal(2), deltareal(3)
  print "real cntr  ";
  print using format$ : realcentre(1), realcentre(2), realcentre(3)
  if view <> 0 then window #view
  get key zz
  if zz < 123 and zz > 119 then
    let view = zz - 119
    window #view
    call orientation(view, hor, vert)
    ask window left, right, bottom, top
  end if
  if zz = 100 then
    window #4
    clear
    print "Current value of step length is " ; 2 * ds
    input prompt "New value ? " : ds
    let ds = ds / 2
    window #view
  end if
  if zz = 114 then
    window #4
    clear
    print "Current value of maximum range is " ; maxrange
    input prompt "New value ? " : maxrange
```

```
  window #view
  set window - maxrange * 1.25, maxrange * 1.25, - maxrange, maxrange
  ask window left, right, bottom ,top
end if
if zz <> 99 and zz <> 113 and view <> 0 then
  if zz = 44 then
    let sliceposn(view) = sliceposn(view) - 2 * ds
  else if zz = 46 then
    let sliceposn(view) = sliceposn(view) + 2 * ds
  else if zz = 48 then
    let sliceposn(view) = 0
  else if zz = 101 or zz = 110 then
    open #5: screen 0, 1, 0, 1
    set window - maxrange * 1.25, maxrange * 1.25, - maxrange, maxrange
    if zz = 110 then
      let galname$ = deviceout$ & chr$(view + 119)
      let galname$ = galname$ & str$(sliceposn(view)) & ".gal"
      open #6 : name galname$, org text, access output, create newold
      erase #6
      print #6 : "Galaxies in slice @ " ; sliceposn(view)
      print #6 : "Thickness =" ; 2*ds; " Range = ";
      print #6 : maxrange ; " X" ; maxrange
      print #6
    end if
  end if
  if zz=44 or zz=46 or zz=48 or zz=101
          or zz=102 or zz=110 or galtot(view)=0 then
    let galtot(view) = 0
    clear
    for i = 1 to suitable_gals
      if abs(pt(view,i)-(cocentre(view)+sliceposn(view))) < ds then
        let hor_coord  = pt(hor,i) - cocentre(hor)
        let vert_coord = pt(vert,i) - cocentre(vert)
        if abs(hor_coord)<maxrange and abs(vert_coord)<maxrange then
          plot hor_coord, vert_coord
          let galtot(view) = galtot(view) + 1
          if zz = 110 then
            print #6 : str$(galtot(view)); " : " ; str$(i) ; " : " ,
            print #6, using " #####  " : hor_coord, vert_coord
            plot text, at hor_coord, vert_coord : str$(galtot(view))
          end if
        end if
      end if
    next i
    close #6
    if zz = 101 or zz = 110 then
      get key zz
      if zz = 115 then
        box keep left, right, bottom, top in picture$
        let picname$ = deviceout$ & chr$(view + 119)
```

```
      let picname$ = picname$ & str$(sliceposn(view)) & ".pic"
      open #10 : name picname$, access output, create newold, org text
        erase #10
        print #10 :  picture$
      close #10
    end if
    let zz = 101
  end if
  call ticks(1000, 1000)
  call frame
  let textposn = maxrange - .10 * maxrange
  plot text, at textposn, 0 : chr$(hor + 119)
  plot text, at 0, textposn - .10 * maxrange : chr$(vert + 119)
  restore
  for i = 1 to no_centres                ! plot centres of other voids
    read name$
    plot text, at (centres(hor,i)-cocentre(hor)),
                          (centres(vert,i)-cocentre(vert)) : name$
  next i
  let corner(view) = sliceposn(view)
  let corner(hor ) = left
  let corner(vert) = bottom
  call octnote(corner, octno)
  plot text, at .8 * left  , .8 * bottom : str$(octno)
  let corner(hor ) = right
  let corner(vert) = bottom
  call octnote(corner, octno)
  plot text, at .8 * right , .8 * bottom : str$(octno)
  let corner(hor ) = right
  let corner(vert) = top
  call octnote(corner, octno)
  plot text, at .8 * right , .8 * top    : str$(octno)
  let corner(hor ) = left
  let corner(vert) = top
  call octnote(corner, octno)
  plot text, at .8 * left  , .8 * top    : str$(octno)
  if zz = 101 then
    get key zz
    clear
    close #5
    mat galtot = (0)
  end if
 end if
end if
if zz = 99 and view <> 0 then
  ! Position the cursor at its previous position in this view with :
  set color 0
  plot horcursor(view), vertcursor(view) ;
  set color 7
  get point : horcursor(view), vertcursor(view)
```

```
    plot
    rem update realcentre and associated uncertainties
    let realcentre(1) = (horcursor(2) + vertcursor(3))/2 + cocentre(1)
    let deltareal(1) = abs(horcursor(2) - vertcursor(3))
    let realcentre(2) = (horcursor(1) + horcursor(3))/2 + cocentre(2)
    let deltareal(2) = abs(horcursor(1) - horcursor(3))
    let realcentre(3) = (vertcursor(1) + vertcursor(2))/2 + cocentre(3)
    let deltareal(3) = abs(vertcursor(1) - vertcursor(2))
  end if
loop until zz = 113
close #4
close #3
close #2
close #1
set mode "text"
end sub


sub calc
do
input prompt "Polar to rectangular, or rectangular
                                to polar conversion (pr/rp) ? " : qu$
loop until qu$ = "pr" or qu$ = "rp"
print
if qu$ = "pr" then
  input prompt "Input latitude, longitude : " : theta, phi
  if phi < 24 then
    print "Is this RA ? (y/n)";
    do
      input qu$
    loop until qu$ = "y" or qu$ = "n"
  end if
  if qu$ = "y" then let phi = phi * 15
  input prompt "Input v : " : v
  let theta = rad(theta)
  let phi = rad(phi)
  let theta = rad(90) - theta
  let x1 = v * sin(theta) * cos(phi)
  let y1 = v * sin(theta) * sin(phi)
  let z1 = v * cos(theta)
  print "x = " ; x1 , "y = " ; y1 , "z = " ; z1
  print "v = " ; v
else
  input prompt "Input x, y, z : " : x1, y1, z1
  let v = (x1^2 + y1^2 + z1^2)^.5
  let theta = acos(z1 / v)
  let phi = arctan(y1 , x1)
  let theta = rad(90) - theta
  let theta = deg(theta)
  let phi = deg(phi)
```

```
  print "v = " ; v , "lat.= " ; theta , "long.= " ; phi
  print ,,, "RA = " ; phi / 15
end if
print "(Press any key when ready ...)"
get key zz
end sub

sub extractbub
clear
print "Extract data from a galaxy catalogue"
print "-----------------------------------"
do
  input prompt "COELIS to extract from which catalogue ? " : filename$
  input prompt "RA/dec or galactic ? (r/g)" : coord$
  input prompt "Are you happy with these values ? (y/n) " : qu$
loop until qu$ = "y"
input prompt "Input a file name for saving" : bubblefile$
print "Prepare drive " ; deviceout$ ; " to receive data, "
print "and hit any key when ready ..."
let bubblefile$ = deviceout$ & bubblefile$ & ".bub"
get key zz

open #9 : name bubblefile$, org text, access output, create newold
erase #9

print
print "Saving to"; bubblefile$
for i = 1 to no_centres
  print #9 : centres(1, i) ; "," ; centres(2, i) ; "," ; centres(3, i)
next i
print #9 : v_lim0 ; "," ; v_lim1 ; "," ;
print #9 : phi_lim0 ; "," ; phi_lim1 ; "," ;
print #9 : theta_lim0 ; "," ; theta_lim1
print #9 : suitable_gals

print "Prepare for galaxy catalogue input from drive " ; devicein$ ;
print " and press any key when ready."
get key zz

open #8 : name filename$, organization text, access input, create old
let i = 0
do while more #8 and i < maxdatano
  line input #8: catline$
  let test = ord(catline$[59:59])
  when error in
    let v = val(catline$[lv_col : rv_col])       ! could use v0 here
    if coords$ = "r" then
      let a$ = catline$[lra_col : rra_col]
      let d$ = catline$[ldec_col : rdec_col]
      let a = val(a$)
```

```
      let d = val(d$)
      let phi = a
      let theta = d
    end if
  use
    let v = 0
  end when
  if test = qu then
        let i = i + 1
        let phi = rad(phi)
        let theta = rad(90 - theta)
        let pt(1, i) = v * sin(theta) * cos(phi)
        let pt(2, i) = v * sin(theta) * sin(phi)
        let pt(3, i) = v * cos(theta)
        print catline$
        print #9 : pt(1,i);",";pt(2,i);",";pt(3,i);
                   ",";str$(i);"::"; catline$[lname_col:rname_col]
  end if
loop

if i = maxdatano then
  print "Too much suitable galaxy data -- hone down the range a bit."
else
  let suitable_gals = i
  print i ; "suitable galaxies were found."
end if
mat cocentre = 0
let xc = 0
let yc = 0
let zc = 0
close #8
close #9
get key zz
end sub


sub loadbub
clear
print "Load bubble-data from bubble-file"
print "--------------------------------"
input prompt "Load bubble data from ? " : bubblefile$
print "Now, prepare drive " ; devicein$ ; " to send data, "
print "and hit any key when ready..."
let bubblefile$ = devicein$ & bubblefile$ & ".bub"
get key zz

open #10 : name bubblefile$, org text, access input, create old
print "Loading " ; bubblefile$
for i = 1 to no_centres
  input #10 : centres(1, i), centres(2, i), centres(3, i)
```

```
next i
input #10 : v_lim0, v_lim1, phi_lim0, phi_lim1, theta_lim0, theta_lim1
input #10 : suitable_gals
for i = 1  to suitable_gals
  input #10 : pt(1, i), pt(2, i), pt(3, i), galname$
next i
mat cocentre = 0
let xc = 0
let yc = 0
let zc = 0
close #10
end sub

sub changedevice
clear
print "Change drive designations"
print "-------------------------"
print "At present the device nos. are"
print "        input  drive : " ; devicein$
print "        output drive : " ; deviceout$
print "Change devices ?"
print "Choose from a or b or c for "
input prompt "  input drive : " : devicein$
input prompt " output drive : " : deviceout$
let devicein$ = devicein$ & ":"
let deviceout$ = deviceout$ & ":"
end sub

sub transformdata
clear
print "Transformations of the data"
print "==========================="
print "Options:"
print "Translating ..................................................... (t)"
print "3-d rotations only (ie. without eigenvectors) ..... (3)"
print "2-d (planar) rot'ns after 3-d rot'ns (ie. with e-vectors) .. (2)"
print "Quitting ........................................................ (q)"
do
  input prompt "Your choice ? " : choice$
loop until choice$ = "t" or choice$ = "3" or choice$ = "2" or choice$ = "q"
if choice$ = "q" then exit sub
print "Real centre so far :";
mat print realcentre
print "Known centres :-"
mat print centres
restore
for i = 1 to no_centres
  read qu$
  print qu$,
next i
```

```
do
  print "Input translation vector or e-vector of largest e-value"
  mat input prompt "relative to the present co-ord system : " : v1
  input prompt "Happy?" : qu$
loop until qu$ = "y"
if choice$ = "t" then
  clear
  print "Translations"
  print "------------"
  print "Transforming ..."
  for  ll = 1 to suitable_gals
    for i = 1 to 3
      let pt(i, ll) = pt(i, ll) - v1(i)
    next i
  next ll
  for ll = 1 to no_centres
    for i = 1 to 3
      let centres(i, ll) = centres(i, ll) - v1(i)
    next i
  next ll
else
  let decision = val(choice$)
  mat v2 = (0)
  clear
  print "Rotations"
  print "---------"
  print choice$ & "-rotating ..."
  if decision = 2 then
    mat input prompt "Input e-vector of 2nd largest e-val : " : v2
  end if
  call rotation(pt,no_centres,centres,v1,suitable_gals,v2,decision)
end if
end sub

end


sub menu(choice$)
  clear
  print "                              COELIS"
  print "                              ======"
  print
  print "Options:"
  print
  print "Load bubble data from a bubble-file ....................... (l)"
  print "Histogram generator for centre checking ................... (h)"
  print "Plot density curves for generated histograms .............. (p)"
  print "Fit by least squares methods .............................. (f)"
  print "Transform the data set .................................... (t)"
  print "Casement displays and ""by hand"" graphics centering ..... (g)"
  print "Calculator (for polar/rect conversion) .................... (c)"
```

```
  print "Extracting bubble data from a galaxy catalogue ..... (e)"
  print "Changing drive designations  ..... (d)"
  print "Quitting  ..... (q)"
  print
  print
input prompt "What is your choice? " : choice$

end sub

def projx(a, d)
  let a = a - pi
  let projx = 2 *sqr(2)*cos(d)*sin(a/2) / sqr(1+cos(d)*cos(a/2))
end def

def projy(a, d)
  let a = a - pi
  let projy = sqr(2) * sin(d) / sqr(1 + cos(d) * cos(a/2))
end def

def arctan(y, x)
  if x <> 0 then
    let phi = atn(y / x)
  else
    let phi = pi / 2
  end if
  if y < 0 or x < 0 then
    let phi = phi + pi
    if x > 0 and y < 0 then let phi = phi + pi
  end if
  let arctan = phi
end def

sub point(x, y, dx, dy)   ! plot large points
  let left = x - dx
  let right = x + dx
  let bottom = y - dy
  let top = y + dy
  box circle left, right, bottom, top
  plot x, y;
end sub

sub octnote(corner(), octno)   ! determine octant
  if corner(3) >= 0 then let octno = 0 else let octno = 4
  if corner(2) >= 0 then
    if corner(1) < 0 then let octno = octno + 1
    let octno = octno + 1
  else
    if corner(1) >= 0 then let octno = octno + 1
    let octno = octno + 3
  end if
```

```
end sub


sub orientation(view, hor, vert)    ! for casement display
  rem  All decisions about orientation of the axes are made here
  if view = 1 then
    let hor = 2
    let vert = 3
  else if view = 2 then
    let hor = 1
    let vert = 3
  else
    let hor = 2
    let vert = 1
  end if
end sub


sub leastsq(pt(,),fitresults(),suitable_gals,xc,yc,zc,
                            residual(),maxrad,op,fop$,ffeed)

declare def cot, sec, csc, asin, acos, acot, asec, acsc
dim sum(0:4, 0:4, 0:4)
dim ellips_ls(9, 9), ellips_c(3, 3), ellips_lsv(9), ellips_cv(3)
dim lambda(3)
for i = 1 to suitable_gals
if (pt(1, i)-xc)^2+(pt(2, i)-yc)^2+(pt(3, i)-zc)^2 <= maxrad^2 then
  let x = pt(1, i)
  let y = pt(2, i)
  let z = pt(3, i)
  let sum(1, 0, 0) = sum(1, 0, 0) + x
  let sum(0, 1, 0) = sum(0, 1, 0) + y
  let sum(0, 0, 1) = sum(0, 0, 1) + z
  let sum(2, 0, 0) = sum(2, 0, 0) + x^2
  let sum(0, 2, 0) = sum(0, 2, 0) + y^2
  let sum(0, 0, 2) = sum(0, 0, 2) + z^2
  let sum(1, 1, 0) = sum(1, 1, 0) + x * y
  let sum(0, 1, 1) = sum(0, 1, 1) + y * z
  let sum(1, 0, 1) = sum(1, 0, 1) + x * z
  let data = data + 1
end if
next i

if data < 3 then
  print "There are not sufficient data points to do a meaningful fit."
  exit sub
end if

rem Construction of coeff. matrix for least-squares for ellipsoid
for i = 1 to 3
```

```
  for j = 1 to 3
    read p$
    let ellips_ls(i, j) = sum(val(p$[1:1]),val(p$[2:2]),val(p$[3:3]))
  next j
  read p$
  let ellips_lsv(i) = sum(val(p$[1:1]), val(p$[2:2]), val(p$[3:3]))
next i

call simeqns2(ellips_ls, ellips_lsv, 3)

rem Results: parameters for ellipse
let ae = ellips_lsv(1)
let be = ellips_lsv(2)
let ce = ellips_lsv(3)

rem Determine standard errors
for i = 1 to suitable_gals
if (pt(1,i)-xc)^2 + (pt(2,i)-yc)^2 + (pt(3,i)-zc)^2 <= maxrad^2 then
  let x = pt(1, i)
  let y = pt(2, i)
  let z = pt(3, i)
  let temp = ae * x + be * y + ce * z -1
  let residual(i) = temp
  let ellips_se = ellips_se + temp^2
else
  let residual(i) = 1e9
end if
next i

let ellips_se = (ellips_se / (data - 3))^.5

if op <> 2 then
  open #1 : printer
else if op = 2 then
  open #2 : name fop$, org text, create old, access output
  set #2 : pointer end
end if
let format$ = "    +#.##^^^^^"
print #op : "MODEL:                    Plane "
print #op
print #op : ae, be, ce
print #op
mat sum = (1/suitable_gals) * sum
print #op : "MEANS              ";
print #op, using " ###### " :sum(1,0,0), sum(0,1,0), sum(0,0,1)
print #op
print #op : "STANDARD ERROR     ";
print #op, using format$: ellips_se
print #op
let ffeed = ffeed + 1
```

```
if op <> 0 then
  print #op : "                -\-\-\-\-\-\-\-\-\-\-\-\-\-"
  print #op
  if ffeed = 2 then
    let ffeed = 0
    print #op : chr$(12)
  end if
  close #op
end if

rem Array of least squares coefficients, and vector (for _ls and _lsv)
data 200, 110, 101,    100
data 110, 020, 011,    010
data 101, 011, 002,    001

end sub

sub simeqns2(b(,), w(), nrow)
rem
rem Solution of simultaneous equations by Gauss-Jordan elimination.
rem (Adapted from AR Miller "Fortran Programs for Scientists & Engineers"
rem  Sybex (1982))
rem

dim index(9, 3)

for i = 1 to nrow
  let index(i, 3) = 0
next i
let determ = 1
for  i = 1 to nrow
  let big = 0
  for j = 1 to nrow
    if index(j, 3) <> 1 then
      for k = 1 to nrow
        if index(k, 3) > 1 then exit for
        if index(k, 3) < 1 and abs(b(j, k)) > big then
          let irow = j
          let icol = k
          let big = abs(b(j, k))
        end if
      next k
      if k < 4 and index(k, 3) > 1 then
        call singular
        exit sub
      end if
    end if
  next j
  let index(icol, 3) = index(icol, 3) + 1
  let index(i, 1) = irow
```

```
  let index(i, 2) = icol
  if irow <> icol then
    let determ = - determ
    for l = 1 to nrow
      call swap(b(irow, l), b(icol, l))
    next l
    call swap(w(irow), w(icol))
  end if
  let pivot = b(icol, icol)
  let determ = determ * pivot
  let b(icol, icol) = 1
  for l = 1 to nrow
    let b(icol, l) = b(icol, l) / pivot
  next l
      let w(icol) = w(icol) / pivot
  for l1 = 1 to nrow
    if l1 <> icol then
      let t = b(l1, icol)
      let b(l1, icol) = 0
      for l = 1 to nrow
        let b(l1, l) = b(l1, l) - b(icol, l) * t
      next l
      let w(l1) = w(l1) - w(icol) * t
    end if
  next l1
next i
for i = 1 to nrow
  let l = nrow - i + 1
    if index(l, 1) <> index(l, 2) then
      let irow = index(l, 1)
      let icol = index(l, 2)
      for k = 1 to nrow
        call swap(b(k, irow), b(k, icol))
      next k
    end if
next i
for k = 1 to nrow
  if index(k, 3) <> 1 then
    call singular
    exit sub
  end if
next k
end sub

sub swap(a, b)
  let hold = a
  let a = b
  let b = hold
end sub
```

```
sub singular
  print
  print "Matrix singular"
  get key zz
end sub

sub rotation(pt(,),no_centres, centres(,),
                        v1(), suitable_gals,v2(), decision)
declare def acos, arctan
dim rot3(1:3, 1:3)
dim rot2(1:3, 1:3)
dim v(1:3)
let r = sqr(v1(1)^2 + v1(2)^2 + v1(3)^2)
let phi = arctan(v1(2), v1(1))
let theta = acos(v1(3) / r)
let rot3(1, 1) = - sin(theta) * cos(phi)
let rot3(2, 1) = - sin(phi)
let rot3(3, 1) = cos(theta) * cos(phi)
let rot3(1, 2) = - sin(theta) * sin(phi)
let rot3(2, 2) = cos(phi)
let rot3(3, 2) = cos(theta) * sin(phi)
let rot3(1, 3) = - cos(theta)
let rot3(2, 3) = 0
let rot3(3, 3) = - sin(theta)
if decision = 2 then
  mat v2 = rot3 * v2
  let phi = arctan(v2(3), v2(2))
  let rot2(1, 1) = 1
  let rot2(2, 1) = 0
  let rot2(3, 1) = 0
  let rot2(1, 2) = 0
  let rot2(2, 2) = cos(phi)
  let rot2(3, 2) = -sin(phi)
  let rot2(1, 3) = 0
  let rot2(2, 3) = sin(phi)
  let rot2(3, 3) = cos(phi)
  mat rot3 = rot2 * rot3
end if
for i = 1 to suitable_gals
  let v(1) = pt(1, i)
  let v(2) = pt(2, i)
  let v(3) = pt(3, i)
  mat v = rot3 * v
  let pt(1, i) = v(1)
  let pt(2, i) = v(2)
  let pt(3, i) = v(3)
next i
for i = 1 to no_centres
  let v(1) = centres(1, i)
  let v(2) = centres(2, i)
```

```
  let v(3) = centres(3, i)
  mat v = rot3 * v
  let centres(1, i) = v(1)
  let centres(2, i) = v(2)
  let centres(3, i) = v(3)
next i
end sub

sub histogram(op,dr,lower,upper,suitable_gals,
              histos(,),r(),oct(),maxdensity,histotype,n$)
if op = 1 then
  open #1 : printer
else if op = 2 then
  open #2 : name n$, org text, create old, access output
  set #2 : pointer end
else
  let op = 0
end if
if histotype = 2 then
  let runs = 8
else
  let runs = 1
end if
let dr = dr / 2
mat histos = (0)
for r0 = lower to upper step (2 * dr)
  let hbin = int(r0/2/dr)
  for i = 1 to suitable_gals
    if abs(r(i) - r0) <= dr then
      if histotype = 2 then
        let histos(oct(i), hbin) = histos(oct(i), hbin) + 1
      else if histotype = 1 then
        if r(i) <> 0 then let histos(1, hbin) = histos(1, hbin) + 1
      end if
    end if
  next i
next r0
print
let maxdensity = 0
for ll = 1 to runs        ! construct the output line
  print #op : repeat$(" ", 30) ; "dr = " ; str$(2 * dr)
  print #op : "r =" & str$(lower)
  print #op : repeat$("_", 20)
  let blocktot = 0
  for r0 = lower to upper step (2 * dr)
    let histo$ = ""
    let hbin = int(r0/2/dr)
    let density = histos(ll, hbin) / ((r0 + dr)^3 - (r0 - dr)^3) * 1e10
    if maxdensity < density then let maxdensity = density
    let histo$ = repeat$(str$(ll), histos(ll, hbin))
```

```
    if len(histo$) > 79 then let histo$ = histo$[1:79]
    let blocktot = blocktot + len(histo$)
    if len(histo$) = 0 then let histo$ = "+"
    print #op : histo$
  next r0
  print #op : repeat$("-", 20)
  print #op : "r ="; str$(upper)
  print #op
  print #op
  print #op : blocktot ; "galaxies are represented here"
  print #op
  print #op : repeat$(" ", 34) & "- - - - - - -"
  print #op : chr$(12)
next ll
if op <> 0 then close #op
end sub
```